T 131

621.38
SHA

CEN
E
cos T 131
27/02/13

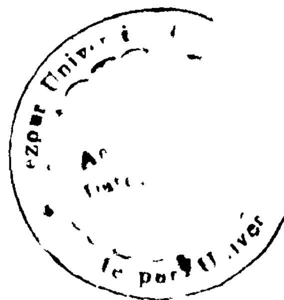

43053

Modeling and Simulation
of
Nanobioelectronic Device
The Cylindrical Ion Sensitive Field Effect Transistor.

A thesis submitted in partial fulfillment of the requirements
for the Degree of Doctor of Philosophy

By

Santanu Sharma

Reg. No-135/99

School of Engineering

Department of Electronics and Communication Engineering

Tezpur University

January, 2009

TEZPUR UNIVERSITY

This is to certify that the thesis entitled "**Modeling and Simulation of Nanobioelectronic Device- The Cylindrical Ion Sensitive Field Effect Transistor**" submitted to the Tezpur University in the Department of Electronics and Communication Engineering under the School of Engineering in partial fulfillment for the award of the degree of Doctor of Philosophy in Electronics and Communication Engineering is a record of research work carried out by Mr. santanu sharma under my supervision and guidance.

All help received by him/her from various sources have been duly acknowledged.

No part of this thesis has been submitted elsewhere for award of any other degree.

Date: 19-01-09

Place: Tezpur

(Dr. Jiten Ch. Dutta)
Supervisor,
Reader,
Department of Electronics and
Communication Engineering,
Tezpur University, Napaam,
Tezpur, Assam, India,
PIN-784028

TEZPUR UNIVERSITY

This is to certify that the thesis entitled "**Modeling and Simulation of Nanobioelectronic Device- The Cylindrical Ion Sensitive Field Effect Transistor**" submitted by Mr. santanu sharma to the Tezpur University in the Department of Electronics and Communication Engineering under the School of Engineering in partial fulfillment for the award of the degree of Doctor of Philosophy in Electronics and Communication Engineering has been examined by us and found to be satisfactory.

The committee recommends for the award of the degree of Doctor of Philosophy.

Supervisor External Examiner

Date:

Abstract

This thesis aims at contributing towards development in pH sensing by proposing a novel device structure of Ion Sensitive Field Effect Transistor (ISFET) and a detailed physico chemical model for its simulation to predict the device characteristics particularly at nano dimension.

Intracellular pH is an important cell function modulator. The activity of proteins depends on pH. Delivery, absorption and effectiveness of drugs can be altered by changing the pH of the local environment . If pH falls below 6.8 or rises above 7.8, the person may die. In certain medical and biotechnological research it becomes necessary to extract signals from within a cell. Intracellular pH difference across the mitochondrial membrane drives the electron transport chain which converts electron energy in to phosphate bonds . For such purpose, sensor capable of extracting information from a single cell is highly essential. In order to achieve clear understanding of what is happening inside a single cell, sensor must meet the physical dimension, detection limit and sensitivity precisely.

The concept of Ion Sensitive Field Effect Transistor was first proposed by Prof. Piet Bergveld, in the year 1970. The basic device is sensitive to H^+ ions and hence it can give a measure of pH of the solution. Field Effect Transistor has shown its suitability as a bioelectronic device for biosensor and has undergone several changes and transitions since its inception in the year 1970. Since then a good number of papers have been published in different journals / conferences. The research work seen so far shows flow of ISFET research mainly in two directions: - one of which shows some experimental results with new samples, new materials to establish the potential of the device in a new direction of application.

In the other direction of research it shows the development of a model -may be a physico- chemical or may be a model based on SPICE (Simulation Program with Integrated Circuit Emphasis) for different sensing materials. The objective of such work is to find out a new material that can be used to make devices with enhanced sensitivity.

A unique feature of all the papers is that, the work is based on the conventional planer device. It has also been observed that no research group or individual has so far worked on a new device geometry or shape for enhancing sensitivity of the ISFET. The potentiometric sensitivity has very weak dependence on device geometry, but the amperometric sensitivity which is highly dependent on deyice transconductance is in turn dependent on the device geometry. By using appropriate material for gate insulator and/or sensing surface of ISFET, the device sensitivity can be enhanced to a particular level. In case of an in vivo sensor it may not always be possible to use the material with highest sensitivity, when the question of biocompatibility arises. In this situation some other methods for sensitivity enhancement will be required, such as new device geometry. In addition ISFET in its planner form when scaled down to deca nanometer dimension comes up with numerous small dimension effects. The Gate All Around MOSFET Structure is very successful against most of these parasitic effects and when these structures are implemented for the ISFET, the sensor amperometric sensitivity shows much higher value. Among all the gate all-around structure, the cylindrical structure is the best because of absence of corner effect. Corner effect gives rise to non uniform gate overdrive and consequently current density also becomes non uniform. This problem is not encountered in Cylindrical Structure.

The main purpose of this work is to develop a Physico chemical model of Cylindrical ISFET of nano dimension. Nano dimension is chosen because; the intended application of this device is for single cell monitoring. Here in this work a complete model of this device has been developed considering the entire major small dimension effects including the quantum mechanical (QM) effects leading to threshold shift. While the initial simulation results (in the sub micron range) have been compared with the data available in literature to evaluate consistency of the model, subsequent results (in the nanometer range that includes QM effect) provides prediction about the device response. This work also gives a rule for reference electrode placement. This finally determines the overall system dimension which depends upon the Debye length corresponding to the highest value of pH to be measured.

The first part of the thesis discusses basics of ISFET, fundamentals of oxide /electrolyte interface of the site binding model and physico chemical modeling of the device. In this part a generalized model for the planer ISFET are discussed based on the site binding model for silicon dioxide as sensing material. Silicon dioxide, when used as pH sensing surface posses only one type of surface site.

Attempts have been made in a very modest way to contribute the following in the present thesis:-

1. First, a novel ISFET structure has been introduced based on the surrounding gate MOSFET which is available in literature. A physico chemical model for the same has been developed in this work. Here the semiconductor charge has been considered as two distinct layers – inversion layer and depletion layer and the simulation results show the followings.

Above threshold condition the inversion charge depends on pH and the depletion charge remains fixed, below threshold, the depletion charge shows its dependence on pH.

The Diffuse layer at the electrolyte insulator interface surrounding the cylindrical device is influenced by cylindrical geometry. This influence is also modeled and analyzed. The device model is simulated in MATLAB and its behavior is analyzed for various pH values. The results show sharper fall in diffuse layer potential compared to the planer geometry. Deviation of device potentiometric sensitivity as a function of reference electrode position relative to the OHP (Outer Helmholtz Plane) has also been analyzed.

The results obtained from simulation leads to the conclusion that there is a definite correlation between the distance from the OHP to the reference electrode and the Debye length of the electrolyte at that particular value of pH. A distance of 3 Debye lengths can give results having one to one relationship between electrolyte oxide interface potential and pH i.e. one value of electrolyte oxide interface potential corresponds only to one value of pH. If the reference electrode is placed at a distance smaller than the Debye length from the OHP in a particular range of pH one value of electrolyte oxide interface potential will correspond to two values of pH

2. A humble attempt has been made to develop the cylindrical ISFET at nano dimension. In this part of work study was carried out giving emphasis on the following factors:

a) The conduction band edge shift at nano dimension has been considered by solving the Schrödinger Wave Equation in cylindrical coordinate.

b) The increase in effective oxide thickness (EOT) that occurs due to shifting of inversion layer centroid away from the insulator semiconductor interface has also been considered.

The study that was carried out on the developed model by considering the above two factors reveals an increased threshold voltage resulting lower drain current at a particular reference electrode voltage and at a particular value of pH.

3. Further, the effect of insulator thickness on the sensitivity of the device was also studied. When the insulator thickness is reduced to nano level, the number of buried (slow responding) sites reduces in number, while the number of surface (Fast responding) sites remains the same. At insulator thickness equal or less than 3 nm, there is no buried site presents, consequently when this effect is incorporated in the model developed in (2) little lesser potentiometric sensitivity obtained, but the output settles faster.

While including the nano dimension effects as discussed in (2) it is observed that the drain current and potentiometric sensitivity of the device decreases, and consequently the amperometric sensitivity also decrease. Even though these three factors pulling the device current and the amperometric sensitivity down at nano dimension, the results are much better while compared with the planer device at similar dimension, which is due to better device transconductance arising out of the device geometry.

When the rule for reference electrode placement is implemented to the cylindrical device, it is observed that, to obtain the same amount of

potentiometric sensitivity, the reference electrode in a cylindrical ISFET can be placed at a smaller distance from the OHP as compared to that in a planer device.

It can therefore be conclude that cylindrical device provides a pH measuring system with smaller dimension with higher amperometric sensitivity as compared to the planer device.

As a future extension of this work, the temperature variation of human body may also be considered in the model because, temperature change in human body under diseased condition may be sufficient to cause drift in the ISFET response *in vivo.*

DECLARATION

I hereby declare that the thesis entitled "**Modeling and Simulation of Nanobioelectronic Device- The Cylindrical Ion Sensitive Field Effect Transistor**" is an outcome of my research carried out at the Department of Electronics and Communication Engineering, School of Engineering, Tezpur University, India. The work is original and has not been submitted in part or full, for any degree or diploma of any other University or Institute.

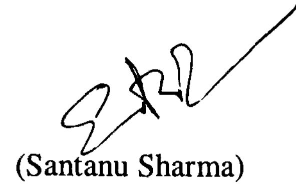

Date: 19.01.2009

(Santanu Sharma)

Dedicated to

My Parents and Family members

Contents **Page**

Abstract		**i**
Declaration		**vii**
Dedication		**viii**
Certificate of Supervisor		**ix**
Certificate of Examiner		**x**
Table of contents		**xi**
List of figures		**xiv**
Acknowledgement		**xix**
List of author's publications		**xx**
Chapter 1:	**Introduction**	**1**
	1.1 Sensing technologies and Ion Sensitive Field Effect Transistors	2
	1.2 Need for suitable device structure for ISFET	4
	1.3 Thesis outline	5
	1.4 References	7
Chapter 2:	**General overview of ISFETs and analysis of conventional ISFET**	**9**
	2.1 Introduction	10
	2.2 Theory of ISFET	10
	2.3 Operation principle of ISFET	15
	2.3.1 Site binding model	15
	2.3.2 Electrical double layer model	17
	2.4 Modeling	17
	2.5 Amperometric sensitivity	27

	2.6 Simulation results and conclusions	30
	2.7 References	35
Chapter 3:	**Novel Device Geometry – The Cylindrical ISFET**	**37**
	3.1 Introduction	38
	3.2 Threshold voltage model of the cylindrical ISFET	38
	3.3 Drain current model of the ISFET	50
	3.4 Potential profile modeling	51
	3.4.1 Electrolyte potential profile	51
	3.4.2 Semiconductor potential profile	56
	3.5 Amperometric Sensitivity	57
	3.6 Simulation results and conclusions	58
	3.7 References	77
Chapter 4:	**Cylindrical ISFET at nano dimension**	**80**
	4.1 Introduction	81
	4.2 Quantum mechanical Effects modeling	81
	4.3 Effective oxide thickness increase	89
	4.4 Effect of insulator nano dimension on ϕ_{eo}	91
	4.5 Conductance of nano cylindrical ISFET	93
	4.6 Parameter fluctuation in very small sensor	93
	4.7 Simulation and results and conclusions.	94
	4.8 References	112
Chapter 5:	**Response of ISFET as a function of Reference electrode position and determination of a rule for reference electrode placement**	**115**
	5.1 Introduction	116
	5.2 Model formulation	117
	5.3 Simulation results and conclusions	126
	5.4 References	131

Chapter 6: Conclusion 132

Appendix 137

Appendix A1 : Amperometric sensitivity 138

Appendix A2 : The cylindrical coaxial capacitance 138

Appendix A3 : The effective channel width of a cylindrical MOSFET 142

Appendix A4 : Calculation of reference electrode potential(E_{ref}) relative to vacuum 145

List of Figures

Chapter -2

Fig. 2.1 (a): Basic MOSFET structure (N-channel enhancement type).

Fig.2.1 (b): Basic ISFET structure.

Fig. 2.2: Site Binding model

Fig. 2.3: Electrical Double layer at the interface model

Fig. 2.4: Charge distribution and potential profiles of an EIS system based on the Site Binding Model explains the reaction at the surface of insulator. This kind of charge distribution occurs for pH> pH_{pzc}.

Fig. 2.5: Charge distribution and potential profiles of an EIS system based on the Site Binding Model explains the reaction at the surface of insulator. This kind of charge distribution occurs for pH< pH_{pzc}.

Fig. 2.6: Electrolyte oxide interface potential vs. pH for Silicon dioxide

Fig. 2.7: Drain Current vs. $V_{ref\ at}$ different values of pH.

Fig. 2.8: Drain Current vs. at different values of pH

Fig. 2.9: Amperometric sensitivity vs. pH

Chapter -3

Fig.3.1: Structure of the Cylindrical ISFET

Fig.3.2: Cross sectional view of a cylindrical ISFET surrounded by electrolyte.

Fig. 3.3: Charge distribution and potential profiles of an EIS system based on the Site Binding Model explains the reaction at the surface of insulator. This kind of charge distribution occurs for pH> pH_{pzc}.

Fig.3.4: Threshold voltage vs. doping concentration for a cylindrical MOSFET

Fig.3.5: Drain current vs. Gate to source voltage

Fig.3.6: Electrolyte oxide interface potential vs. pH

Fig.3.7: Drain current vs. pH

Fig.3.8: Surface buffer capacity vs. pH

Fig.3.9: Diffuse layer capacitance vs. pH

Fig.3.10: Double layer capacitance vs. pH

Fig.3.11: Debye length vs. pH

Fig.3.12: Normalized potential vs. distance from the OHP

Fig.3.13: Comparison of Normalized potential vs. distance from the OHP at pH=4

Fig.3.14: Comparison of Normalized potential vs. distance from the OHP at pH=7

Fig.3.15: Comparison of Normalized potential vs. distance from the OHP at pH=10

Fig: 3.16: Drain current vs. Drain to source voltage at different value of pH

Fig: 3.17: Drain current vs. the voltage applied to the reference electrode at different value of pH.

Fig.3.18: (a) Inversion Charge Density vs. pH (V_{ref}=10 V)

(b) Depletion Charge Density vs. pH (V_{ref}=6 V)

Fig.3.19: Amperometric sensitivity of planar and cylindrical ISFET

Chapter -4

Fig.4.1: Potential of an electron in a homogeneous field

Fig.4.2: The triangular potential well. The Eigen function of the problem is chosen in such way that on the left side of the interface i.e. for $\rho \geq \rho_{Si}/2$, $\psi(\rho)$ vanishes.

Fig.4.3: Threshold shift vs. silicon pillar diameter

Fig.4.4: Shift of inversion layer centroid (Δr) vs. total carrier concentration (Inversion and depletion charges)

Fig.4.5: Drain current vs. voltage applied to the reference electrode at pH=4, t_{si}=10nm

Fig.4.6: Drain current vs. voltage applied to the reference electrode at pH=7, t_{si}=10nm

Fig.4.7: Drain current vs. voltage applied to the reference electrode at pH=10 and t_{si}=10nm

Fig.4.8: Drain current vs. voltage applied to the reference electrode at pH=4, tsi=5nm, t_{si}=10nm and t_{si}=20nm

Fig.4.9: Drain current vs. voltage applied to the reference electrode at pH=7, tsi=5nm, t_{si}=10nm and t_{si}=20nm

Fig.4.10: Drain current vs. voltage applied to the reference electrode at pH=10, tsi=5nm, t_{si}=10nm and t_{si}=20nm

Fig.4.11: Drain current vs. drain to source voltage (tsi=10nm)

Fig.4.12: Reduction of electrolyte oxide interface potential due to nano dimension

Fig.4.13: Drain current vs. drain to source voltage at tsi=10nm (including QME only and QME+ effect of nano dimension insulator)

Fig.4.14: Amperometric Sensitivity vs. pH

Fig.4.15: Conductivity of the cylindrical ISFET at nano dimension vs. pH at V_{ref}= 8.5 volts

Fig.4.16: Conductivity of the cylindrical ISFET at nano dimension vs. pH at V_{ref}=9volts

Chapter -5

Fig.5.1: Potential profile of the Electrolyte Insulator Semiconductor structure for a planar surface when the reference electrode is placed in the bulk electrolyte i.e. sufficiently away from the OHP

Fig.5.2: Potential profile of the Electrolyte Insulator Semiconductor structure for a planar surface when the reference electrode is placed inside the diffuse layer.

Fig.5.3: Effective electrolyte oxide interface potential (ϕ_{eo_eff}) vs. pH when the reference electrode is placed at a distance of 30.8 nm from the OHP.

Fig.5.4: Effective electrolyte oxide interface potential (ϕ_{eo_eff}) vs. pH when the reference electrode is placed at a distance of 975 nm from the OHP.

Fig.5.5: Effective electrolyte oxide interface potential (ϕ_{eo_eff}) vs. pH when the reference electrode is placed at a distance of 308375 nm from the OHP.

Appendix

Fig.A1: Cylindrical capacitance cross sectional view

Fig.A2: Cross sectional view of a cylindrical ISFET surrounded by electrolyte.

Fig.A3: Channel of a planar MOSFET

Fig.A4: Cylindrical silicon pillar

Acknowledgements

I would like to thank those people whose help and support has made this work possible.

At the outset, I would like to express my sincere gratitude to my research supervisor Dr. Jiten Ch. Dutta, Department of Electronics and Communication Engineering, Tezpur University for his enthusiasm and guidance during my research and also for his patience while the thesis was being written. I greatly appreciate his care and dedication in constructively criticizing my works, including my thesis.

I would also like to thank all the members of the Department of Electronics and Communication Engineering, Tezpur University for their constant encouragement and support.
I would like to extend my special thanks to Mr N M Kakoty and Dr T Medhi for their help during my thesis work.

I would like to thank my family members for their constant support and encouragement during my entire research period.

Last but not the least; I would like to thank all my well wishers for their encouragement and help.

Santanu Sharma

List of author's publications

Journals

1. J C Dutta, S. Sharma, S Roy "Ion Sensitive Field Effect Transistors (ISFETs): Transducers for Biosensors" IE(I)-ET, Vol.88, July 2007

Conference Proceedings

1. R Borgohain, S. Sharma, J C Dutta, "Modeling Cylindrical nano size ISFET for biosensor applications" Proceedings of International Conference CODEC-06, Kolkata., December 18-20, 2006
2. J C Dutta, S Sharma R Borgohain, "Mixed Domain Modeling And Simulation Of Nano Size ISFET For Bioelectronic Device" International Conference on Recent Trends on Nanoscience and Technology (ICRTNT-06) Jadavpur University 7-9th December, 2006
3. S Sharma, J Bora, J C Dutta "Simulation of pH Sensitive ISFET based on site binding and Electrical Double Layer Theory" Proceedings of International Conference CODIS-04, Kolkata., January 8-10,2004
4. S. Sharma, J C Dutta, J Bora "Simulation of Cylindrical ISFET based on site binding model" Proceedings of International Conference CODEC-04, Kolkata., January 1-3,2004
5. R. Borgohain, S. Sharma, J. C. Dutta "Modeling Cylindrical Nano Size ISFET for Biosensor Applications" Seminar on Bioelectronics, Department of ECE, Tezpur University, 27 March,07.

Chapter 1

Introduction

1.1 Sensing technologies and Ion Sensitive Field Effect Transistors

Over the past thirty five years astounding progress has been made on multifold applications of chemical sensing technology. The field of chemical sensor mainly includes electro chemical sensor and optical sensor, while the concept of biosensing gives a new leap to it. Ion Sensitive Field Effect Transistor (ISFET), which is basically a chemical sensor, was first reported by Bergveld in 1970 [1]. ISFET bears the potential of fast response, smaller size and low cost due to the well established metal oxide semiconductor (MOS) technology. Initially silicon dioxide was used in ISFET as its sensing surface. It was sensitive to hydrogen ions, an inherent property of inorganic oxide. The circuit is completed by using one reference electrode. This concept was developed by Matsu and Wise [2] in 1974. Structurally ISFET is almost similar to metal oxide semiconductor field effect transistor (MOSFET) barring the metal gate electrode and adding a reference electrode immersed in the electrolyte solution. In this structure the gate insulator is exposed to the electrolyte solution and the reference electrode which is also inside the solution, completes the loop.

Wise et al. [3] used silicon as substrate for micro electrodes for electrophysiological measurement. But a systematic progress started with the inception of the ISFET. Since then several researchers carried out various studies on ISFET and other field effect transistor (FET) based devices. Most of them described ISFET as future tools for electrophysiological measurement [4]

Attempts have been made by the researchers to improve some characteristics like sensitivity, temperature effect, drift phenomenon etc using various inorganic oxides as dielectric materials. In the search for enhancement of pH and other chemical and biological sensing, several approaches have been made by different

researchers. For example some researchers have presented their work on nanowires: It has strong confinement for carriers in two dimensions and weak confinement in one direction. These devices possess capability of pH detection/ detection of chemical and biological species in aqueous solution [5]. The work in [5] states that it was carried out without an external gate, but the dynamic range can be extended for such sensors by using a side gate. However during the measuring process the changes in the surface charge can chemically gate the silicon nanowire. The silicon nanowire pH sensor presented in [6] uses a side gate to control the accumulation or depletion of the surface carrier on the nanowire. The side gate also provides ability to control the nanowire conductance necessary for optimization of detection sensitivity. The conductance of nanowire sensor presented in [6, 7] as a function of pH also uses a side gate for conductivity modulation. The work presented in [8] uses a nanowire for measurement of pH, detection of bio molecules like DNA with complimentary strand and detection of ATP binding. In this work the nanowire is used for direct detection of chemical and biological species. This explains how the nanowire is chemically or biologically gated without using any external gate. This paper also reports about the sensitivity limitation of a planar FET sensor over a nanowire FET sensor. In a cylindrical nanowire sensor the molecules that are being sensed can come from any direction. This makes it more likely to sense a molecule than a traditional planar sensor [9]. The work reported in [5] enunciates some advantage of nanowire over nanotube sensor such as- a metallic device does not function as expected. In this case the methods for preparation of selective interface required for a nanotube sensor is not well established. As the nanowire can be conveniently modified with receptors and ligands, it is very suitable for specific detection of biological and chemical species. In this connection it is worth mentioning that a recent work done in the year 2007 [10] reports that

penetrating a living cell having larger diameter compared to a semiconducting nanowire is not fatal to the cell and that cell remains functional for a few days after penetration. The results reported in this paper and also in [11] shows possibility of in vivo pH measurement and monitoring metabolic activity inside a single cell. In the above cases cylindrical shape nanowires have been used for detection and measurement of the analytes. Some of them have not used any external gate whereas the others have used an external gate but only sideways. Here the author gives a humble attempt to model a new device geometry concept at nano size. A comparison with a planar ISFET and nanowire sensor is also presented here.

1.2 Need for suitable device structure for ISFET

A high-throughput bimolecular analysis requires bio molecular detection at lower concentration and demands ultra sensitive sensors [12]. By using appropriate material for gate insulator and/or sensing surface of ISFET, the device sensitivity can be enhanced to some extent. In vivo sensor may not use the material with highest sensitivity, due to lack of biocompatibility. In such situations some other methods of sensitivity enhancement will be adopted, such as new device geometry. In addition, ISFET in its planner form, when scaled down to deca nanometre dimension comes up with number of small dimension effects. In this regard, it is worth mentioning the work presented in [8]. The Double Gate or the Gate All around MOSFET/Cylindrical MOSFET structure are very much successful against the most cases of these parasitic effect. On simulation these structures show much higher sensitivity. Consequently an ISFET based on these structure also posseses similar electrostatic nature. Cylindrical silicon nanowire is currently drawing much attention of the

researchers. As mentioned in the previous section, some of the research works carried out so far shows the use of nano wire without an external gate [5, 8]. Unfortunately without an external gate it is not possible to adjust the conductance which is necessary for optimization of detection sensitivity [6, 7]. On the other hand some works have been reported [6, 7] on the use of a side gate and a suitable voltage for optimization of sensitivity. A cylindrical nano MOSFET surrounded by the control gate [13] is azimuthally symmetric but a nanowire sensor with a side gate is not a symmetric device. Electrons travelling from source to the drain suffer from mobility degradation due to lateral electric field. The lateral electric field component in this case is induced by the side gate voltage [14, 15]. A cylindrical ISFET with a surrounding reference electrode leads to a symmetric distribution of electric field. Consequently the normal component of the electric field will have a cancelling effect in the middle of the silicon body as in the case of a double gate MOSFET [16]. For this reason, in case of optimization of detection sensitivity, it can be expected that use of a surrounding reference electrode will have much less mobility degradation effect than that of a side gate.

1.3 Thesis outline

The 2nd Chapter discusses the basics of ISFET and the fundamentals of oxide /electrolyte interface of the site binding model along with physico chemical modeling of the device. In this chapter a generalized model for the planer ISFET has been developed based on the site binding model for silicon dioxide used as insulating material. Silicon dioxide, when used as pH sensing surface possess only one type of surface site. Consequently, the model developed is much simple.

The simulation results in this case (presented at the end of the chapter) gives a clear insight of the device.

In the 3rd Chapter the novel ISFET structure i.e. the Cylindrical ISFET, has been introduced for developing a physico chemical model for the same. In this chapter we have considered separate layer of charges for inversion and depletion layers and they are included in the model. The potential drop across the depletion layer and oxide layer has been modeled as a function of pH. The diffuse layer surrounding the cylindrical device is influenced by cylindrical geometry. This influence is also analyzed and modeled. The device model is simulated in MATLAB for the analysis of its behaviour at various pH values. The result shows distinct potential variation from inversion layer to the depletion layer as a function of pH and deviation in the device sensitivity as a function of the position of reference electrode relative to the Outer Helmholz Plane (OHP).

In the 4th Chapter Scaling Issues related to downsizing of ISFET to nano dimension is discussed and accordingly the model developed in Chapter 3 has been modified to include the nano dimensional effects. The model includes threshold voltage shift due to quantum mechanical energy band shift, oxide capacitance reduction due to effective oxide thickness increase and sensitivity reduction due to decrease in number of sites per unit area Finally the model is simulated using a MATLAB program and a comparison is made with the ideal case. A comparison with a nanowire sensor is also presented towards the end of this chapter.

The 5th Chapter a novel rule for reference electrode placement has been framed. This rule can be helpful in determining the complete dimension of the pH measuring system using ISFET.

Finally Chapter 6 carries a summary of this dissertation and suggestion for future work is given.

1.4 References:

1. P.Bergveld, "Development of an ion-sensitive solid- state device for neuro physiological measurements", IEEE Trans. Biomed. Eng. BME-17, pp.70-71, 1970
2. T. Matsuo, K.D. Wise, "An integrated field effect electrode for biopotential recording", IEEE Trans. Biomed. Eng. BME-21, pp. 485- 487,1974
3. K.D. Wise, J.B. Angell, A. Starr, "An integrated circuit approach to extra cellular microelectrodes", IEEE Trans. Biomed. Eng. BME-17(3), pp.238-247, 1970.
4. P.Bergveld, "Thirty years of ISFETOLOGY what happened in the past 30 years and what may happen in the next 30 years", Sensors and Actuators B ,Vol-88, pp. 1-20, 2003.
5. Yi Cui and Charles M Lieber "Functional Nanoscale Electronic Devices Assembled Using Silicon Nanowire Building Blocks" Science, vol.291, pp.851-853, 2 February2001.
6. Alireza Kargar, Jennifer M Blain Christen "Theoritical Investigation of Silicon Nanowire pH Sensor" Proceedings of the 2nd Biennial IEEE/RAS-EMBS International Conference on Biomedical Robotics and Biomechatronics, Scottsdale, AZ, USA, October 19-22, 2008.

7. Alireza Kargar "Modeling of Silicon Nanowire pH Sensor with Nanoscale Side Gate Voltage" Chinese Physical Letter, Vol.26, No.6(2009)060701, June 2009, (4pp).
8. Fernando Patolsky and Charles M Lieber "Nanowire nanosensors" Materials Today, Volume 8, Issue 4, April 2005, Pages 20-28.
9. Websource http://www.eetimes.com/showArticle.jhtml?articleID=205208762
10. Stephen J. Pearton, Tanmay Lele, Yiider Tseng, F Ren "Penetrating living cells using semiconductor nanowires" TRENDS in Biotechnology, Vol. 25, No. 11, pp.481-482, 2007
11. Olga Korostynska, Khalil Arshak, Edric Gilland Arousian Arshak "Materials and Technique for *In Vivo* pH Monitoring" IEEE Sensor Journal, Vol.8, No.1, January 2008, pp.20-28.
12. T Edwin. Carlen, Albert van den Berg "Nanowire electrochemical sensors: can we live without labels?" Lab on a Chip, 7(1), pp.19–23, 2007.
13. Mark Lundstrom and Jing Guo, *Nanoscale MOSFETs: Device Physics Modeling and Simulation,* Springer, 2006.
14. John P. Uyemura, *CMOS Logic Circuit Design*, Kluer Academic Publishers, 2001.
15. Ben G Streetman and Sanjay Banerjee, *Solid State Electronic Devices, 5th Ed.* Prentice Hall of India,November, 2001.
16. S. Christoloveanu, "SOI MOSFET Scaling and Innovative Solutions", International Semiconductor Device Research Symposium Proceedings, 1999, pp.389-391.

Chapter 2

General overview of ISFETs and analysis of conventional ISFET

2.1 Introduction

Ion Sensitive Field Effect Transistor (ISFET) was first reported in 1970 by Prof. P. Bergveld [1] who described it as a tool for electrophysiological measurement of ionic and effluxes around a nerve. This work was described in details in 1972 [2], which is now cited by many authors as pioneering publication in the field of ISFET investigation. In this publication he demonstrated that if the metal gate of ordinary metal oxide field effect transistor (MOSFET) is omitted and the silicon dioxide layer is exposed to an electrolyte solution, the characteristic of the device is then affected by ionic activity of the electrolyte solution and hence the device functions as an ion sensitive transducer. At the same time Matsu and Wise developed a similar device [3] using silicon nitride as insulating layer. After these pioneering works, many other groups started to publish their research findings on ISFETs and related devices. Since 1970, led by Prof P.Bergveld, more than 700 publications appeared which were devoted to various aspects of ISFET development [4]. The latest investigations concern the application of extended gate polycrystalline silicon thin film transistors as ISFETs to the development of DNA hybridization sensors, the miniaturization of reference electrodes compatible with silicon chip technology and development of nanoscale ISFETs [5].

In this chapter the basic theoretical principles of ISFET, operation mechanism and simulation results based on site binding theory [6] is presented here.

2.2 Theory of ISFET

The Schematic representation of a MOSFET and an ISFET is given in fig 2.1. The characteristic of a MOS device is determined by its flat band voltage. This

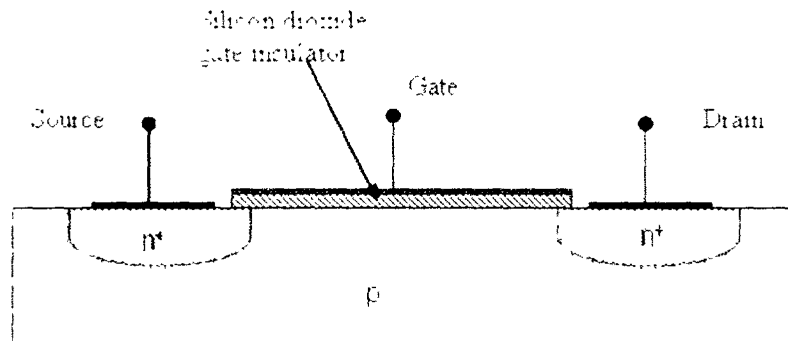

Fig. 2.1 (a): Basic MOSFET structure (n channel enhancement type).

can be defined as summation of the work function difference between the gate material and potential due to the trapped charge between the oxide and the semiconductor, mobile ionic charge and fixed charges. A change in the magnitude of these charges causes change in the threshold voltage of the MOS device [7]. In an ISFET the flat band voltage changes due to the chemical changes that occur at the oxide electrolyte interface.

In a MOSFET the various layers are positioned as follows [8]

BODY METAL	SEMICONDUCTOR SUBSTRATE	GATE INSULATOR	GATE METAL

The Threshold voltage of an n channel enhancement type MOSFET is given as follows [9]

$$V_{th(mos)} = V_{fb(mos)} + 2|\phi_f| + Q_{depletion}/C_{ox} \qquad \text{----------------2.1}$$

$$V_{fb} = \phi_m - \phi_s + (Q_f + Q_m + Q_{it})/C_{ox} \qquad \text{-----------------2.2}$$

$$\phi_f = \frac{KT}{q}\ln\left(\frac{N_a}{n_i}\right) \qquad \text{-----------------2.3}$$

$$Q_{depletion} = -\sqrt{4\varepsilon_{si} q N_a |\phi_f|} \qquad \text{----------------2.4}$$

$$C_{ox} = \varepsilon_{ox}/t_{ox} \qquad \text{----------------2.5}$$

$Q_{depletion}$ = Depletion charge per unit area (coulomb/metre^2)

Q_f = Fixed charge per unit area (within 3nm of Si-SiO_2 interface) (coulomb/metre^2)

Q_m = Mobile ionic charge per unit area (coulomb/metre^2)

Q_{it} = Oxide trapped charge per unit area (coulomb/metre^2)

The charges Q_f, Q_m, Q_{it} can be neglected considering ideal condition.

Now, if the metal gate of the MOS structure in the Fig. 2.1(a) is replaced by a reference electrode and an electrolyte solution, a structure as shown in fig.2.1 (b) is obtained. This structure is known as electrolyte insulator semiconductor (EIS) structure and it is analogous to MOS structure, a reference electrode closes the circuit [10].

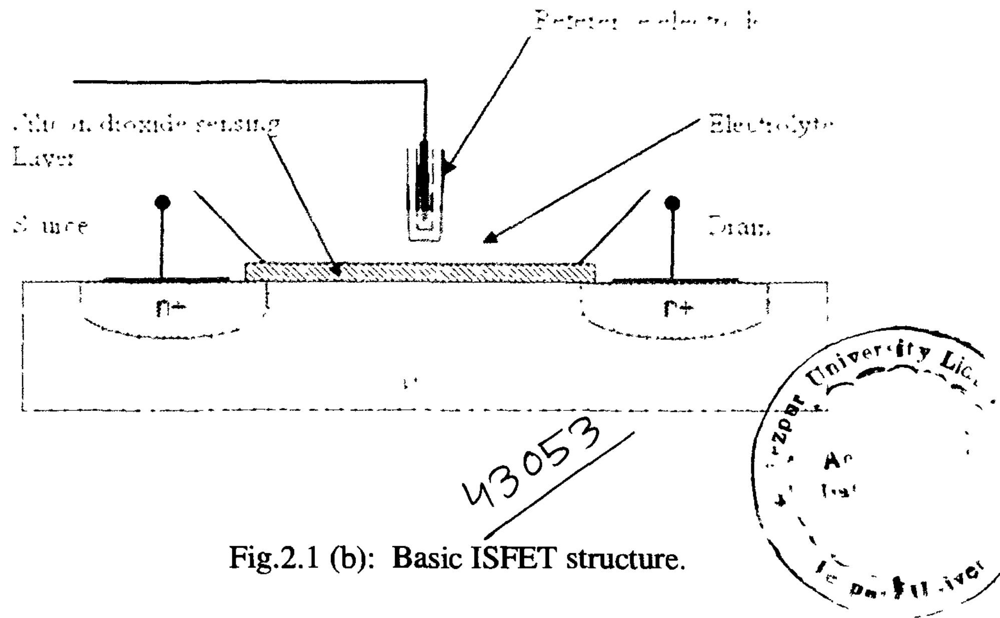

Fig.2.1 (b): Basic ISFET structure.

The threshold voltage for EIS structure is given as follows [7]

$$V_{th(isfet)} = (E_{ref} + \varphi_{lj}) - (\varphi_{eo} - \chi_e) - \phi_{Si} + \frac{Q_{depletion}}{C_{ox}} + 2|\phi_f| \text{ ----------2.6}$$

$$V_{fb} = (E_{ref} + \varphi_{lj}) - (\varphi_{eo} - \chi_e) - \phi_{Si} \qquad \text{--------------------2.7}$$

V_{fb} flat band voltage of the ISFET in volts.

E_{ref} reference electrode potential relative to vacuum in volts.

ϕ_{lj} is the liquid-junction potential difference between the reference solution and the electrolyte in volts;

ϕ_{eo} is the potential drop in the electrolyte at the insulator-electrolyte interface in volts;

χ_e is the surface dipole potential of the solution in volts;

ϕ_{si} is the work function of Si in volts;

C_{ox} the insulator capacitance per unit area (F/m^2)

In the expression of V_{fb} of MOSFET, the terms in parenthesis are replaced by the work function of the containing metal (ϕ_m). A change in work function of the gate causes change in threshold voltage. Similarly, the flat-band voltage and therefore the threshold voltage, changes with change in chemical quantity.

The threshold voltage equation for ISFET can be expressed in terms of MOSFET threshold as [7],

$$V_{th(isfet)} = V_{th(mosfet)} + E_{ref} + \phi_{lj} + \chi_e - \phi_{eo} - \phi_m \quad \text{------------------2.8}$$

ϕ_m - is the work function of the metal or polysilicon gate material relative to vacuum in volts

The drain current expression in the non saturated mode for MOSFET and ISFET is given respectively as follows [4]

$$I_{DS(mos)} = \mu C_{ox} \frac{W}{L}\left((V_{GS} - V_{th(mos)})V_{DS} - \frac{V_{DS}^2}{2} \right) \text{------------------------} 2.9$$

$$I_{DS(isfet)} = \mu C_{ox} \frac{W}{L}\left((V_{GS} - V_{th(isfet)})V_{DS} - \frac{V_{DS}^2}{2} \right) \text{---------------------} 2.10$$

2.3 Operation Principle of ISFET

2.3.1. Site Binding Model

The response of the ISFET to pH can be explained by using site-binding model as shown in fig 2.2. This model can give a more fundamental explanation of operation of ISFET.

The presence of an insulator in contact with the electrolyte solution introduces a new kind of charge distribution caused by the formation of surface groups that transforms the EIS structure into a pH sensor. The exchange of hydrogen ions between the electrolyte and the reactive sites at the insulator surface causes the change in potential at the electrolyte insulator interface. The ions present in the solution react with positively or negatively charged active sites present at the dielectric surface creating hydrogen active site pairs and consequently changing the total value of the active site charge at the insulator surface and thus forms the electrical double layer. The ion concentration in the electrolyte influences the gate potential, which in turn modifies the threshold voltage. The ISFETs are usually operated under the constant drain current mode, which means that the change of drain current due to the change of the ion concentration in the

electrolyte is compensated by the adjustment of the voltage applied to the reference electrode.

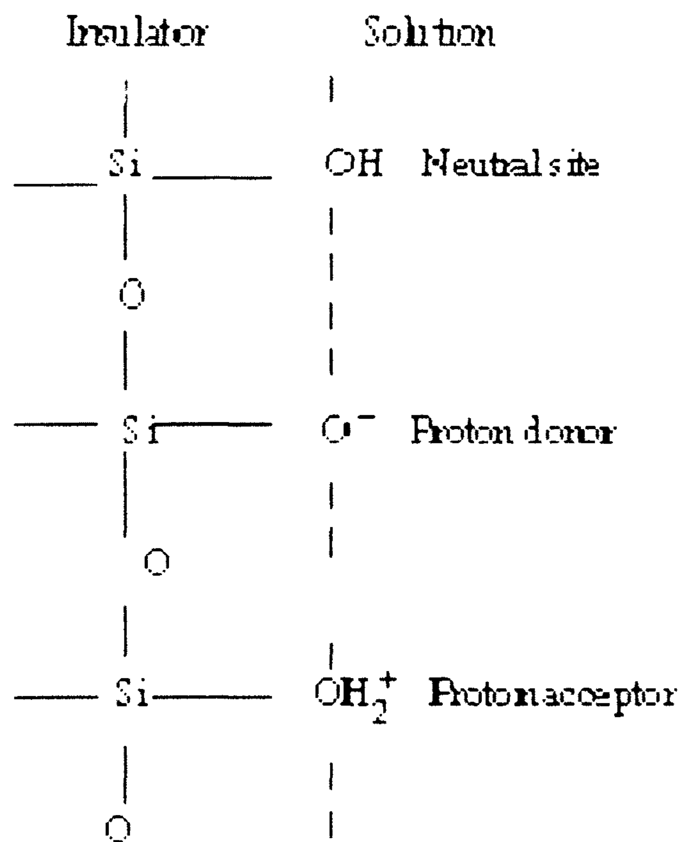

Fig. 2.2 Site Binding model

2.3.2. Electrical Double Layer Model

Electrical double layer model can be used to describe the ion distribution and potential variation near a solid liquid interface. Figure 2.3 depicts the nature of this interface.

- Some ions are held tightly right next to the surface. This layer of ions is known as the Inner Helmholtz Plane (IHP). The ions in this layer immobile. These ions are attracted by the solid surface and assumed to approach the electrode surface and form a layer which tries to balance the electrode charge. The distance of approach is assumed to be limited by the radius of the ion. These ions have lost their solvation shell. Consequently IHP can be defined as the distance from the electrode surface to the centre of an ion which has lost its solvation shell.

- Beyond the IHP the other ions are held relatively loosely. As we further away the ions are more loosely held. This starting plane of these loosely bound ions is known as the Outer Helmholtz Plane (OHP). The layer of charge beyond the OHP is known as diffuse layer.

2.4 Modeling

Let us consider SiO_2 as the insulator. Generally its surface contains site in three forms: $Si\text{-}O^-$, Si-OH and $Si\text{-}OH_2^+$ as shown in fig 2.2. The acidic and basic characters of neutral site Si-OH are characterized by the equilibrium constants K_a and K_b respectively and can be written as the following equation [7] [11]

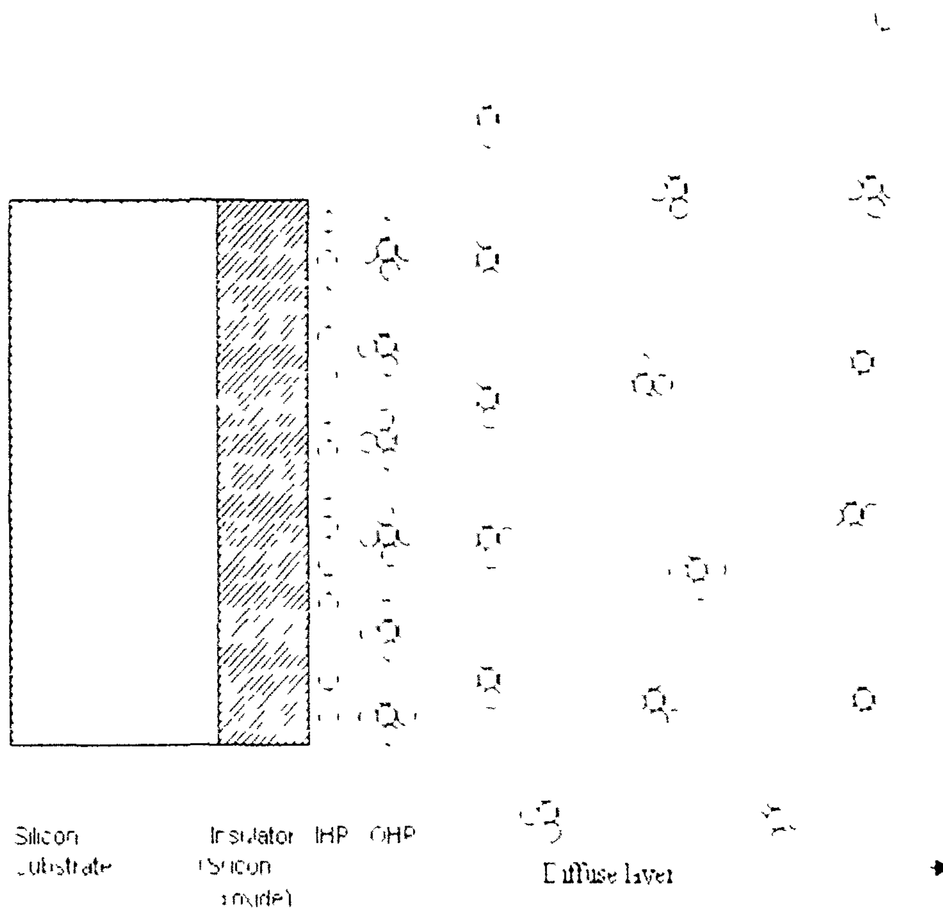

Fig. 2.3 Electrical Double layer at the interface model

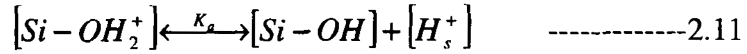

$$\left[Si-OH_2^+\right] \xleftrightarrow{K_a} \left[Si-OH\right] + \left[H_s^+\right] \qquad \text{-------------2.11}$$

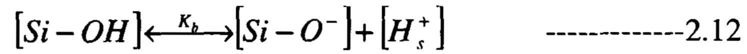

$$\left[Si-OH\right] \xleftrightarrow{K_b} \left[Si-O^-\right] + \left[H_s^+\right] \qquad \text{-------------2.12}$$

Now the dissociation constants can be defined as

$$K_a = \frac{[Si-OH][H^+]_s}{[Si-OH_2^+]} \qquad \text{------------2.13}$$

$$K_b = \frac{[SiO^-][H^+]_s}{[\ SiOH\ ]} \qquad \text{------------2.14}$$

In the equations 2.11 to 2.14 $Si\text{-}OH_2^+$, Si-OH and $Si\text{-}O^-$ represent positive, neutral and negative surface sites respectively and $[Si\text{-}OH_2^+]$, [Si-OH] and $[Si\text{-}O^-]$ are the numbers of these sites per surface area. The subscript 's' in $[H^+]_s$ signifies the concentration of proton near the surface of the insulator. The surface to bulk relationship i.e. $[H^+]_s$ and $[H^+]_{bulk}$ follows the Boltzmann distribution. Therefore

$$\left[H^+\right]_s = \left[H^+\right]_{bulk} \exp\left(\frac{-q\phi_{eo}}{kT}\right) \qquad \text{-------------2.15}$$

Where,

ϕ_{eo} Electrolyte insulator interface potential in volts.

q charge of an electron

T Absolute temperature

k Boltzman constant

This surface potential is generated by the net surface charge,

$$\sigma_o = q([Si-0H_2^+]-[Si-0^-]) \qquad \text{------------------2.16}$$

The total number of sites per unit area is given by

$$N_S = [Si-OH]+[Si-O^-]+[Si-OH_2^+] \qquad \text{------------------2.17}$$

From equations 2.11 to 2.17 the expression for surface charge density σ_0 becomes

$$\sigma_o = q \times N_s \frac{[H^+]_s^2 - K_a K_b}{[H^+]_s^2 + K_a[H^+]_s + K_a K_b} \qquad \text{------------2.18}$$

The relation among pH, σ_o and ϕ_{eo} can be established by using equations 2.11 to 2.17 as given in [12]

$$[H^+] = \left(\frac{K_a}{k_b}\right)^{1/2} \exp(y_0).\frac{\left[\frac{\alpha_0}{\delta}+1+\left(\frac{\alpha_0}{\delta}\right)^2(1-\delta^2)\right]^{1/2}}{1-\alpha_0} \qquad \text{---------------2.19}$$

Where

$$y_0 = \frac{q\phi_{eo}}{kT} \quad \text{--------------------2.20}$$

$$\alpha_0 = \frac{\sigma_0}{qN_S} \quad \text{--------------------2.21}$$

$$\delta = 2.(K_a K_b)^{1/2} \quad \text{--------------------2.22}$$

Now it can be seen that $\delta << 1$, and consequently putting $1-\delta^2 \approx 1$ in equation 2.18 we get

$$[H^+] = \left(\frac{K_a}{k_b}\right)^{1/2} \exp(y_0).\frac{\left[\frac{\alpha_0}{\delta}+1+\left(\frac{\alpha_0}{\delta}\right)^2\right]^{1/2}}{1-\alpha_0} \quad \text{--------------------2.23}$$

When the electrolyte oxide interface potential is zero, the surface becomes neutral and hence we get

$$y_0 = 0$$

$$\sigma_0 = 0$$

And consequently at this value of hydrogen ion concentration becomes

$$[H^+] = \left(\frac{K_a}{k_b}\right)^{1/2} \quad \text{--------------------2.24}$$

Taking logarithm on both the sides we get

$$\ln[H^+] = \ln\left(K_a / k_b\right)^{1/2} \qquad \text{--------------------2.25}$$

Where

$$-\ln\left(K_a / k_b\right)^{1/2} = -2.303\log\left(K_a / k_b\right)^{1/2} = 2.303 pH_{PZC} \qquad \text{---------------2.26}$$

pH_{pzc} is the value of pH at which the surface becomes neutral.

By taking logarithm of the equation 2.22 we get

$$\ln[H^+] = \ln\left(K_a / k_b\right)^{1/2} + y_0 + \ln\left[\frac{\alpha_0}{\delta} + 1 + \left(\frac{\alpha_0}{\delta}\right)^2\right]^{1/2} - \ln(1-\alpha_0)$$

$$\Rightarrow \ln[H^+] - \ln\left(K_a / k_b\right)^{1/2} = y_0 + \sinh^{-1}\left(\frac{\alpha_0}{\delta}\right) - \ln(1-\alpha_0)$$

$$\Rightarrow 2.303(pH_{PZC} - pH) = y_0 + \sinh^{-1}\left(\frac{\alpha_0}{\delta}\right) - \ln(1-\alpha_0) \qquad \text{......................2.27}$$

In the above equation the last term represents saturation of pH response when the surface charge σ_0 increases and consequently α_0 approaches one. For Silicon dioxide the last term of the equation 2.26 may be neglected

$$\Rightarrow 2.303(pH_{PZC} - pH) = y_0 + \sinh^{-1}\left(\frac{\alpha_0}{\delta}\right) \qquad \text{---------------2.28}$$

According to Gouy Chapman Stern Theory, the electrolyte oxide interface potential is exactly the summation of the potentials across the stern layer and the potential across the diffused layer i.e.

$$\phi_{eo} = -2(kT/q)\sinh^{-1}\left(\frac{\sigma_d}{(8\varepsilon_{diffuse}kTC_0)^{1/2}}\right) - \frac{\sigma_d}{C_d} \qquad \text{---------------2.29}$$

Where

$\varepsilon_{diffuse}$ permittivity of the diffuse layer

For small value of diffuse layer charge σ_d, the equation 2.21 can be approximated as

$$\phi_{eo} = \left(\frac{-2(kT/q).\sigma_d}{(8\varepsilon_{diffuse}kTC_0)^{1/2}}\right) - \frac{\sigma_d}{C_d} \qquad \text{---------------2.30}$$

$$\Rightarrow \phi_{eo} = -\frac{\sigma}{C_D} - \frac{\sigma_d}{C_d} \qquad \text{---------------2.31}$$

$$\Rightarrow \phi_{eo} = -\frac{\sigma_d}{C_d} \qquad \text{---------------2.32}$$

Where

$$\frac{1}{C_d} = \frac{1}{C_D} + \frac{1}{C_H} \qquad \text{---------------2.33}$$

Where the diffuse layer capacitance is expressed as

$$C_D = -\frac{d\sigma_{diffuse}}{d\phi_{eo}} \approx \left(\sqrt{8\varepsilon_{diffuse}\, kTC_0}\right)\left(\frac{zq}{2kT}\right) \qquad \text{-------------2.34}$$

In absence of applied voltage to the reference electrode, the diffuse layer charge is given by

$$\sigma_{diffuse} = -\left(\sqrt{8\varepsilon_{diffuse}\, kTn_0}\right)\sinh\left(\frac{zq\,\phi_{e0}}{2kT}\right) \approx -\left(\sqrt{8\varepsilon_{diffuse}\, kTn_0}\right)\left(\frac{zq\,\phi_{e0}}{2kT}\right)$$

-------2.35

And the Helmholz capacitance is

$$C_H = \frac{1}{\frac{1}{C_{IHP}} + \frac{1}{C_{OHP}}} \qquad \text{-----------------2.36}$$

Where C_{IHP} and C_{OHP} are the capacitance of the Inner Helmholz Plane (IHP) and Outer Helmholz Plane (OHP). The can be expressed as

$$C_{IHP} = \frac{\varepsilon_{IHP}}{t_{IHP}} \qquad \text{-----------------2.37}$$

$$C_{OHP} = \frac{\varepsilon_{OHP}}{t_{OHP}} \qquad \text{----------------2.38}$$

From the condition of charge neutrality it can be written as [13]. Fig 2.4 and fig. 2.5 shows the charge density and potential profile of an EIS system.

$$\sigma_{diffuse} + \sigma_{IHP} + \sigma_{insulator} + Q_{semiconductor} = 0 \qquad \text{---------------2.39}$$

Where

$$Q_{inversion} + Q_{depletion} = Q_{semiconductor} \qquad \text{---------------2.40}$$

$$\sigma_{IHP} + \sigma_{insulator} = \sigma_0 \qquad \text{--------------2.41}$$

Using 2.40 and 2.41 we may write equation 2.39 as follows

$$\sigma_{diffuse} + \sigma_0 + Q_{inversion} + Q_{depletion} = 0 \qquad \text{-------------2.42}$$

In absence of reference electrode applied voltage (V_{ref}), inversion charge is zero and the depletion charge $(Q_{depletion})$ is also negligibly small. Consequently we may write

$$\sigma_{diffuse} + \sigma_0 \approx 0 \quad \text{Or} \quad \sigma_{diffuse} \approx -\sigma_0 \qquad \text{--------------2.43}$$

Consequently, with introduction of the equation 2.43 in the equation 2.29, we get

$$2.303(pH_{PZC} - pH) = y_0 + \sinh^{-1}\left(\frac{-\sigma_{diffuse}/qN_S}{2(K_a K_b)^{1/2}} \right) \qquad \text{--------------- 2.44}$$

$$\Rightarrow 2.303(pH_{PZC} - pH) = y_0 + \sinh^{-1}\left(\frac{\frac{C_d \phi_{eo}}{qN_S}}{2(K_a K_b)^{1/2}}\right) \quad \text{----------------2.45}$$

$$\Rightarrow 2.303(pH_{PZC} - pH) = y_0 + \sinh^{-1}\left(\frac{y_0}{\frac{q^2 N_S 2(K_a K_b)^{1/2}}{kTC_d}}\right) \quad \text{---------------- 2.46}$$

$$\Rightarrow 2.303(pH_{PZC} - pH) = y_0 + \sinh^{-1}\left(\frac{y_0}{\beta}\right) \quad \text{--- ------------ 2.47}$$

Where

$$\beta = \frac{q^2 N_S 2(K_a K_b)^{1/2}}{kTC_d} \quad \text{---------------2.48}$$

β is known as Dimensionless Sensitivity Parameter.

The asymptotic behaviors of equation 2.47 are as follows.

$$\varphi_{eo} = 2.303\frac{kT}{q}(pH_{PZC} - pH)\frac{\beta}{1+\beta}, \quad \text{For} \quad y_0 << \beta \quad \text{------------2.49}$$

And

$$2.303(pH_{PZC} - pH) = y_0 + \ln\left(\frac{2y_0}{\beta}\right) \approx \ln\left(\frac{2y_0}{\beta}\right) \text{ For } y_0 >> \beta \quad \text{------- } 2.50$$

In our analysis we have used the first expression for pH, because in the present analysis the value of $y_0 << \beta$.

2.5 Amperometric Sensitivity:

Let us define the term amperometric sensitivity as $\frac{dI_{DS}}{dpH}$. It is the variation of drain current in response to change in pH. This can mathematically be expressed as follows [appendix A1]

$$\frac{dI_{DS}}{dpH} = \mu C_{ox} V_{DS} \frac{W}{L} \cdot \frac{d}{dpH}(\phi_{eo}) \quad \text{-------------}2.51$$

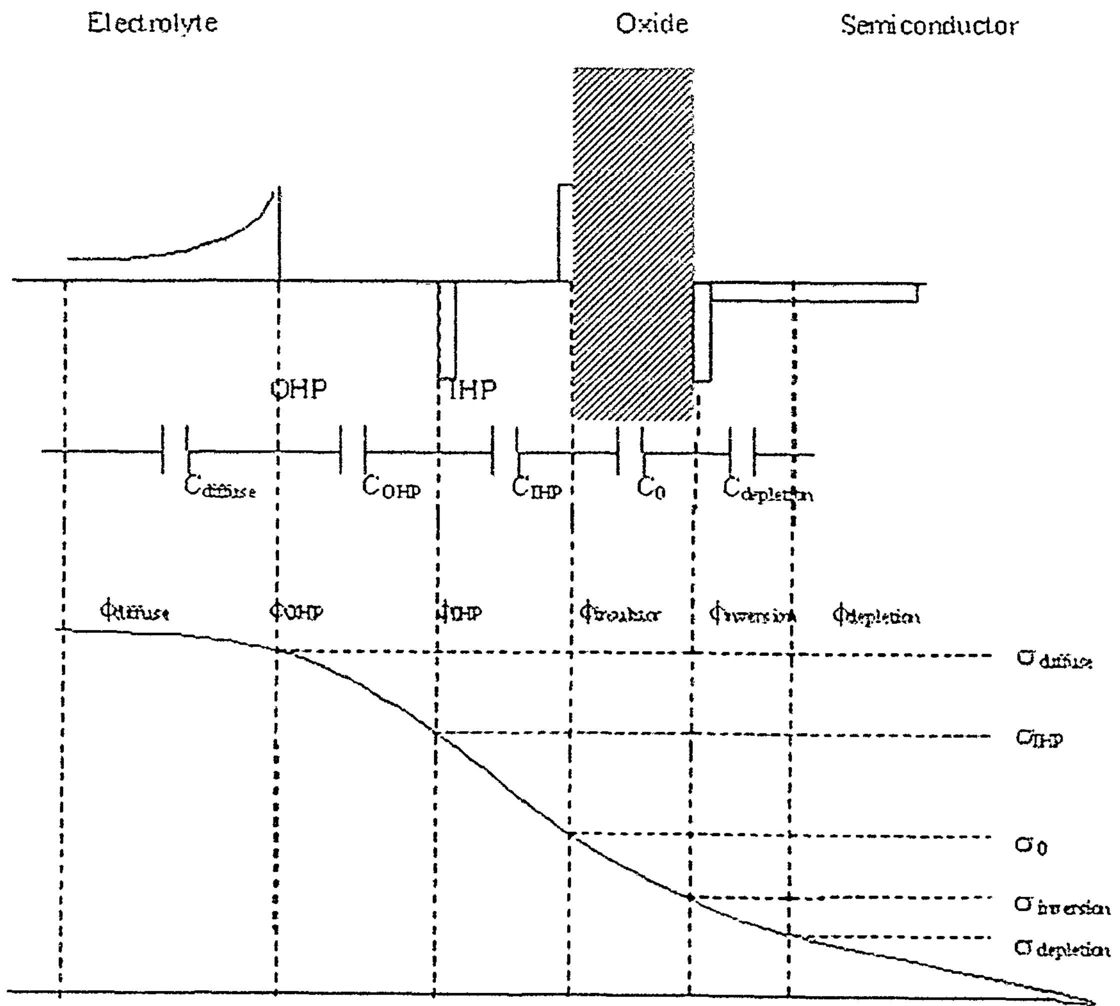

Fig 2.4: Charge distribution and potential profiles of an EIS system based on the Site Binding Model explains the reaction at the surface of insulator. This kind of charge distribution occurs for pH> pH_{pzc} .

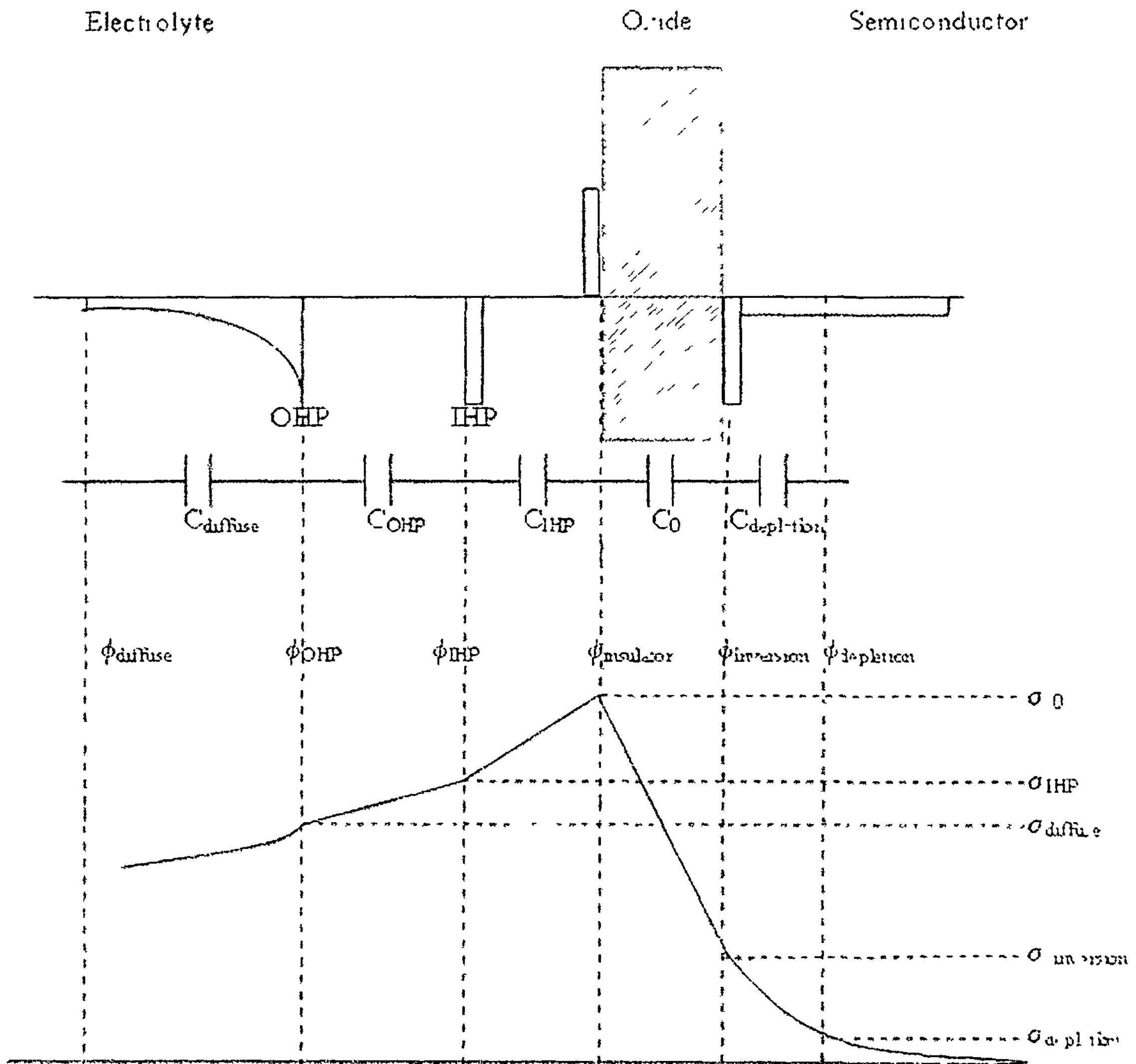

Fig 2.5: Charge distribution and potential profiles of an EIS system based on the Site Binding Model explains the reaction at the surface of insulator. This kind of charge distribution occurs for pH< pH_{pzc} .

2.6 Simulation results and conclusions :

Figure 2.6 shows variation of electrolyte oxide interface potential with pH. In this figure it can be observed that the electrolyte oxide interface potential varies linearly with pH except at very low value of pH. At low value of pH, the value of β decreases and due to this the electrolyte oxide interface potential decreases in magnitude. As the value of pH decreases i.e. the ionic concentration increases, the value of double layer capacitance increase and this results in lower value of β.

Figure 2.7 shows the relationship between drain current and voltage applied to the reference electrode at different value of pH. This gives an indication of variation of the drain current with pH, when the drain to source voltage is kept constant. As the pH changes the electrolyte oxide interface potential also change and due to this the threshold voltage of the ISFET changes. This variation of threshold voltage causes the change in drain current which is observed in this figure.

Figure 2.8 shows the relationship between drain current and drain to source voltage, at different value of pH. This gives an indication of variation of the drain current with pH, when the voltage applied to the reference electrode is kept constant.

Figure 2.9 shows the newly defined parameter Amperometric sensitivity of ISFET as a function of pH. At very low value of pH, the amperometric sensitivity is positive. When the value of pH increases, this value decreases to zero and attains negative value and remains fixed thereafter. From this figure it is clear that the current increases slightly and then decreases nonlinearly, as the of

pH increases from 1 to just over 2. After that, the current starts decreasing linearly with increasing pH

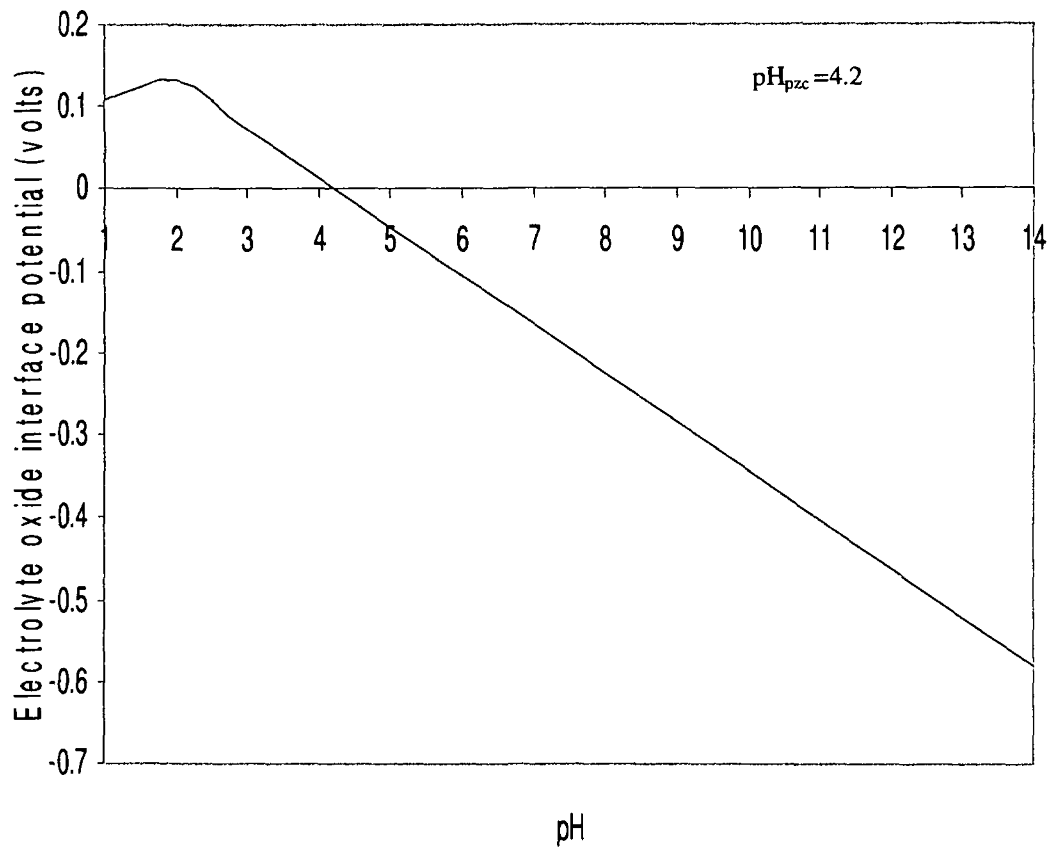

Fig. 2.6 Electrolyte oxide interface potential vs. pH for Silicon dioxide

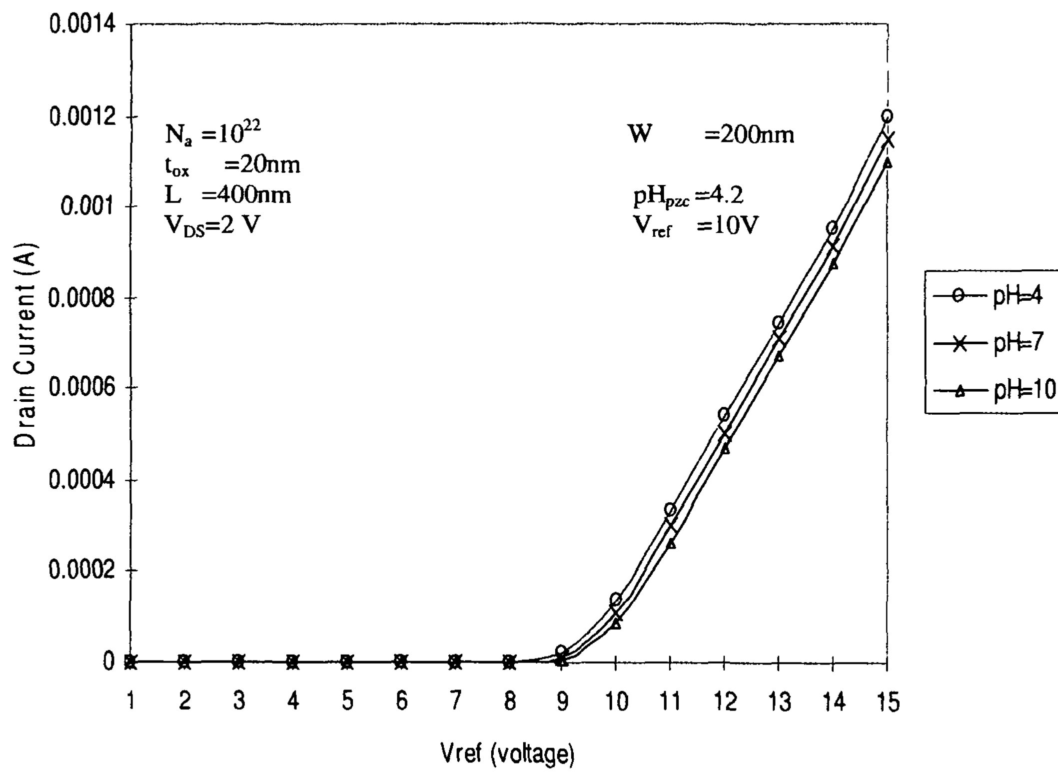

Fig. 2.7: Drain Current vs. V_{ref} at different values of pH .

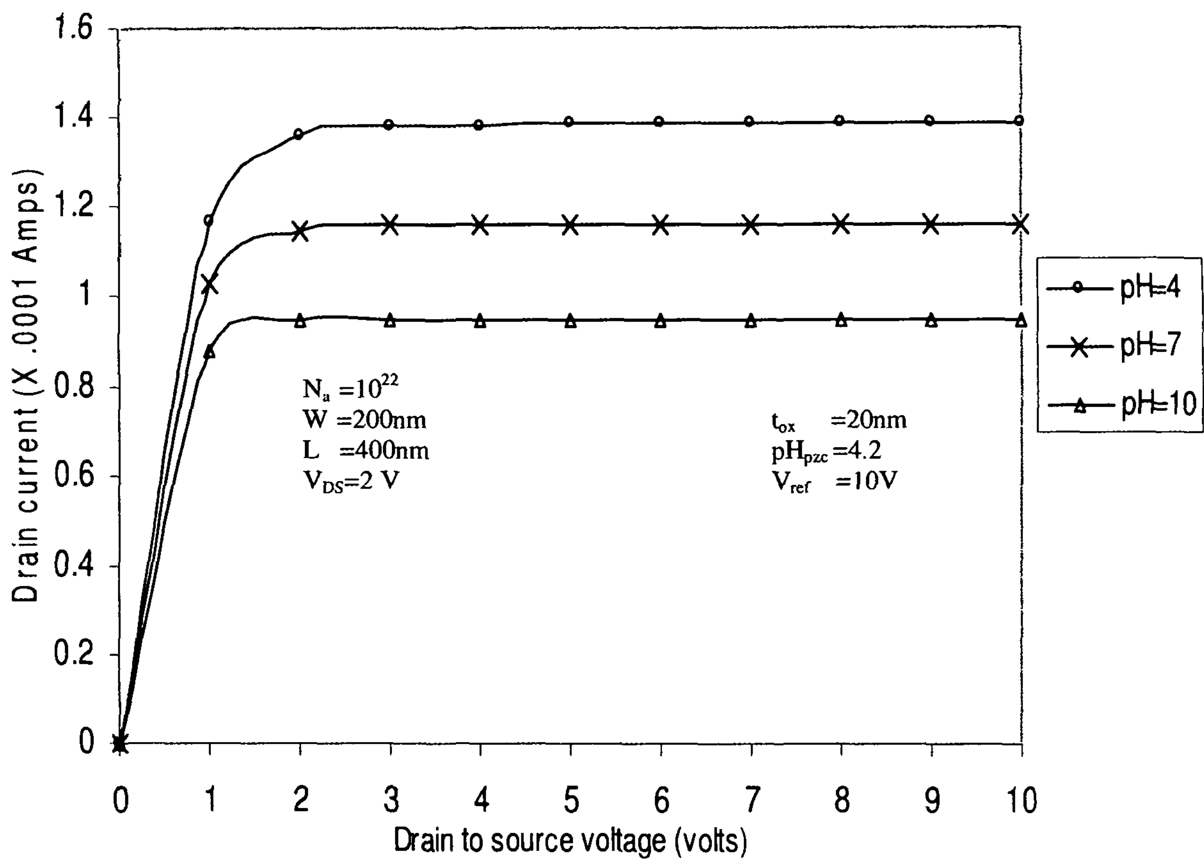

Fig. 2.8 Drain Current vs. Drain to source voltage at different values of pH

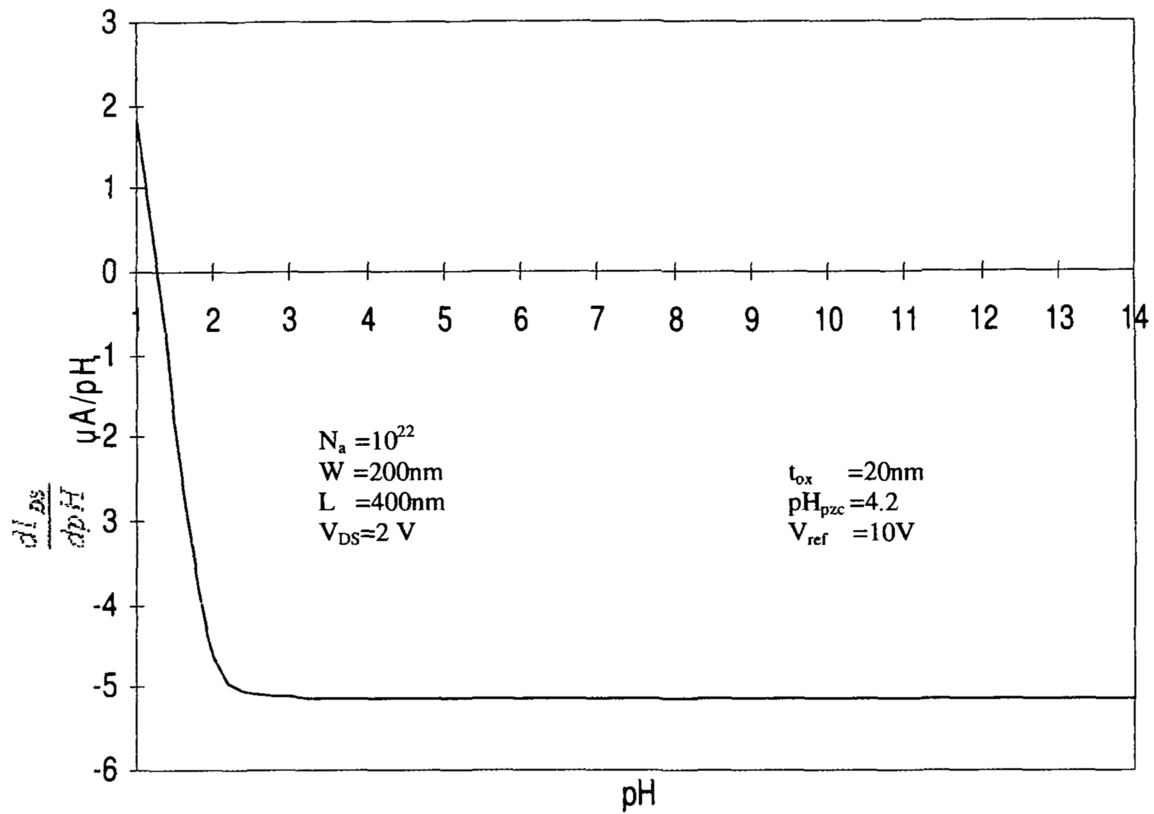

Fig 2.9 Amperometric sensitivity vs. pH

2.7 References

1. P. Bergveld, "Development of an Ion-Sensitive Solid-State Device for Neurophysiological Measurements" IEEE Transactions on Biomedical Engineering, Vol.17, No-1,pp.70-71, 1970
2. P. Bergveld "Development, Operation, and Application of the Ion-Sensitive Field-Effect Transistor as a Tool for Electrophysiology" IEEE Transactions on Biomedical Engineering, Vol.-19, No-5,pp.342-351, 1972
3. Tadayuki Matsuo, Kensall D Wise, "An Integrated Field-Effect Electrode for Biopotential Recording" IEEE Transactions on Biomedical Engineering, Vol.-21, No. 6, pp.238-247,1974
4. P.Bergveld , "Thirty years of ISFETOLOGY - What happened in the past 30 years and what may happen in the next 30 years", Sensor and Actuators B 88, pp. 1-20, 2003
5. Massimo Grattarola, Giusseppe Massobrio, Sergio Martinoia "Modeling H^+- Sensitive FET's with SPICE" IEEE Transaction on Electron Devices , vol 39, No 4, pp.813-819,1992.
6. David E Yates, Samuel Levine, Thomas W Healy " Site binding Model of the Electrical Double Layer at the Oxide/ Water Interface" Journal of Chemical Society, Faraday Transaction I70,pp1807-1818,1974
7. M. Grattarola , M. Giuseppe, *Bioelectronics Handbook*, McGraw Hill, 1998.
8. M Waleed Shinwari, M Jamal Deen, Dolf Landheer "Study of electrolyte insulator semiconductor field effect transistor(EISFET) with applications in biosensors design" Microelectronics Reliability, Vol. 47, No- 12, pp 2025-2057, 2007

9. S.M.Sze, *Semiconductor Devices Physics and Technology,* John Wiley and Sons (Asia) Pte. Ltd, 2002
10. P.Bergveld , "ISFET Theory and Practice", IEEE Sensor Conference, October,pp.1-26, 2003
11. Clifford D Fung, Peter W Chung, Wen H Ko, "A Generalized Theory of an Electrolyte – Insulator –Semiconductor Field Effect Transistor" IEEE Transaction on Electron Devices, Vol. ED-33, No 1,pp.8-18, 1986.
12. Luc Bousse, Nico F De Rooji, P. Bergveld "Operation of Chemically Sensitive Field Effect Sensors As a Function of the Insulator Electrolyte Interface" IEEE Transaction on Electron Devices , Vol. ED-30, No 10, pp.1263-1270, 1983.
13. William M. Siu, Richard S. C. Cobbold "Basic Properties of the Electrolyte –SiO_2- Si System: Physical and Theoretical Aspects" IEEE Transactions on Electron Devices, Vol. ED-26. No. 11, pp.1805-1815, 1979

Chapter 3

Novel Device Geometry – The Cylindrical ISFET

3.1 Introduction

In the last few years, surrounding gate cylindrical MOSFET has attracted an increased research interest because it possesses better electrostatic gate control [1]. The cylindrical structure MOSFET can be scaled down to sub few nm, indicating its suitability for use in bioelectronic devices oriented for biomedical and bioanalytical practices in vivo. Cylindrical MOSFET can be rendered H^+ sensitive by eliminating its surrounding gate electrode by a series combination of a surrounding reference electrode and an electrolyte solution. In this chapter we propose a physico chemical model of threshold voltage, electrolyte potential profile model and drain current of the Cylindrical ISFET based on the solution of Poisons equation and Poisson Boltzmann equation in cylindrical coordinate. As far as semiconductor side is concerned, it is validated by comparing it with the model given in reference [2], while the electrolyte modeling is validated by comparing the result given in reference [3]. Good agreement is found with the models already available. The surface phenomenon of the device is based on the site binding theory [4] and the implementation of the corresponding model is done in cylindrical coordinate using basic formulae viz. the diffuse layer capacitance and normalized potential are developed for cylindrical geometry.

3.2 Threshold Voltage model of the Cylindrical ISFET

Structurally, cylindrical ISFET is obtained by replacing the surrounding metal gate of cylindrical MOSFET by the series combination of a surrounding reference electrode, electrolyte solution and a chemically sensitive insulator. Cylindrical MOSFET is basically a Gate All Around MOSFET with a cylindrical geometry. The schematic description of cylindrical ISFET structure is shown in fig 3.1

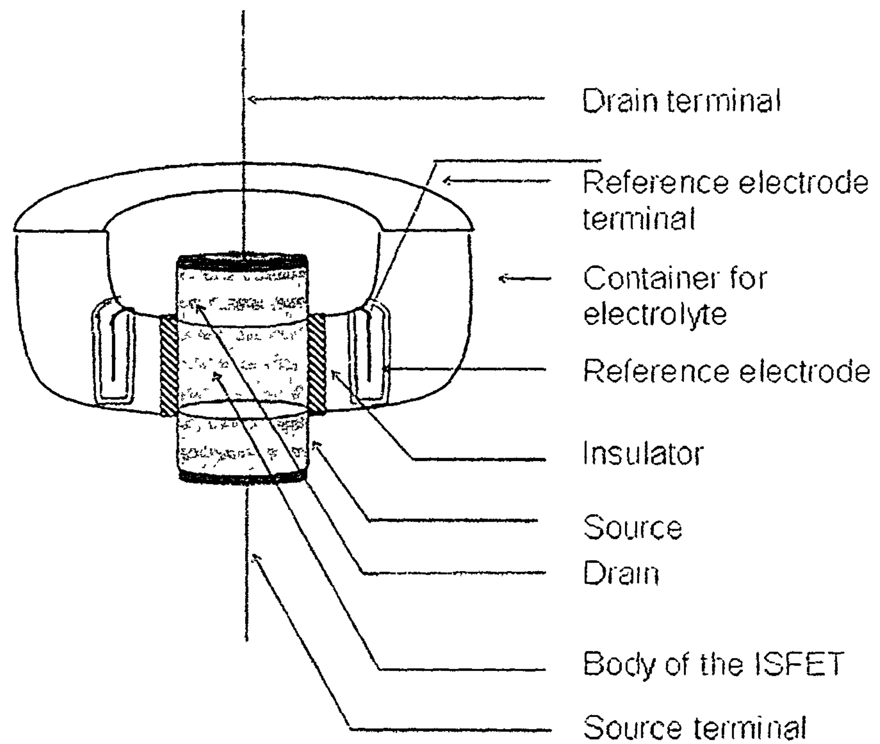

Fig.3.1 Structure of the Cylindrical ISFET

The one dimensional Poisson's equation for a MOS structure in cylindrical coordinate is given by

$$\frac{1}{r}\frac{\partial}{\partial r}\left(r\frac{\partial}{\partial r}\phi(r)\right)=-\frac{\rho}{\varepsilon_{Si}} \qquad \text{-------3.1}$$

Where

$$\rho = q\left(N_d^+ - N_a^- + p - n\right) \qquad \text{-------3.2}$$

$\phi(r,)$	potential distribution in the cylindrical silicon pillar,
N_a	Acceptor doping concentration (per metre^3)
N_d	Donor doping concentration (per metre^3)
q	Charge of an electron ($1.6\text{x}10^{-19}$ coulomb)
r	radial direction of the cylindrical coordinate (metre)
ε_{si}	is the dielectric permittivity of silicon.
	($\varepsilon_{si} = \varepsilon_0\varepsilon_r = 103.59\text{x}10^{-12}$ F/m)

For a p-type semiconductor $N_d = 0$ and equation 3.2 becomes

$$\rho = q\left(-N_a^- + p - n\right) \qquad \text{-------3.3}$$

For a moderately doped semiconductor $p >> n$, and therefore the equation 3.3 reduces to

$$\rho = q\left(-N_a^- + p\right)$$

$$\Rightarrow \rho = q\left\{- N_a^- + p_o \exp\left(-{}^{q\phi}\!/_{KT}\right)\right\}$$

$$\Rightarrow \rho = q\left\{- N_a^- + N_a^- \exp\left(-{}^{q\phi}\!/_{KT}\right)\right\}$$

$$\Rightarrow \rho = qN_a^-\left\{\exp\left(-{}^{q\phi}\!/_{KT}\right) - 1\right\} \qquad \text{--------3.4}$$

Putting this expression of charge density into the equation 3.1 we get

$$\frac{1}{r}\frac{\partial}{\partial r}\left(r\frac{\partial}{\partial r}\phi(r)\right) = -\frac{qN_a^-\left\{\exp\left(-{}^{q\phi}\!/_{KT}\right) - 1\right\}}{\varepsilon_{Si}} \qquad \text{-----------3.5}$$

Expanding the exponential term and neglecting the higher order terms we get

$$\frac{1}{r}\frac{\partial}{\partial r}\left(r\frac{\partial}{\partial r}\phi\right) = \left(\frac{q^2 N_a^-}{\varepsilon_{Si} KT}\right).\phi \qquad \text{-------3.6}$$

The equation 3.6 can finally be reduced to

$$r^2\frac{d^2\phi}{dr^2} + r\frac{d\phi}{dr} - \left(\frac{q^2 N_a^-}{\varepsilon_{Si} KT}\right).r^2\phi = 0$$

$$\Rightarrow r^2\frac{d^2\phi}{dr^2} + r\frac{d\phi}{dr} - A.r^2\phi = 0 \qquad \text{-------3.7}$$

Where $A = \left(\frac{q^2 N_a^-}{\varepsilon_{Si} KT} \right) = L_D^{-2}$.

L_D. is the extrinsic Debye length of the bulk semiconductor.

The equation 3.7 is Hyperbolic Bessel's Differential Equation and the solution of this equation is given as [5]

$$\phi(r) = B.I_0\left(\sqrt{A}\, r\right) \quad \text{-------3.8}$$

Where $I_0\left(\sqrt{A}\, r\right)$ is the Bessel's function of first kind of order zero which is given as follows [6]

$$I_0\left(\sqrt{A}\, r\right) = \sum_{k=0}^{\infty} \frac{\left\{ \frac{1}{4} \left(\sqrt{A}.r\right)^2 \right\}^k}{(k!)^2}. \quad \text{-------3.9}$$

'B' is a constant. Its value can be found by using the boundary condition.

$$\phi\big|_{r=t_{Si}/2} = \phi_s \quad \text{-------3.10}$$

And at threshold condition

$$\phi_s = 2\left|\phi_f\right| = 2\left|\frac{KT}{q}\right| \ln\left(\frac{N_a}{n_i}\right) \quad \text{-------3.11}$$

Therefore at the onset of inversion the equation 3.8 becomes

$$2|\phi_f| = B.\sum_{k=0}^{\infty}\frac{\left\{\frac{1}{4}\left(\sqrt{A}.r\right)^2\right\}^k}{(k!)^2} \qquad \text{-------3.12}$$

$$\Rightarrow B = \frac{2|\phi_f|}{\sum_{k=0}^{\infty}\frac{\left\{\frac{1}{4}\left(\sqrt{A}.r\right)^2\right\}^k}{(k!)^2}}.$$

$$\Rightarrow B = \frac{2\left|\frac{KT}{q}\right|\ln\left(\frac{N_a}{n_i}\right)}{\sum_{k=0}^{\infty}\frac{\left\{\frac{1}{4}\left(\sqrt{A}.r\right)^2\right\}^k}{(k!)^2}}. \qquad \text{-------3.13}$$

Now the bulk charge or depletion charge term for a cylindrical ISFET can be expressed as $Q_{depletio_cyln}$ at threshold condition is given by

$$Q_{depletion_cyl} = -\varepsilon_{SiO_2}E_S \qquad \text{-------3.14}$$

Where E_S is the electric field at the semiconductor surface at threshold condition.

$$E = -\frac{d\phi}{dr} = -B\sum_{k=0}^{\alpha}\frac{\left(\frac{1}{4}\right)^{k} A^{k}.2k.r^{2k-1}}{(k!)^{2}}$$ -------3.15

$$E_S = E\big|_{\phi=2|\phi_{ff}|,\, r=t_{si}/2} = -B.\sum_{k=0}^{\alpha}\frac{\left(\frac{1}{4}\right)^{k} A^{k}.2k\left(t_{si}/2\right)^{2k-1}}{(k!)^{2}}$$ -------3.16

The threshold voltage of a planar MOSFET is given as [7]

$$V_{th(mosfet)} = V_{fb(mosfet)} + 2|\phi_f| + \frac{|Q_{depletion}|}{C_{OX}}$$ ----3.17

And consequently, the same for a cylindrical device can be written as

$$V_{th_cyl(mosfet)} = V_{fb(mos)} + 2|\phi_f| + \frac{|Q_{depletion_cyl}|}{C_{ox_cyl}}$$ ----3.18

ϕ_f : Fermi potential of the doped silicon pillar (in volts)

$V_{fb(mos)}$: Flat band voltage (in volts) of the MOS structure and is given by equation 2.2

C_{ox_cyl} : Oxide capacitance per unit area for the cylindrical device (F/m^2)

$Q_{depletion_cyl}$: Depletion charge per unit area for a cylindrical ISFET (F/m^2)

$$C_{ox_cyl} = \frac{2\varepsilon_{ox}}{t_{si}\left(\ln(1+\frac{2t_{ox}}{t_{si}})\right)} \quad \text{-------3.19}$$

ε_{SiO_2} : Dielectric constant of the oxide

t_{Si} : Diameter of the silicon pillar

Now using the reference [9], [10] and combining it with equation 3.18 the threshold voltage for the cylindrical ISFET can be written as

$$V_{th_cyl(isfet)} = V_{fb(mos)} + 2|\phi_f| + \frac{|Q_{depletion_cyl}|}{C_{ox}} + E_{ref} + \phi_{lj} + \chi_e - \phi_{eo} - \phi_m \quad \text{------3.20}$$

$$V_{th_cyl(isfet)} = V_{fb(isfet)} + 2|\phi_f| + \frac{|Q_{depletion_cyl}|}{C_{ox}} \quad \text{-------3.21}$$

Where

$$V_{fb(isfet)} = V_{fb(mos)} + E_{ref} + \phi_{lj} + \chi_e - \phi_{eo} - \phi_m \quad \text{------- 3.22}$$

E_{ref} : Reference electrode potential (in volts)

ϕ_{lj} : Liquid junction potential (in volts)

χ_e : Liquid dipole potential (in volts)

ϕ_{eo} : Electrolyte oxide interface potential (in volts)

The electrolyte oxide potential ϕ_{eo} is given by [11], [12]

$$\phi_{eo} = 2.303\frac{KT}{q}(pH_{PZC} - pH)\left(\frac{\beta}{1+\beta}\right) \qquad \text{-------3.23}$$

Where

pH_{PZC} : The value pH of the electrolyte at which the surface becomes neutral

β : Dimensionless sensitivity factor [13] given by

$$\beta = \frac{2q^2 N_S (k_a k_b)^{1/2}}{kTC_d} \qquad \text{-------3.24}$$

The two equilibrium constants are given by

$$k_a = \frac{[Si-O^-][H^+]_S}{[Si-OH]} \qquad \text{-------3.25}$$

$$k_b = \frac{[Si-OH_2^+]}{[Si-OH][H^+]_S} \qquad \text{-------3.26}$$

N_S = Number of binding sites per unit area

The equivalent double layer capacitance per unit area C_d is given by [14]

$$\frac{1}{C_d} = \frac{1}{C_D} + \frac{1}{C_H} \qquad \text{-------3.27}$$

Where, C_H is the Helmholz capacitance per unit area. The Helmholz capacitance is the series combination of two capacitances – Inner Helmholz Plane (IHP) capacitance per unit area and Outer Helmholz Plane (OHP) capacitance per unit area [14].

$$C_H = \frac{1}{\frac{1}{C_{IHP}} + \frac{1}{C_{OHP}}} \qquad \text{-------3.28}$$

For planer device C_{IHP} and C_{OHP} are given as

$$C_{IHP} = \frac{\varepsilon_{IHP}}{t_{IHP}} \qquad \text{-------3.29}$$

$$C_{OHP} = \frac{\varepsilon_{OHP}}{t_{OHP}} \qquad \text{-------3.30}$$

For a cylindrical device, it may be shown that IHP capacitance per unit area and OHP capacitance per unit area are given as (Appendix-2)

$$C_{IHP_cyl} = \frac{2\varepsilon_{IHP}}{(t_{si} + 2t_{OX})\left(\ln(1 + \frac{2t_{IHP}}{t_{si} + 2t_{OX}}) \right)}$$ -------3.31

$$C_{OHP_cyl} = \frac{2\varepsilon_{OHP}}{(t_{si} + 2t_{OX} + 2t_{IHP})\left(\ln\left(1 + \frac{2t_{OHP}}{t_{si} + 2t_{OX} + 2t_{IHP}} \right) \right)}$$ -------3.32

The general expression for diffuse layer capacitance per unit area C_D is

$$C_D = \frac{d\sigma_{dl}}{d\phi_{eo}}$$ -------3.33

σ_{dl} Is the charge in the diffuse layer [15]

$$\sigma_{dl} = -\left(\sqrt{8\varepsilon_0 \varepsilon_r kTn_0}\right)\sinh\left(\frac{ze\,\phi_{e0}}{2kT}\right)$$ -------3.34

Where $n_0 = c_0 \times 1000 \times N_{AV}$ -------3.35

N_{AV} : Avogadro's number(6.023×10^{23} per mol)

c_0 : molar concentration (mol/L)

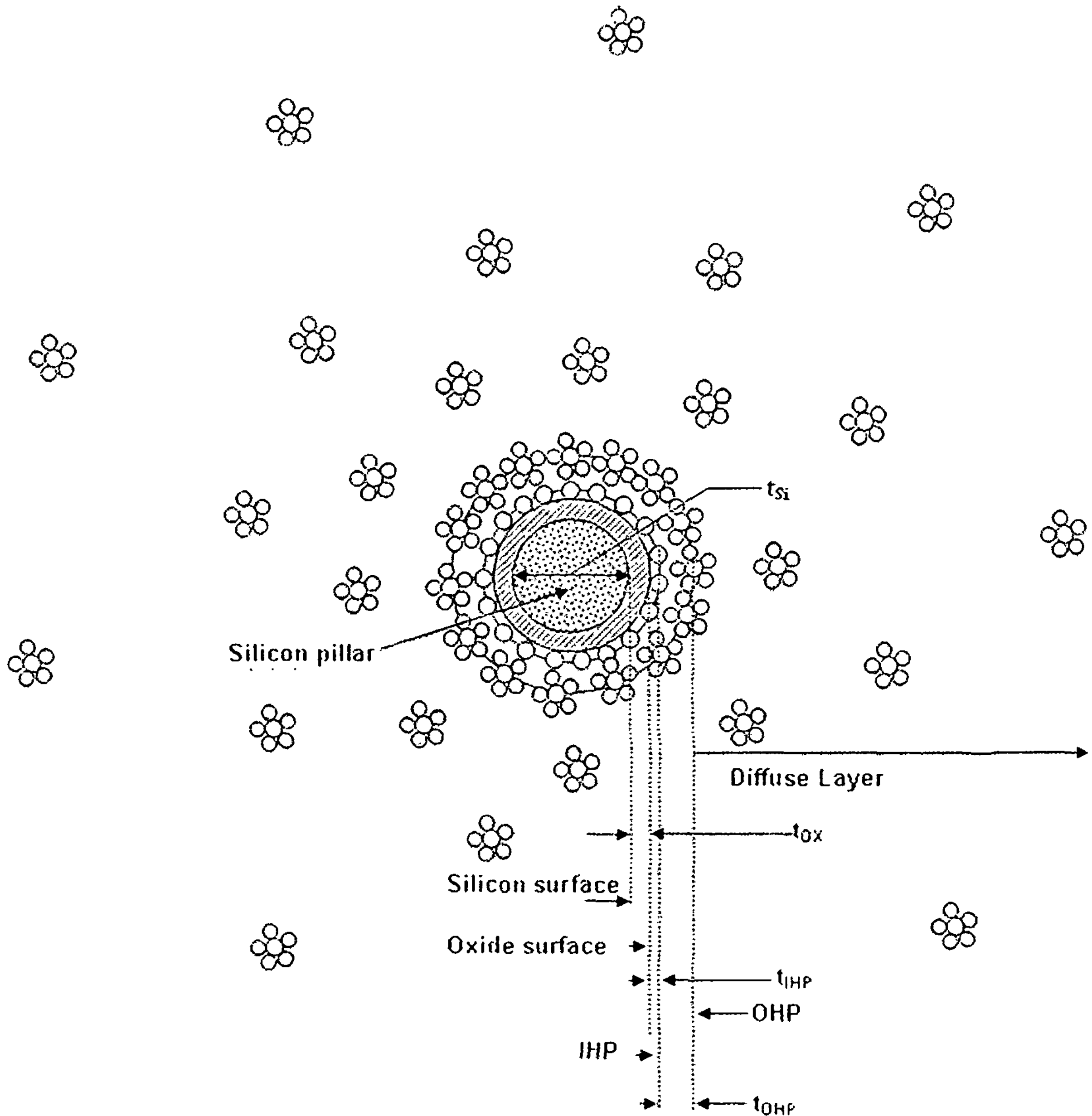

Fig.3.2: Cross sectional view of a cylindrical ISFET surrounded by electrolyte.

3.3 Drain Current Model of the ISFET

In a planer MOSFET the drain current is given by [16]

$$I_{DN} = \mu C_{OX} \frac{W}{L}\left((V_{GS} - V_{TH})V_{DS} - \frac{V_{DS}^2}{2}\right)$$

$$V_{GS} - V_{TH} > V_{DS}$$ Active region------- 3.36

$$I_{DN} = \mu C_{OX} \frac{W}{L}\frac{(V_{GS} - V_{TH})^2}{2}$$

$$V_{GS} - V_{TH} < V_{DS}$$ Saturation region-------3.37

Where 'W' is the channel width for a planner device. In case of a cylindrical MOSFET 'W' is the effective width of the current path given by the following equation (Appendix-3)

$$W = \frac{\pi\left[t_{Si}^2 - (t_{Si} - t_{inv})^2\right]}{4t_{inv}}$$ -------3.38

Where t_{inv}= thickness of the inversion layer. So the equation 3.36 and 3.37 the drain current equations for a cylindrical ISFET can be expressed as

$$I_{DN} = \mu C_{ox_cyl} \frac{\pi\left[t_{Si}^2 - (t_{Si} - t_{inv})^2\right]}{4Lt_{inv}}\left((V_{GS} - V_{th_cyl(isfet)})V_{DS} - \frac{V_{DS}^2}{2}\right)$$

$$V_{GS} - V_{th_cyl(isfet)} > V_{DS}$$ Active region -------3.39

$$I_{DN} = \mu C_{ox_cyl} \frac{\pi\left[t_{Si}^2 - (t_{Si} - t_{inv})^2\right]}{4Lt_{inv}} \times \frac{\left(V_{GS} - V_{th_cyl(isfet)}\right)^2}{2}$$

$V_{GS} - V'_{th_cyl(isfet)} < V_{DS}$ Saturation region -------3.40

3.4 Potential profile modeling

Potential profile modeling of ISFET includes potential profile of the electrolyte and that of the semiconductor side.

3.4.1 Electrolyte Potential Profile

i) Stern Layer potential profile

In the stern layer there exist two charge layers viz. IHP and OHP. In between these charge layers there exist no charges and hence the Gauss law reduces to Laplace equation and consequently its solution yields a linear potential variation from the insulator surface to IHP and from IHP to OHP as given below.

$$\phi_{insulator} - \phi_{IHP} = -\frac{\sigma_0 + Q_{inversion} + Q_{depletion}}{C_{IHP}} \quad \text{------- 3.41}$$

$$\phi_{IHP} - \phi_{OHP} = -\frac{\sigma_{diffuse}}{C_{OHP}} \quad \text{-------3.42}$$

From the condition of charge neutrality we get

$$\sigma_{diffuse} + \sigma_{IHP} + \sigma_{insulator} + Q_{inversion} + Q_{depletion} = 0 \quad \text{-------3.43}$$

Again the potential at any point in between insulator surface and IHP the potential is given as

$$\phi_{IH_region}(r) = \phi_0 + \left(\frac{\phi_{IHP} - \phi_{insulator}}{t_{IHP}}\right)\left(r - \left(\frac{t_{si}}{2} + t_{ox}\right)\right) \quad \text{-------3.44}$$

For $\left(\frac{t_{si}}{2} + t_{ox}\right) \le r \le \left(\frac{t_{si}}{2} + t_{ox}\right) + t_{IHP}$

$$\phi_{OH_region}(r) = \phi_{IHP} + \left(\frac{\phi_{OHP} - \phi_{IHP}}{t_{OHP} - t_{IHP}}\right)\left(r - \left(\frac{t_{si}}{2} + t_{ox} + t_{IHP}\right)\right) \quad \text{-------3.45}$$

For $\left(\frac{t_{si}}{2} + t_{ox} + t_{IHP}\right) \le r \le \left(\frac{t_{si}}{2} + t_{ox}\right) + t_{OHP}$

ii) Diffuse layer potential profile

Since the device is of cylindrical shape, the surrounding electrolyte also takes the same form. The diffuse layer potential decays in the radial direction of the cylinder. This can be derived using the Poisson Boltzmann equation in cylindrical coordinate as [17]

$$\frac{1}{r}\frac{d}{dr}\left(r\frac{d\phi}{dr}\right)=\frac{2qzn_0}{\in}\sinh\left(\frac{zq\phi}{k_BT}\right) \qquad \text{-------3.46}$$

Where, z is the valence of the electrolyte ions.

For small value of $\phi < 0.025V$ the term $\left(\frac{zq\phi}{k_BT}\right)$ is smaller than unity and therefore the above equation can be approximated as

$$\frac{1}{r}\frac{d}{dr}\left(r\frac{d\phi}{dr}\right)=\frac{2q^2z^2n_0}{\in}\frac{\phi}{k_BT} \qquad \text{-------3.47}$$

or

$$\frac{1}{r}\frac{d}{dr}\left(r\frac{d\phi}{dr}\right)=k^2\phi \qquad \text{-------3.48}$$

Where,

$$k^2=\frac{2q^2z^2n_0}{\in k_BT} \qquad \text{-------3.49}$$

and

$$k^{-1}=L_D \qquad \text{-------3.50}$$

L_D is known as Debye length of the electrolyte solution. It is a measure of double layer thickness comprising of Helmholtz and Diffuse layer. At this length

the potential falls to around 33% that of the insulator surface if the surface is planar. For a curved surface this percentage is even smaller.

Now using the boundary conditions

$$\phi(0)=\phi_0 \quad \text{and} \quad \left.\frac{d\phi}{dr}\right|_{r=\alpha}=0 \qquad \text{------3.51}$$

The solution of the above equation is given below [17] .This gives the potential profile in
the Diffused layer

$$\phi(r)=\phi_0 \frac{K_0(k\,r)}{K_0(k..(t_{si}+2t_{ox}))} \qquad \text{-------3.52}$$

Where, K_0 is the modified Bessel function of zeroth order [18][19]

$$\frac{\phi(r)}{\phi_0}=\frac{K_0(k\,r)}{K_0(k..(t_{si}+2t_{ox}))} \qquad \text{-------3.53}$$

The equation 3.53 gives the normalized potential profile in the diffused layer.

The diffuse layer charge density can be found as

$$\sigma_{dl}=\varepsilon\left.\frac{d\phi}{dr}\right|_{r=\frac{t_{si}+2t_{ox}}{2}} \qquad \text{-------3.54}$$

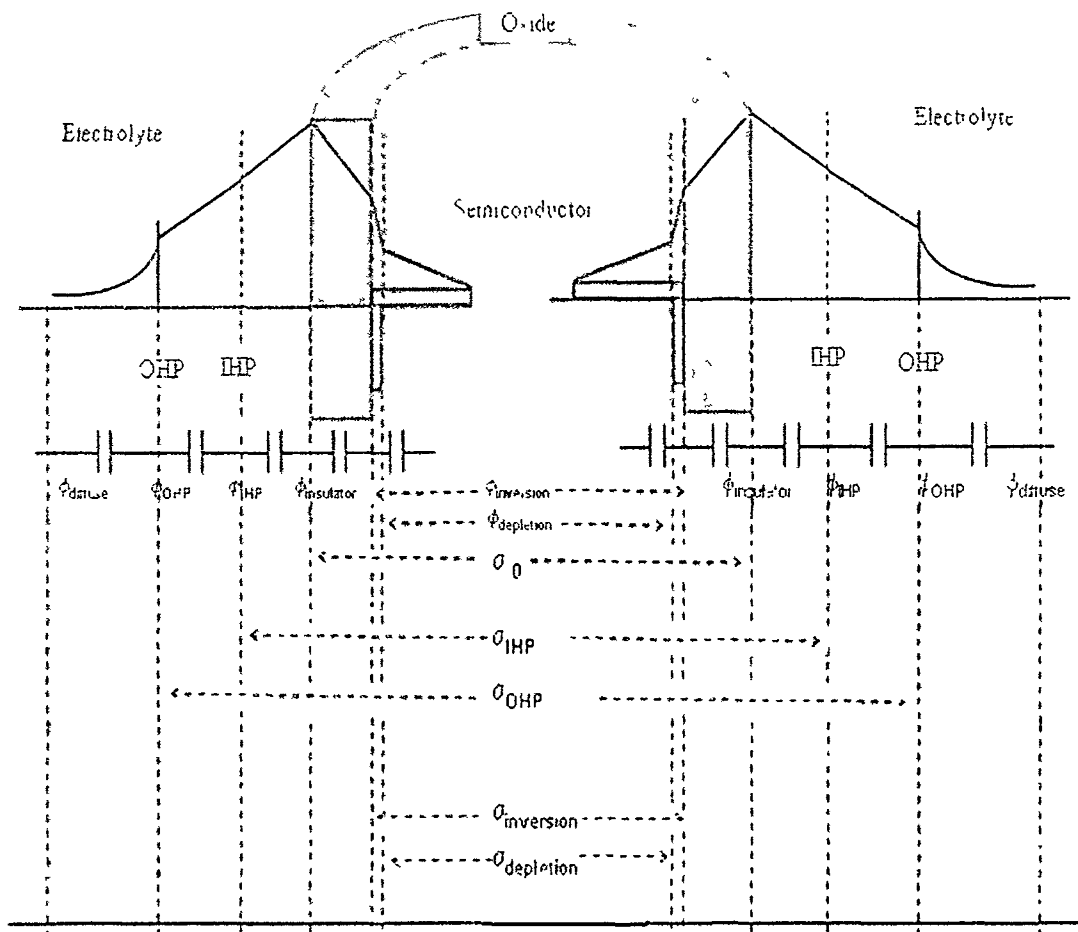

Fig 3.3: Charge distribution and potential profiles of an EIS system based on the Site Binding Model explains the reaction at the surface of insulator. This kind of charge distribution occurs for pH> pH_{pzc} .

3.4.2 Semiconductor Potential Profile

For this part of modeling, two assumptions

i) Inversion layer is situated exactly at the semiconductor insulator interface. The inversion charge density for a cylindrical MOSFET is given by

$$Q_{inv} = -C_{ox_cyl}\left(V_{ref} - V_{mCYL(MOSFET)}\right) \quad \text{----3.55}$$

$$Q_{inv} = -C_{ox_cyl}\left(V_{ref} - V_{mCYL(ISFET)}\right) \quad \text{---3.56}$$

ii) Under depletion approximation the maximum thickness of the depletion layer is $W_{depletion_\max}$ i.e. the depletion layer starts at the semiconductor–insulator interface and extends towards the far side of the interface up to $W_{depletion_\max}$. The depletion charge density is given by equation 3.14 as follows.

$$Q_{depletion} = -\varepsilon_{SiO_2} E_S \quad \text{-----3.57}$$

Using the above, the potential drop across the inversion layer can be expressed as follows

$$\phi_{insulator} - \phi_{inversion} = -\frac{Q_{inv} + Q_{depletion}}{C_{ox}} \quad \text{-------3.58}$$

And similarly the potential variation across the depletion can be found by the following expression

$$\phi_{inversion} - \phi_{depletion} = -\frac{Q_{depletion}}{C_{depletion}} \quad ----3.59$$

3.5 Amperometric Sensitivity

As defined in the chapter 2, amperometric sensitivity is expressed as follows

$$\frac{dI_{DS}}{dpH} = \mu C_{ox} V_{DS} \frac{W}{L} \cdot \frac{d}{dpH}(\phi_{eo}) \quad ---------3.60$$

For a cylindrical device, the effective channel width of the cylindrical device is considered here. The effective width of a cylindrical device is as given in equation 3.38 is

$$W_{cyl} = \frac{\pi\left[t_{Si}^2 - (t_{Si} - t_{inv})^2\right]}{4t_{inv}} \quad ---------3.61$$

Therefore the amperometric sensitivity of a cylindrical device is

$$\frac{dI_{DS}}{dpH} = \mu C_{ox} V_{DS} \frac{W_{cyl}}{L} \cdot \frac{d}{dpH}(\phi_{eo}) \quad -------3.62$$

3.6 Simulation results and conclusions

The main goal of this work is to evaluate the behaviors of a cylindrical ISFET from its simulation results and compare the same with a planar ISFET. For this purpose a cylindrical ISFET has been modeled considering a long channel.

The simulation result in Fig. 3.4 shows variation of threshold voltage with change in acceptor doping concentration. Here a comparison is shown between the threshold voltage model developed in present work for a cylindrical MOSFET and model available in [2] equation no.(29). From low to moderately high doping concentration, good consistency of the simulation result of the present model is seen with results obtained from available literature, but at higher doping concentration the present model shows considerable deviation. This happens due to the fact that, during development of the model the assumptions were made for low to moderate doping concentration and not for high doping concentration.

Fig 3.5 shows drain current vs. gate to source voltage of the cylindrical MOSFET and same is compared model available in [2] equation no.(29).

Fig. 3.6 shows variation of electrolyte oxide interface potential vs. pH. This relation is almost linear throughout the range except at very low value of pH. This happens because at low value of pH, the value of β is small. As the value of pH increases, β also increases and consequently $\beta/_{\beta+1} \approx 1$ and hence the ϕ_{eo} becomes linear. This variation of β is shown in the fig. 6.

The fig. 3.7 shows variation of drain current of cylindrical ISFET vs. pH. As the pH value increase, electrolyte oxide interface potential decreases and this result in increase in threshold voltage of the ISFET. Consequently, an increase in

pH causes decrease in drain current. The figure shows a linear variation of the drain current for varying pH.

Fig. 3.8: shows relationship between pH and the dimensionless sensitivity factor β of the electrolyte oxide interface. This factor remains almost constant from pH=5 to 14. This range may be different for different material. For pH below 5, the value of this factor decreases and becomes stable around pH≤2.5. This transition is linear and sharp around the value of pH_{PZC} which is 4.2.

In the Fig.3.9:, the variation of diffuse layer capacitance is shown as a function of pH. For high value of pH i.e. at lower ionic concentration this capacitance is low. But as the pH decreases and falls below pH_{PZC}, this capacitance sharply increases. This happens because of high ionic concentration at low value of pH.

The variation of double layer capacitance with pH is shown in Fig.3.10: This also shows similar variation of capacitance as in the case of diffuse layer capacitance around pH_{PZC}.

Fig. 3.11 shows variation of Debye length as pH varies. For low value of pH the Debye length is few nanometers only, but as the pH increases the Debye length increases considerably.

The normalized potential profile vs. distance from the OHP is shown in Fig. 3.12. The normalized potential decays fast for low value of pH, whereas there is very slow variation of this at high value of pH. This is the main reason behind the sharp increase in the diffused layer capacitance at low pH.

Fig.3.13: shows the comparison of the normalized potential profile of a cylindrical and a planar ISFET at pH= 4. From this figure it can be observed that

the normalized potential decays faster in case of a cylindrical device as compared to that of a planar device.

Fig.3.14: and Fig.3.15: shows the comparison of the normalized potential profile of a cylindrical and a planar ISFET at pH= 7 and pH=10 respectively. From these three figures it can be observed that as the value of pH increases, the normalized potential decay for a cylindrical device becomes faster as compared to that for a planar device, but in absolute terms both becomes slow at high value of pH (fig.11).

Fig.3.16 shows the device Drain current variation with variation of Drain to source voltage at various pH. From this figure we can get indication of threshold voltage shift with pH by linear extrapolation.

Fig.3.17: shows drain current of the cylindrical ISFET vs. V_{ref} at different pH indicating pH response of the Cylindrical Device. When this figure is compared with the figure 2.7 of chapter 2, the increase in amperometric sensitivity for the cylindrical ISFET is observed which is presented in figure 3.19.

Fig.3.18 (a) shows variation of inversion charge density with pH. A decrease in inversion charge density is observed with increase in pH. Fig. 3.18 (b) shows variation of depletion charge density with pH. For this analysis the reference electrode voltage is kept at V_{ref} = 6.5 volts, so that inversion does not occur at any value of pH. A decrease in inversion charge density is observed with increase in pH.

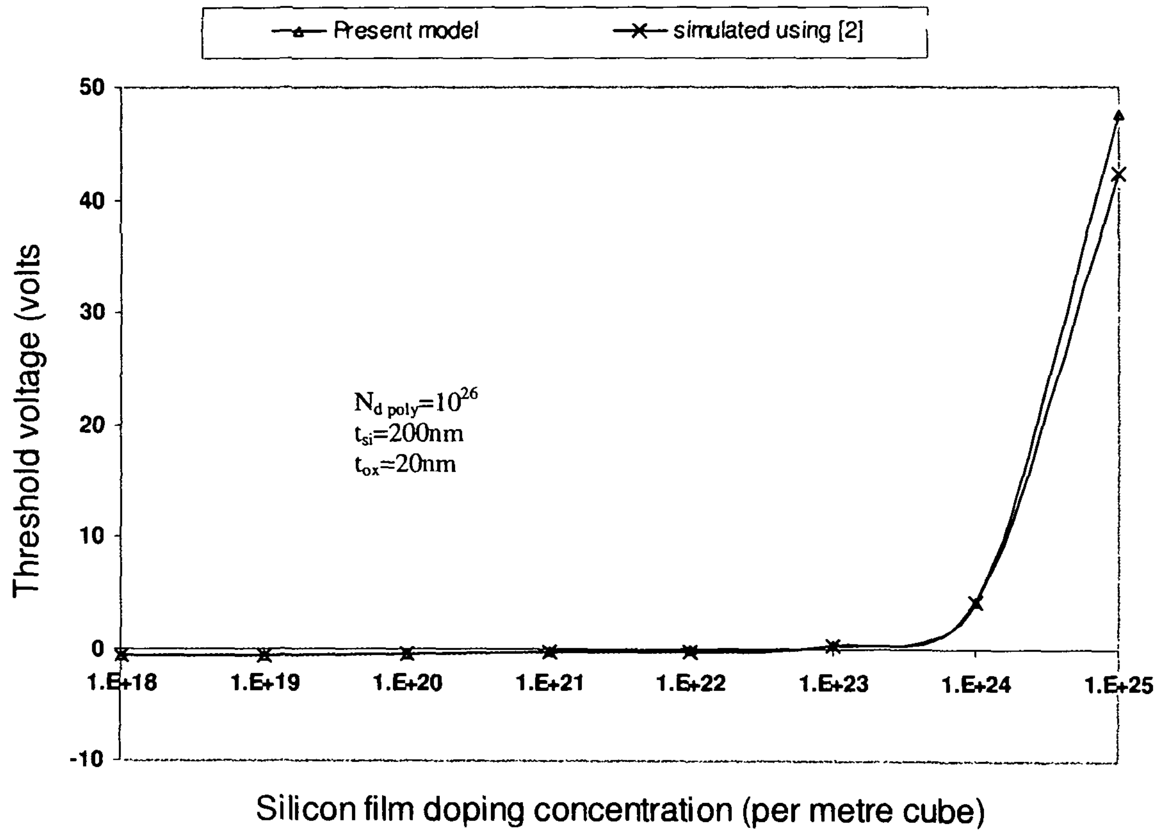

Fig.3.4: Threshold voltage vs. Doping concentration for a cylindrical MOSFET

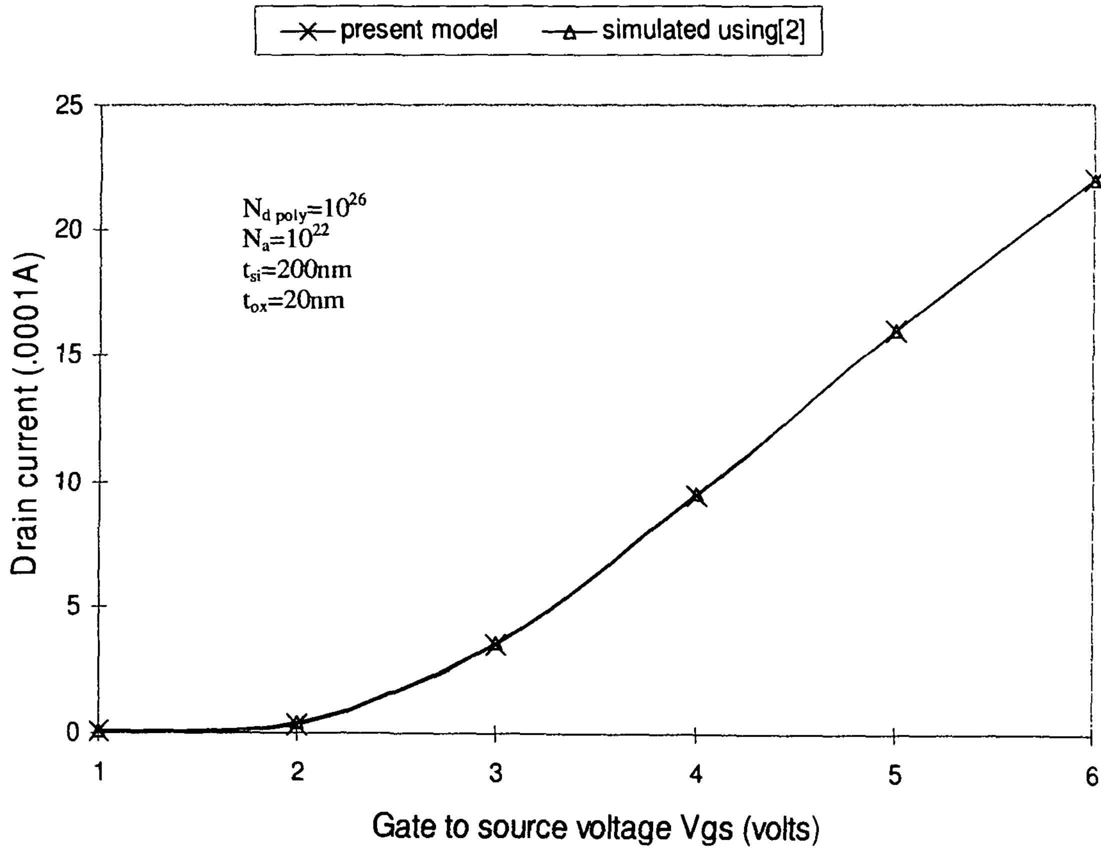

Fig.3.5: Drain current vs. Gate to source voltage

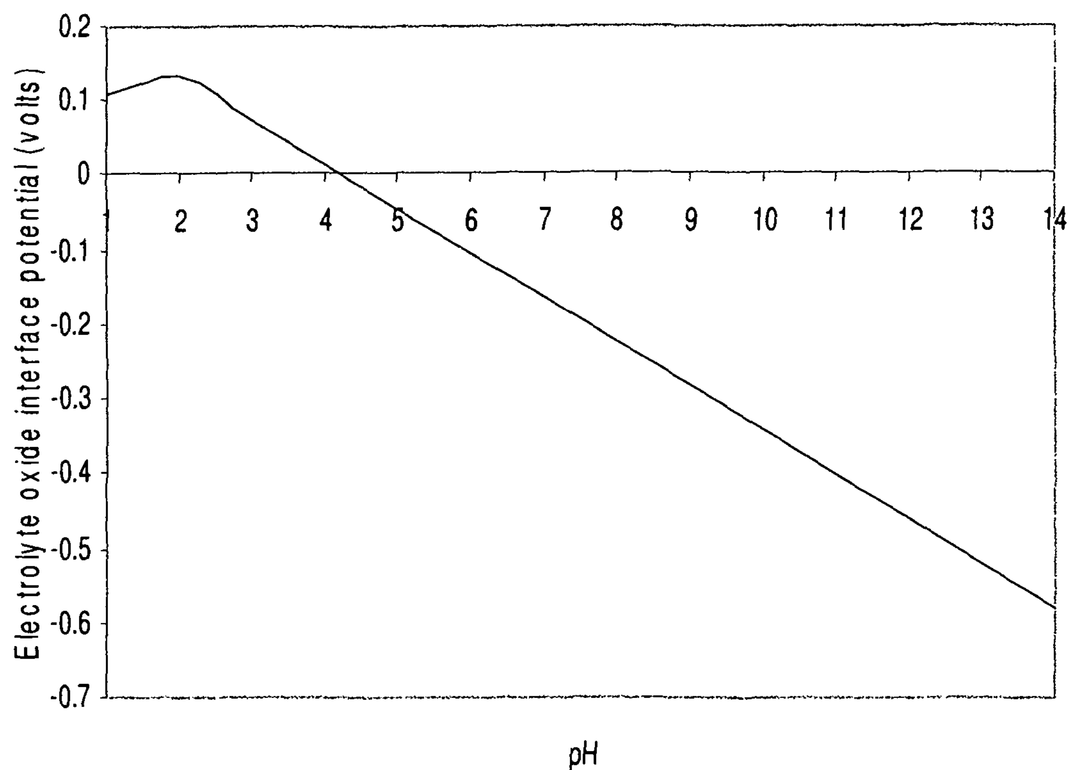

Fig. 3.6: Electrolyte oxide interface potential vs. pH

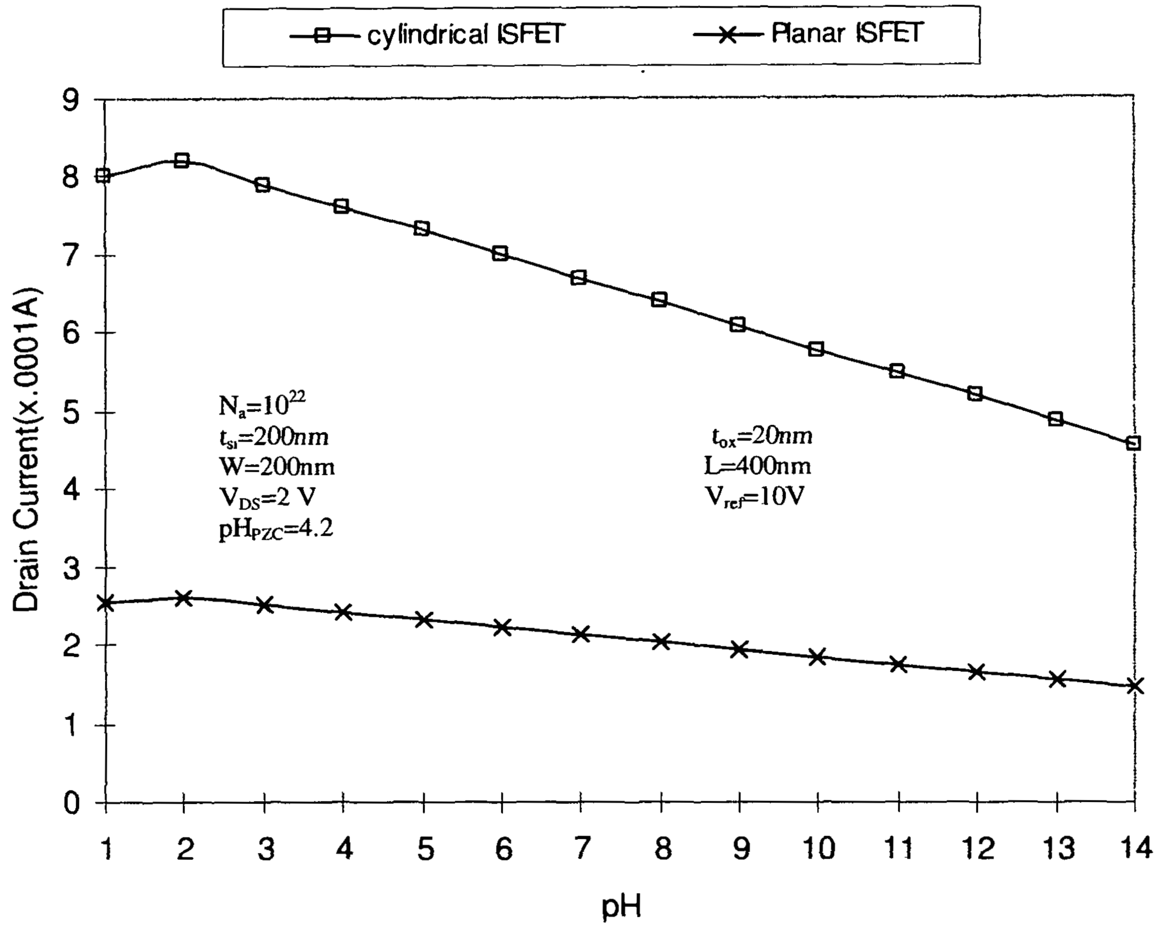

Fig.3.7: Drain current vs. pH

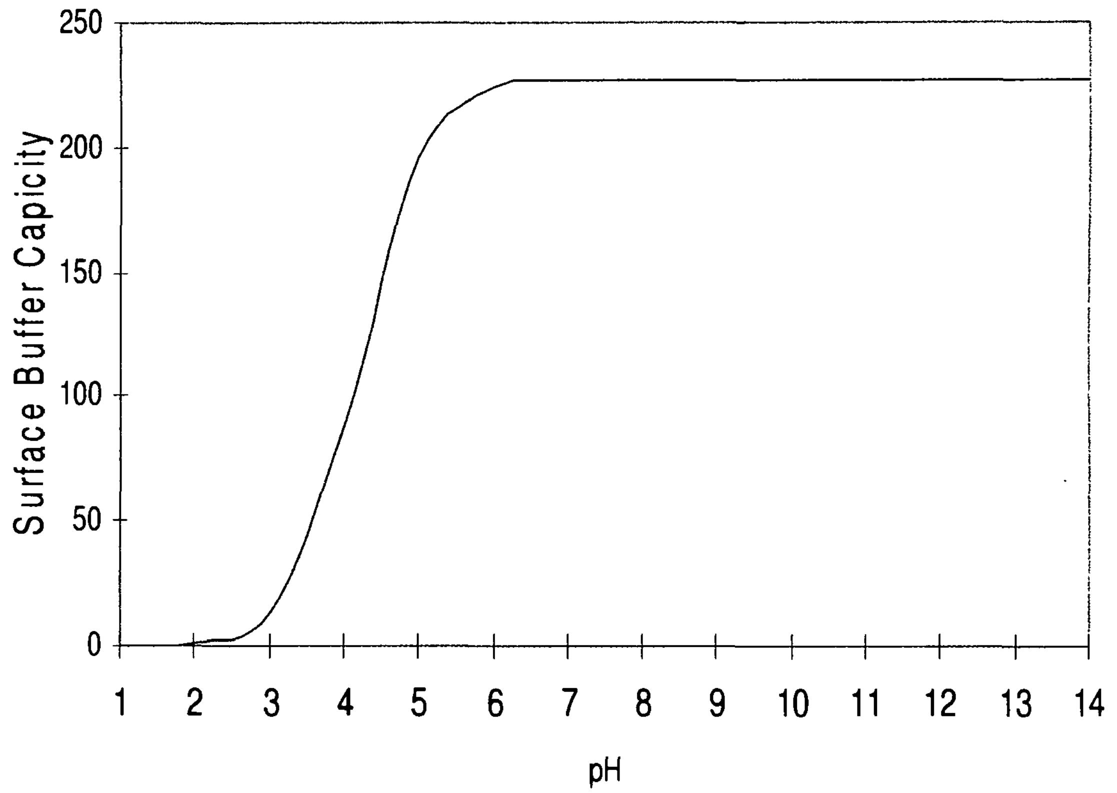

Fig.3.8: Surface buffer capacity vs. pH

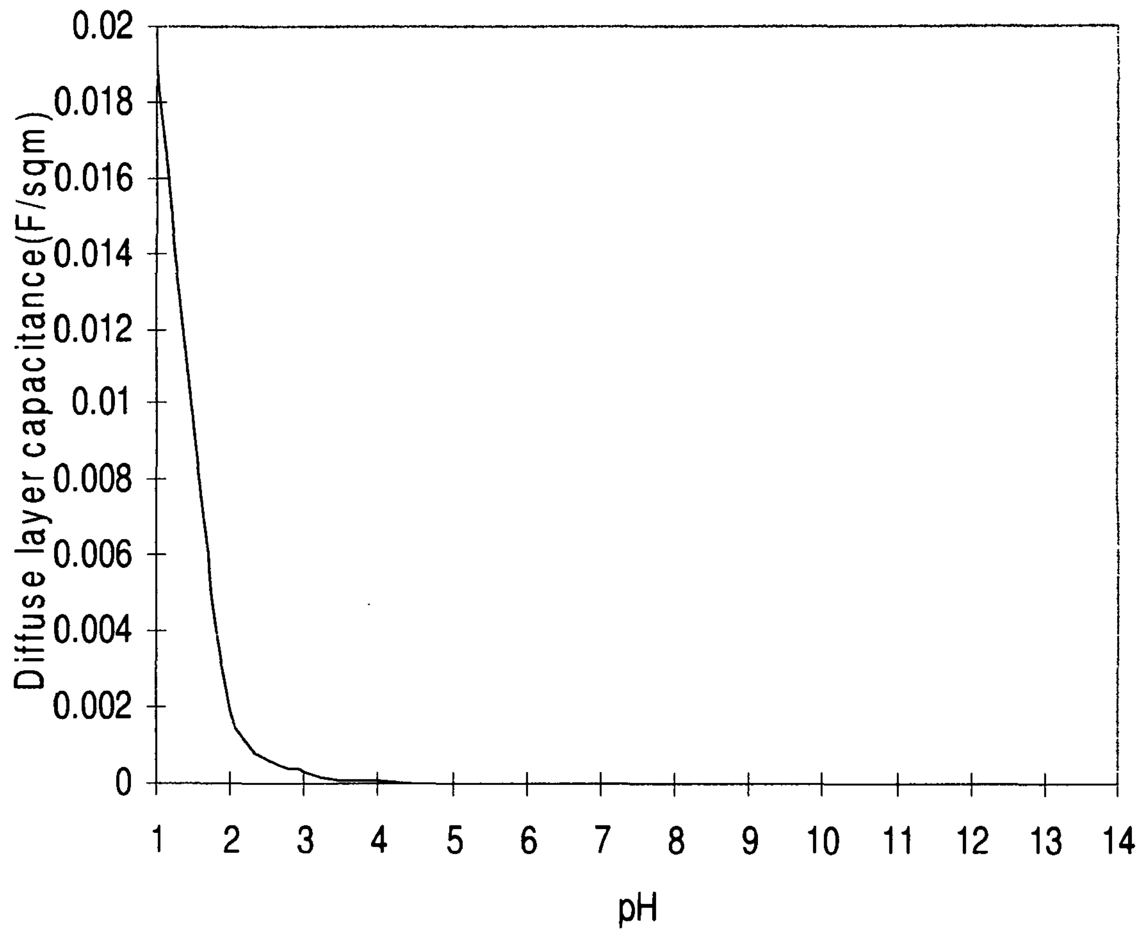

Fig.3.9: Diffuse layer capacitance vs. pH

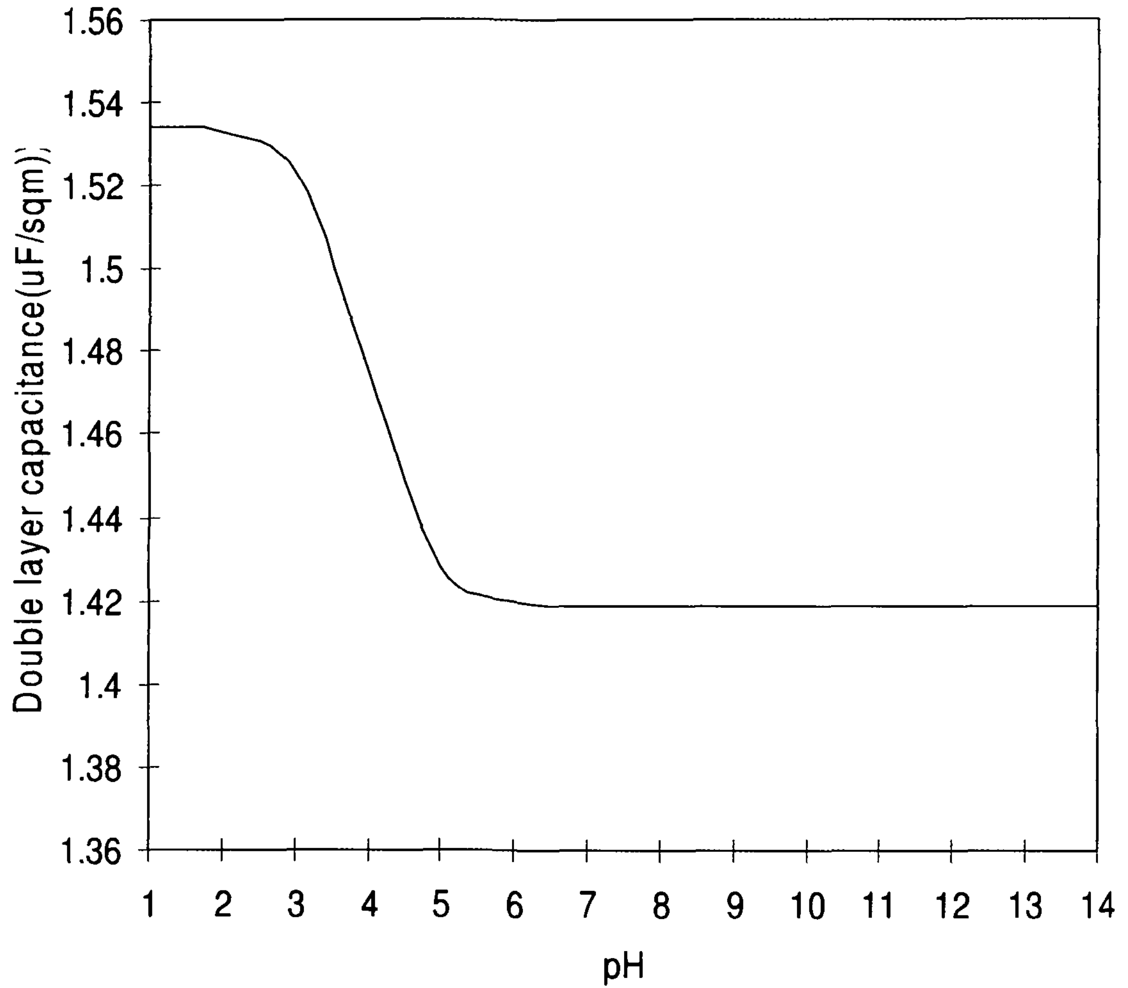

Fig.3.10: Double layer capacitance vs. pH

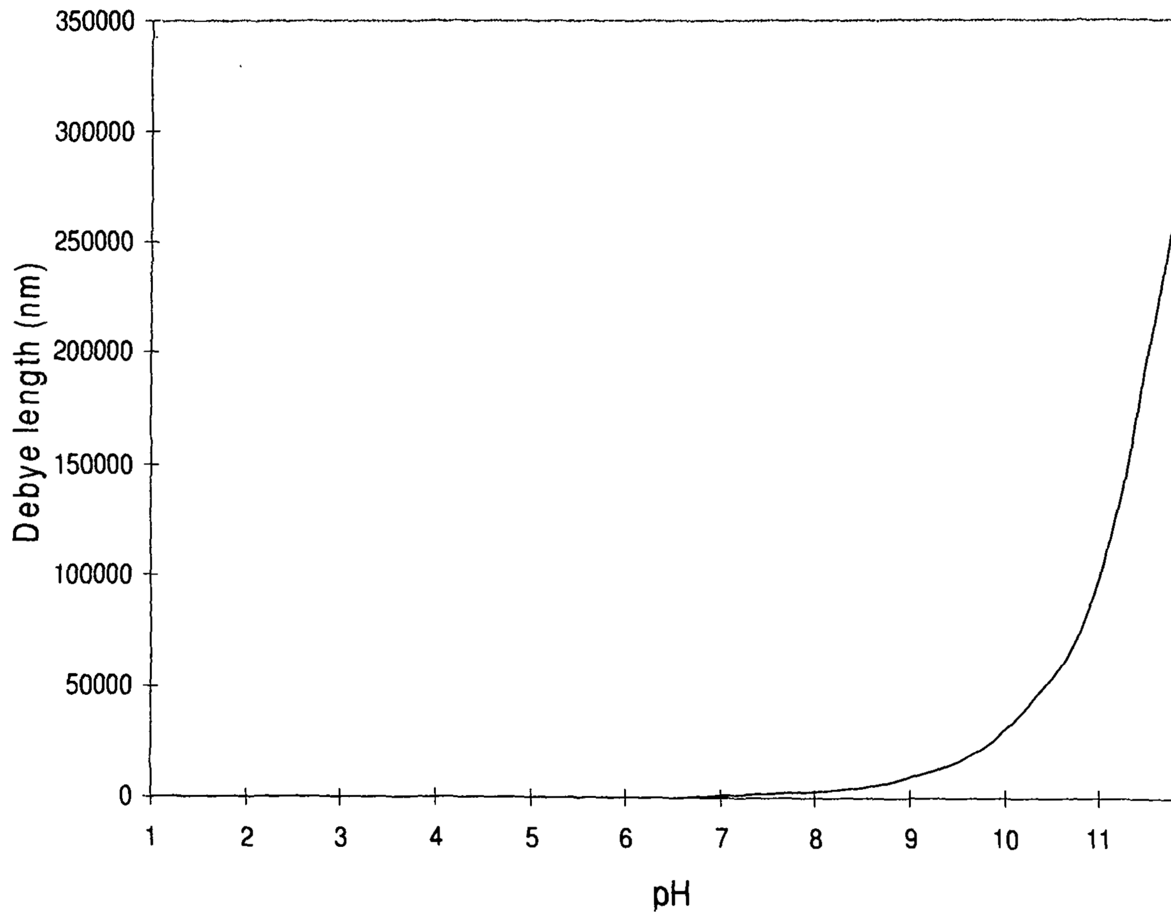

Fig.3.11: Debye length vs. pH

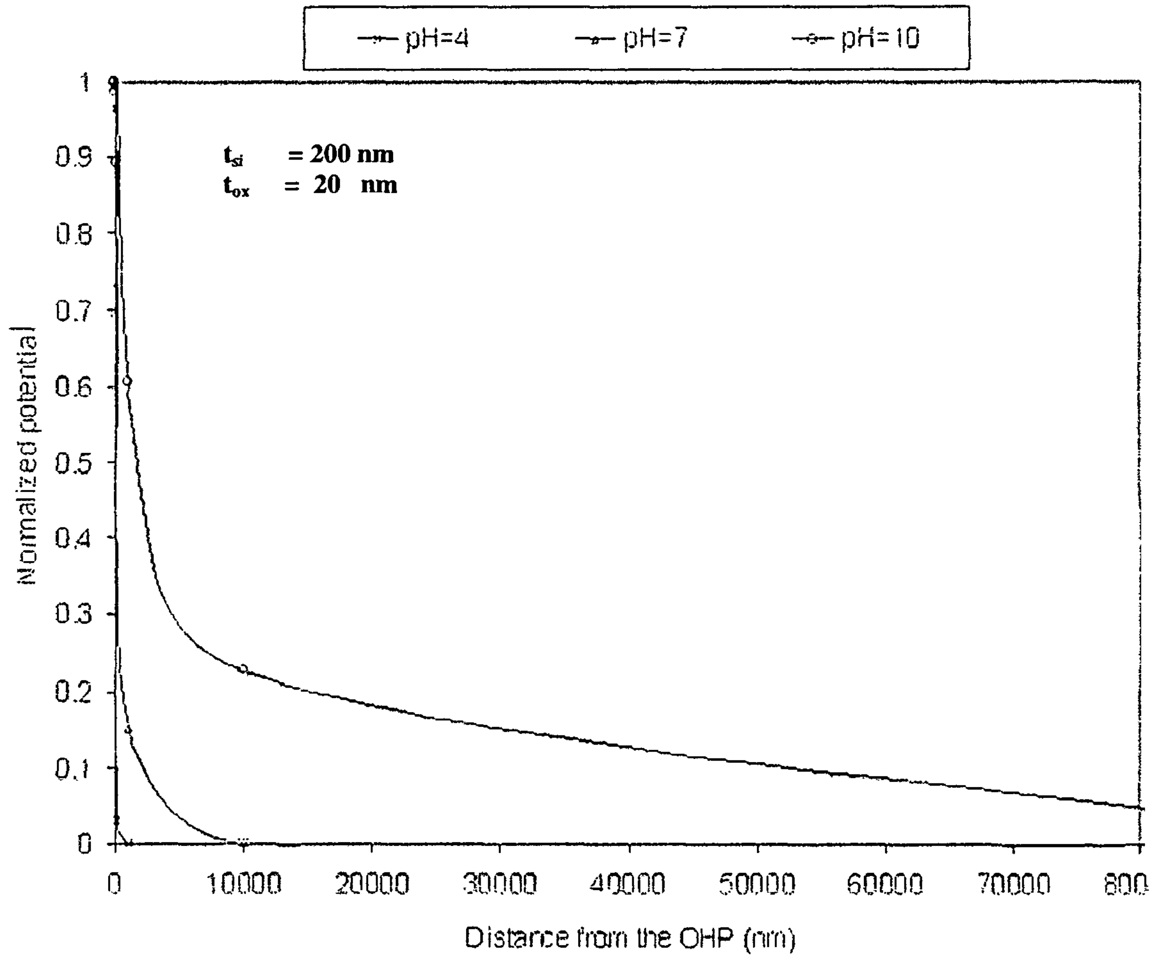

Fig.3.12: Normalized potential vs. distance from the OHP

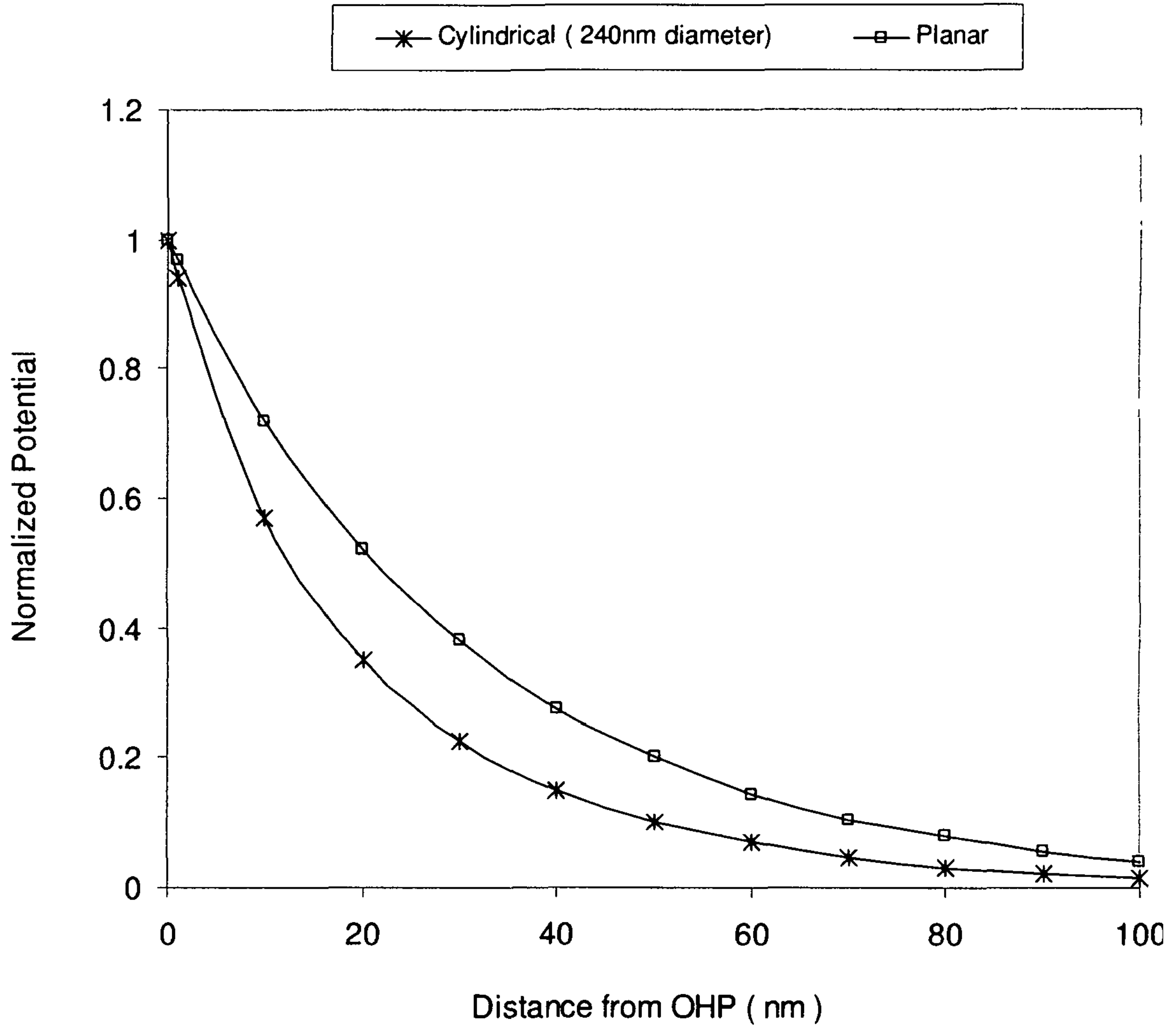

Fig.3.13: Comparison of Normalized potential vs. distance from the OHP at pH=4

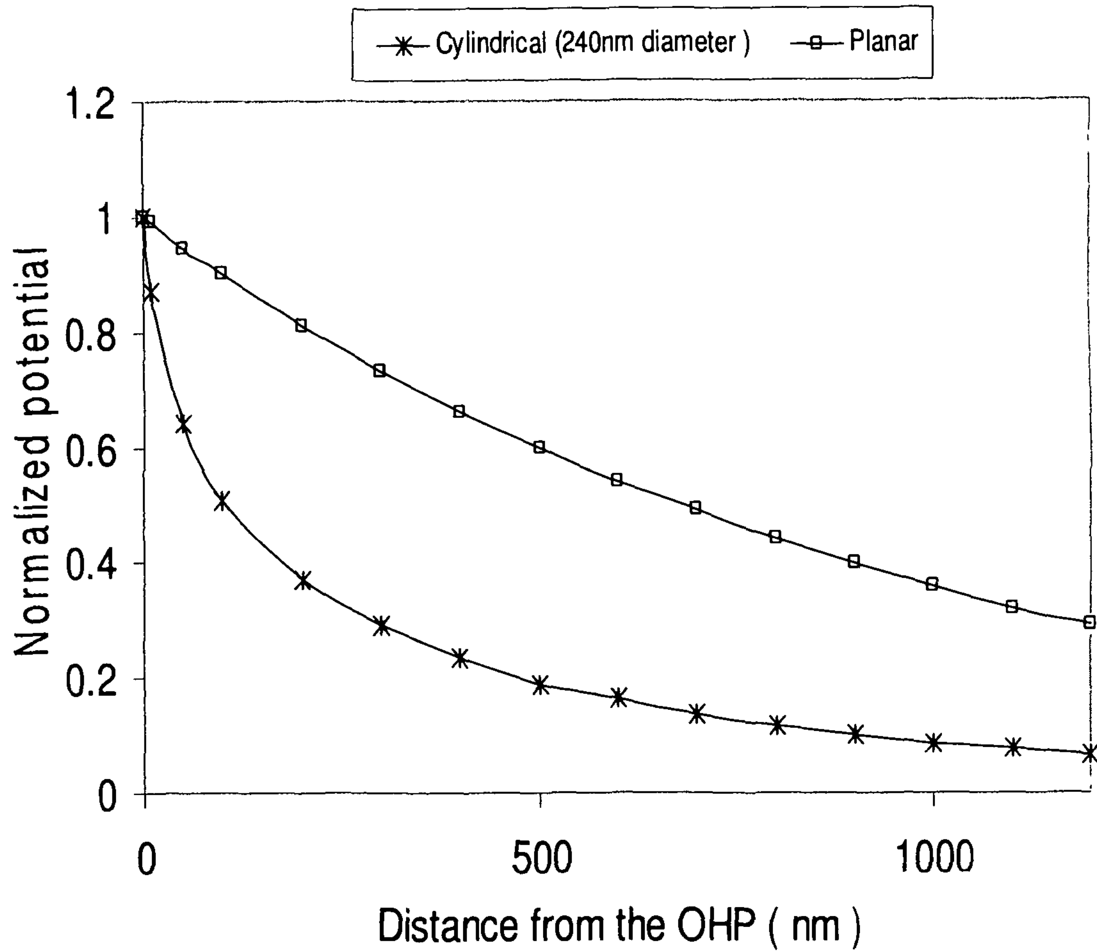

Fig.3.14: Comparison of Normalized potential vs. distance from the OHP at pH=7

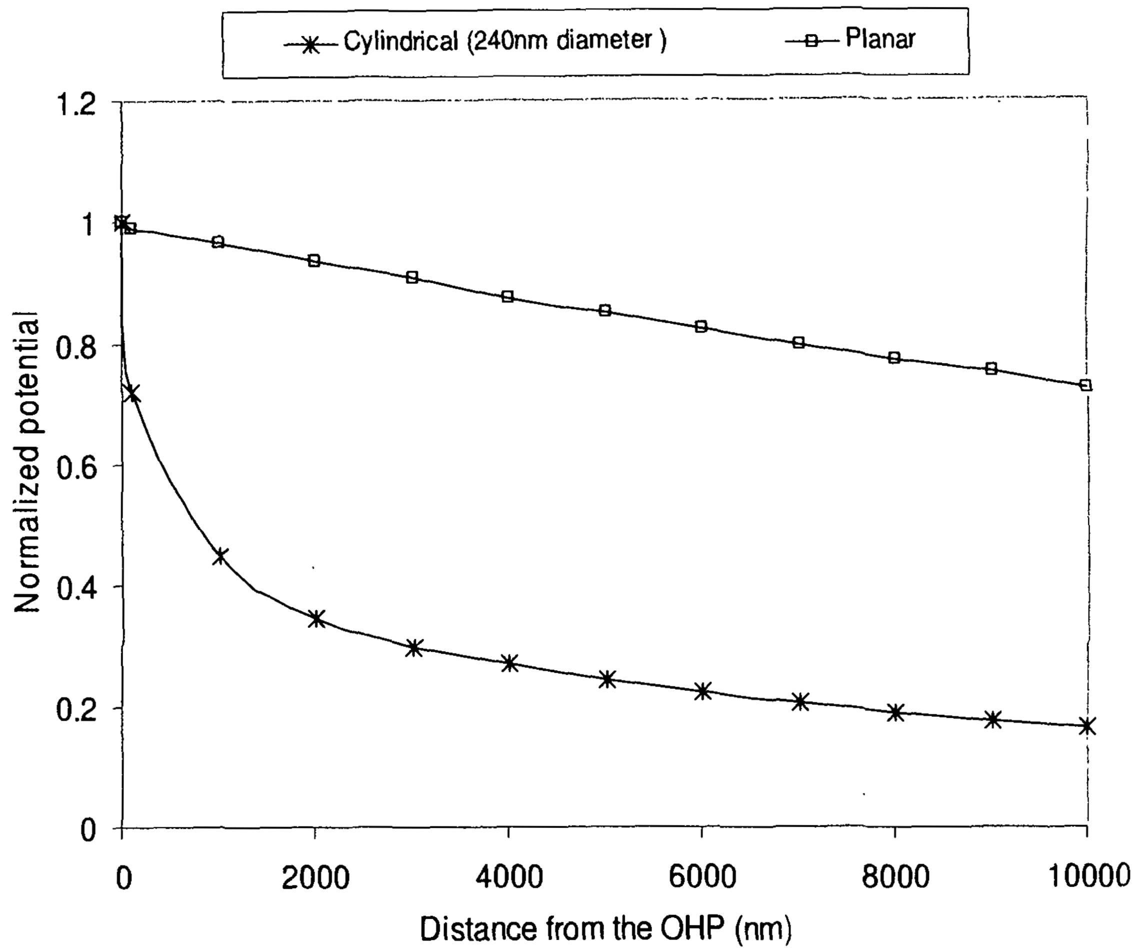

Fig.3.15: Comparison of Normalized potential vs. distance from the OHP at pH=10

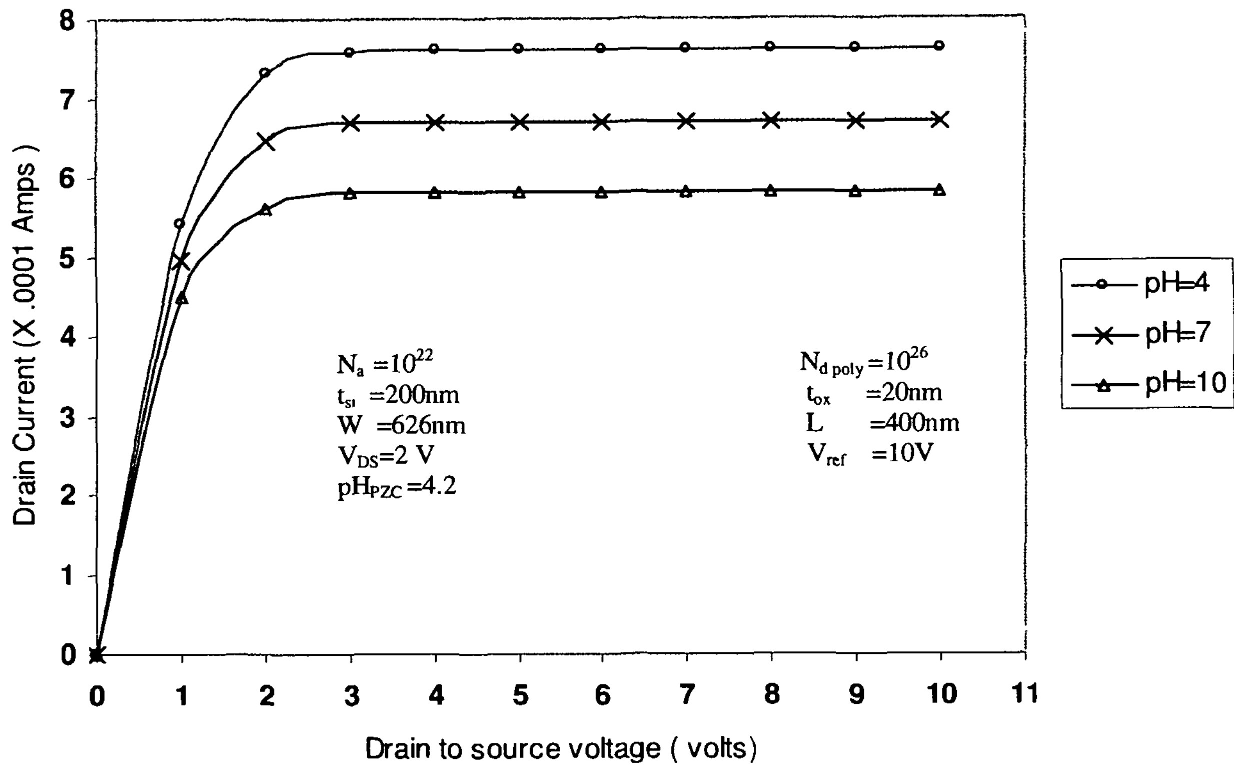

Fig: 3.16: Drain current vs. Drain to source voltage at different value of pH

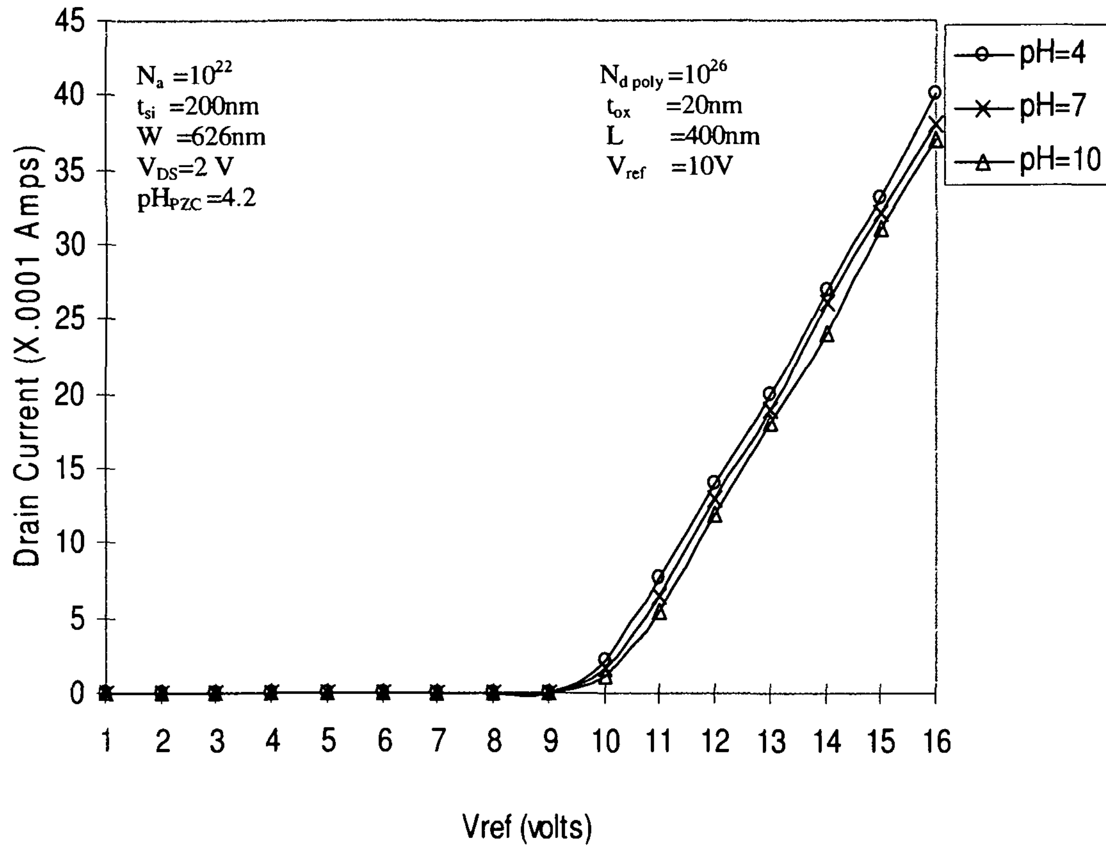

Fig: 3.17: Drain current vs. the voltage applied to the reference electrode at different value of pH.

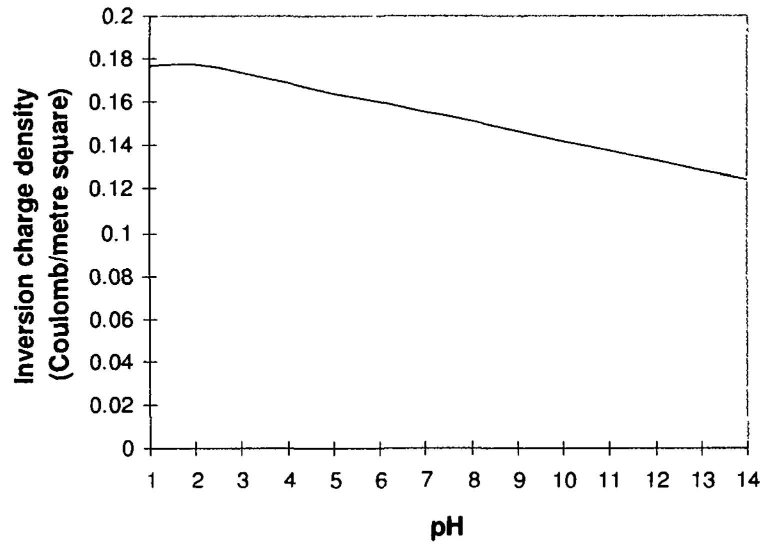

(a)

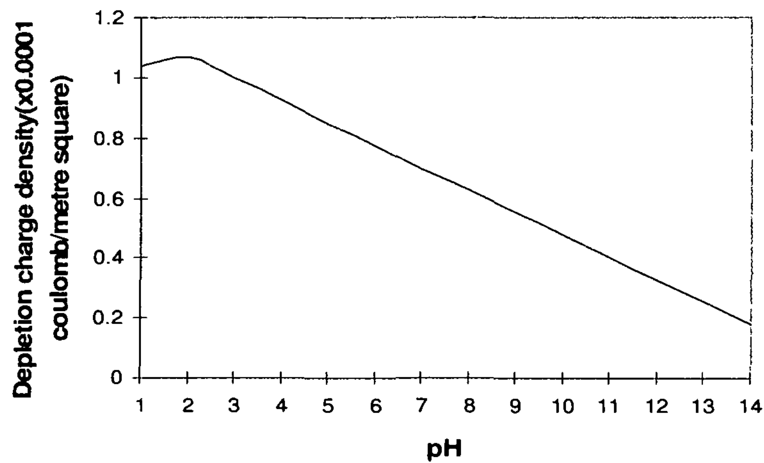

(b)

Fig. 3.18: (a) Inversion layer charge density vs. pH (V_{ref}=10V).

(b) Depletion charge density vs. pH (V_{ref}= 6.5 V)

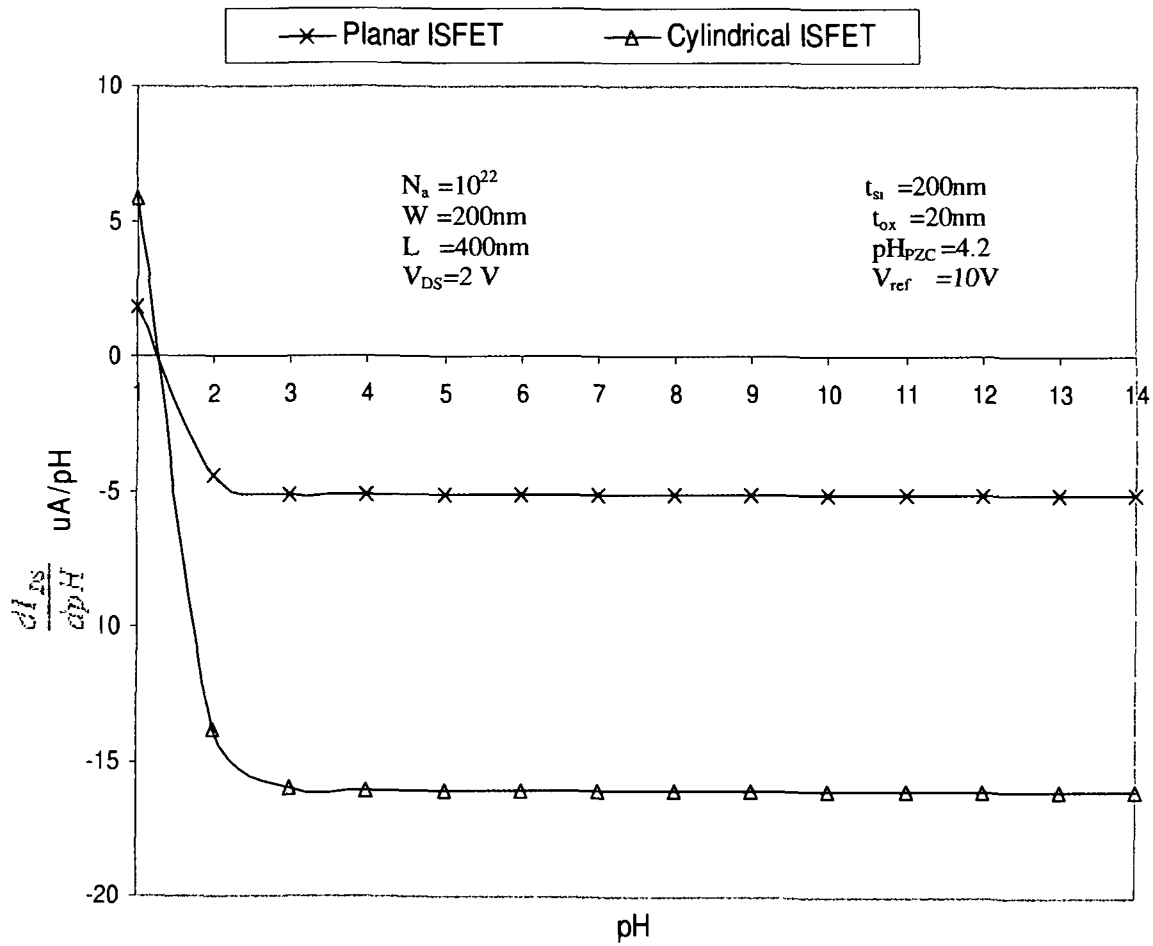

Fig. 3.19: Amperometric sensitivity of planar and cylindrical ISFET

3.7 References

1. Sang –Hyun Oh, J.M. Hergenrother, "Analytic Description of short-channel Effects in Fully-depleted Double-Gate and Cylindrical Surrounding-Gate MOSFETs" IEEE Electron Device letters, Vol.21, No.9, pp.445-44, 2000.
2. Abdellah Aouaj, Ahmed Bouziane, Ahmed Nouacry "Analytical 2D modeling for potential distribution and threshold voltage of the short channel fully depleted cylindrical/surrounding gate MOSFET" International Journal of Electronics, Vol.92, No. 8, 437-443, 2005.
3. Jacob H Masliyah, Subir Bhattacharjee, *Electrokinetic and Colloid Transport Phenomena,* John Wieley & Sons, Inc, 2006.
4. Yates, Levine, Healy, - "Site binding model of the electrical double layer at the oxide/water interface", J. Chem. Soc. Faraday Trans. 70, pp. 1807-1818,1974.
5. Hyun-Jin Cho, James D Plummer "Modeling of Surrounding Gate MOSFETs With Bulk Trap States" IEEE Transactions on Electron Devices, Vol. 54, no.. 1, pp.166-169, 2007
6. Weisstein, Eric W. "Modified Bessel Function of the First Kind." From MathWorld—A Wolfram Web Resource. http://mathworld.wolfram.com/ModifiedBesselFunctionoftheFirstKind.html
7. S.M.Sze, *Semiconductor Devices Physics and Technology,* John Wiley and Sons (Asia) Pte. Ltd, 2002
8. Rang Hong Yan, Abbas Ourmazd, Kwing F Lee "Scaling the Si MOSFET: From Bulk to SOI to Bulk" IEEE Transactions on Electron Devices, vol. 39, no. 7,pp. 1704-1710, 1982.

9. Abhinav Kranti , S Haldar, R S Gupta "Analytical model for threshold voltage and I V characteristics of fully depleted short channel cylindrical/surrounding gate MOSFET" Microelectronic Engineering 56, pp.241-259, 2001
10. P.Bergveld "ISFET, Theory and Practice" IEEE Sensor Conference Toronto, October, 2003.
11. Luc Bousse, Nico F De Rooji, P. Bergveld "Operation of Chemically Sensitive Field Effect Sensors As a Function of the Insulator Electrolyte Interface" IEEE Transaction on Electron Devices , Vol. ED-30, No 10, pp.1263-1270, 1983.
12. P Bergveld. "Thirty years of ISFETOLOGY What happened in the past 30 years and what may happen in the next 30 years" Sensors and actuators B 88, pp.1-20, 2003.
13. Sergei V Dzyadevych, Alexey P Soldatkin, Anna V El'skaya, Claude Martelet, Nicole Jaffrezic-Renault "Enzyme Biosensors Based on ion – sensitive field-effect transistor" Analytica Chimica Acta 568, pp. 248-258, 2006.
14. Jung Chung Chou, Cheng Yu Weng, Hsjian Ming Tsai. "Study on the temperature effects of Al_2O_3 gate pH-ISFET" Sensors and Actuators B 81, 152-157, 2002.
15. Sergio Martinoia, Giuseppe Massobrio, Leandro Lorenzelli "Modeling ISFET microsensor and ISFET based Microsystems: a review" Sensor and Actuator B 105, 14-17, 2005.
16. Massimo Grattarola, Giuseppe Massobrio, *Bioelectronics Handbook: MOSFETs, Biosensors and Neurons*, Mc Graw Hill.
17. Ben Streetman , Sanjay Banerjee, *Solid State Electronic Devices*, PHI.2001

18. Jacob H. Masliyah, Subir Bhattacharjee, *Electrokinetic and Colloid Transport Phenomena*, JohnWiley & Sons, Inc., Hoboken, New Jersey
19. Arfken, G., Hans J. Weber, *Mathematical Methods For Physicists*, 3rd ed. Orlando, Academic Press, 2001.

Chapter 4

Cylindrical ISFET at Nano dimension

4.1 Introduction

Application of solid state ion sensor is continuously increasing since its inception. Everyday, there comes new field of applications, such as monitoring metabolic activity, pH inside a single cell, which require specific features of the sensor. Recently successful penetration of mouse embryonic stem cell with silicon nanowire (90nm diameter) has been reported [1]. In this process the cells survived, provided the silicon nanowire diameter was small as compared to the cell size.

Consequently, if any measurement has to be done within a cell, the size of the sensing device must be smaller than the cell size, for survival of the cells. To achieve this criterion, when the device (in present study it is an ISFET) is scaled down to such small dimension, some unwanted effect arises. For an MOSFET, when the gate oxide thickness is scaled to less than 10 nm, the transverse electric field becomes very large [2], [3] leading to a sharp band bending. The effect is quantization of energies above conduction band. Under this condition the first the lowest allowed energy level of electrons becomes little higher than the bottom of the conduction band. As a result of this, the gate voltage required is little more to bring the conduction band below the Fermi level by same amount. In other words, the threshold voltage increases. The same effect appears in an ISFET also because of similar structure on the semiconductor side. If the device dimension is less than 100 nm, threshold voltage shift due to quantum confinement is also needed to be considered [3].

4.2 Quantum Mechanical Effect Modeling

The general threshold voltage of a cylindrical MOSFET can be expressed as given as follows

$$V_{th_cyl(MOS)} = V_{fb(MOS)} + 2\left|\phi_f\right| + \frac{\left|Q_{depletion_cyl}\right|}{C_{ox_cyl}} \quad \text{-----4.1}$$

And that of a cylindrical ISFET is given as

$$V_{th_cyl(ISFET)} = V_{fb(MOS)} + 2\left|\phi_f\right| + \frac{\left|Q_{depletion_cyl}\right|}{C_{ox_cyl}} + E_{ref} + \phi_{lj} + \chi_e - \phi_{eo} - \phi_m \quad \text{---4.2}$$

The above equations are valid for a long channel bulk device. To estimate the quantum mechanical V_T-shift with a 2-D confinement in a cylindrical structure, it is required to solve the Schrödinger equation and poisons equation self consistently. Although this method gives accurate result, it is quite troublesome. A simple approximation for this problem is triangular potential well approximation [2]. Here a triangular potential well approximation in the cylindrical geometry has been assumed. As per this assumption, the potential is given as follows

$$V(r) = F\left(\frac{t_{si}}{2} - r\right), \quad r \le t_{si/2} \quad \text{-----4.3}$$

$$V(r) = \infty \quad , r > t_{si/2} \quad \text{-----4.4}$$

In the case of a particle in the cylindrical quantum well with the infinite potential barrier, as shown in Fig. 4.1[4]

The Schrödinger equation in cylindrical coordinate with a triangular potential well can be presented as follows

$$-\frac{\hbar^2}{2m^*}\nabla^2\psi + F\left(\frac{t_{Si}}{2}-|r|\right) = E\psi \qquad \text{-----4.5}$$

$$\Rightarrow -\frac{\hbar^2}{2m^*}\frac{1}{r}\frac{\partial}{\partial r}\left(r\frac{\partial\psi}{\partial r}\right) - \frac{\hbar^2}{2m^*}\frac{1}{r^2}\left(\frac{\partial^2\psi}{\partial\phi^2}\right) - \frac{\hbar^2}{2m^*}\left(\frac{\partial^2\psi}{\partial z^2}\right) + F\left(\frac{t_{Si}}{2}-|r|\right) = E\psi$$

-----4.6

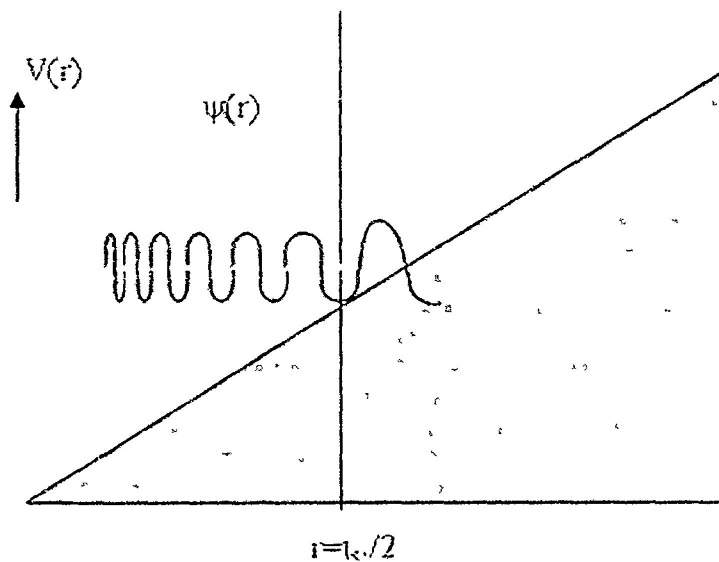

Fig.4.1 Potential of an electron in a homogeneous field

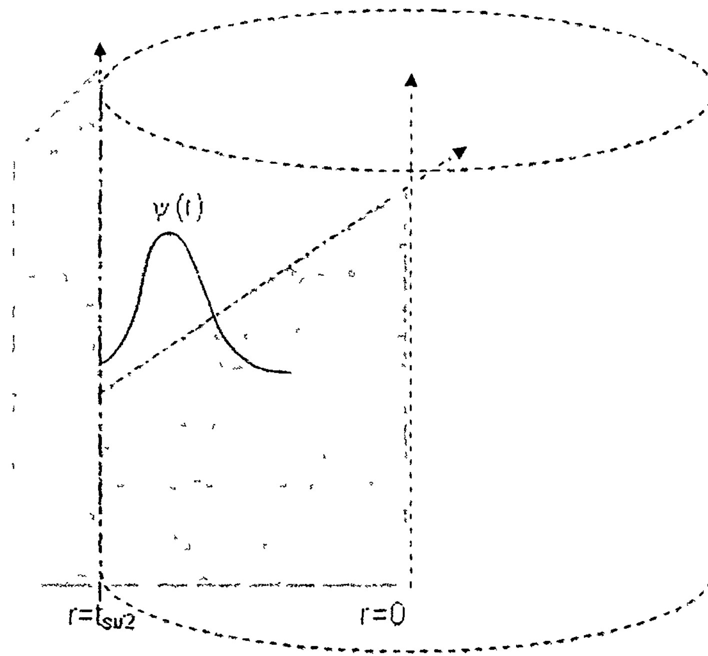

Fig. 4.2: The triangular potential well. The Eigen function of the problem is chosen in such way that on the left side of the interface i.e. for $\rho \geq \rho_{Si}/2$, $\psi(\rho)$ vanishes.

The ground-state wave function obtained is independent of 'z' and 'θ'.So the above equation can be reduced to

$$\Rightarrow -\frac{\hbar^2}{2m^*}\frac{1}{r}\frac{\partial}{\partial r}\left(r\frac{\partial \psi}{\partial r}\right)+F\left(\frac{r_{Si}}{2}-|r|\right)=E\psi \qquad \text{-----4.7}$$

Which can be finally be reduced to the following form

$$\frac{\partial^2\psi}{\partial r^2}+\frac{1}{r}\frac{\partial\psi}{\partial r}+\frac{2m^*}{\hbar^2}\left[E-F\left(\frac{r_{Si}}{2}-|r|\right)\right]\psi=0 \qquad \text{-----4.8}$$

$$\Rightarrow\frac{\partial^2\psi}{\partial r^2}+\frac{1}{r}\frac{\partial\psi}{\partial r}+\frac{2m^*}{\hbar^2}\left[\left(E-F\frac{t_{Si}}{2}\right)+F|r|\right]\psi=0 \qquad \text{-----4.9}$$

From the above figures 4.1 and 4.2 it is seen that the second term in the above equation can be neglected near the semiconductor insulator interface. Consequently the Schrödinger equation becomes

$$\frac{\partial^2\psi}{\partial r^2}+\frac{2m^*}{\hbar^2}\left[\left(E-F\frac{t_{Si}}{2}\right)+F|r|\right]\psi=0 \qquad \text{-----4.10}$$

Now let us introduce the variable ξ, where

$$\xi=\left(r+\frac{E-F.\frac{t_{Si}}{2}}{F}\right)\left(\frac{2m^*F}{\hbar^2}\right)^{1/3} \qquad \text{-----4.11}$$

And the Schrödinger equation reduces to

$$\frac{\partial^2\psi}{\partial\xi^2}+\xi\psi=0 \qquad \text{----4.12}$$

The solution of this equation is

$$\psi(\xi) = A.\phi(-\xi) \qquad \text{-----4.13}$$

$$.\phi(\xi) = \frac{1}{\sqrt{\pi}}\int_0^{\alpha}\cos\left(\frac{1}{3}u^3 + u\xi\right)du \qquad \text{-----4.14}$$

$.\phi(\xi)$ is known as Airy function and 'A' is known as normalization constant[4].

$$A = \frac{(2m)^{1/3}}{\pi^{1/2}F^{1/6}\hbar^{2/3}} \qquad \text{-----4.15}$$

$$F = qE_S \qquad \text{-----4.16}$$

E_S is the effective electric field at the semiconductor surface region and can be expressed as [5].

$$E_S = -\frac{0.5Q_{inv} + Q_{depletion}}{\varepsilon_{Si}} \qquad \text{-----4.17}$$

For a MOSFET device the inversion charge density is given by [6] [7]

$$Q_{inv} = C_{ox}\left(V_{GS} - V_{th(MOS)}\right) \qquad \text{-----4.18}$$

Consequently for a cylindrical device the same can be expressed as

$$Q_{inv} = C_{ox_cyl}\left(V_{GS} - V_{th_cyl(MOS)}\right) \qquad \text{-----4.19}$$

And the depletion charge is given by

$$Q_{depletion} = -\varepsilon_{Si} E_S \qquad \text{-----4.20}$$

Where $E_S = \left.\frac{\partial \psi}{\partial \rho}\right|_{\rho=\frac{t_{Si}}{2}}$ is the electric field at the surface when the width of depletion layer is maximum [7].

The asymptotic behaviors of Airy functions are as follows (similar to [5])

$$\phi(\xi) \approx \frac{A}{2|\xi|^{1/4}} \exp\left(\frac{2}{3}|\xi|^{3/2}\right) \quad \text{For } \xi < o \qquad \text{-----4.21}$$

$$\phi(\xi) \approx \frac{A}{2\xi^{1/4}} \sin\left(\frac{2}{3}\xi^{3/2} + \frac{1}{4}\pi\right) \quad \text{For } \xi > o \qquad \text{-----4.22}$$

At $r = \frac{t_{Si}}{2}$, the value of $\xi = \frac{E}{F}\left(\frac{2m^* F}{\hbar^2}\right)^{1/3} > o$. Therefore the second form has to be used for this.

At $r = \frac{t_{si}}{2}$, $\psi(\xi) = 0$ and hence the second asymptotic function becomes as shown below

$$0 = \frac{A}{2\left[\frac{E_S}{F}\left(\frac{2m^* F}{\hbar^2}\right)^{1/3}\right]^{1/4}} \sin\left[\frac{2}{3}\left\{\frac{E}{F}\left(\frac{2m^* F}{\hbar^2}\right)^{1/3}\right\}^{3/2} + \frac{\pi}{4}\right]$$

$$\Rightarrow n\pi = \sin\left[\frac{2}{3}\left\{\frac{E_n}{F}\left(\frac{2m^* F}{\hbar^2}\right)^{1/3}\right\}^{3/2} + \frac{\pi}{4}\right]$$

$$\Rightarrow E_n = \left(\frac{\hbar^2}{2m^*}\right)^{1/3}\left(\frac{3}{2}\pi F\right)^{2/3}\left(n - \frac{1}{4}\right)^{2/3} \qquad \text{-----4.23}$$

For $n = 1,2,3..........$

For a moderately doped semiconductor, and at a low gate voltage there is low electron density, hence it can be considered that only the lowest sub band (n=1) is occupied.

$$E_1 = \left(\frac{\hbar^2}{2m^*}\right)^{1/3}\left(\frac{3}{2}\pi F\right)^{2/3}\left(\frac{3}{4}\right)^{2/3} \qquad \text{-----4.24}$$

Now, using the expression of E_1, the effective increase in threshold voltage can be expressed as follows

$$\Delta V_{th_qm} = \frac{E_1}{q} \qquad \text{-----4.25}$$

$$C_{ox-cyl)} = \frac{2\varepsilon_{ox}}{t_{Si}\ln\left(1+\left(\frac{2t_{ox}}{t_{Si}}\right)\right)} \qquad \text{-----4.26}$$

4.3 Effective oxide thickness increase

This effect occurs due to spatial distribution of inversion charge. The classical analysis shows peak of the inversion charge at the oxide –semiconductor interface. In case of quantum mechanical analysis, the peak of the charge distribution occurs [8] at a distance around less than a nanometer from the Si-SiO_2 interface. This leads to an effective increase in the oxide thickness, which can be found out using the following expression [9] [10]

$$t_{ox_eff} = t_{ox} + \frac{\varepsilon_{ox}}{\varepsilon_{si}} \Delta r \qquad \text{-----4.27}$$

Where

$$\Delta r = \frac{2E_n}{3q.F} \qquad \text{-----4.28}$$

Δr represents the value by which the thickness of the oxide increases and actually it is the average separation of carriers in the nth subband from the interface. The centroid of the carriers passes through a line situated at a distance Δr from the oxide–semiconductor interface. Since here only first subband is considered, consequently Δr becomes $2E_1/3q.F$.

As evident from the expression of t_{ox_eff}, that with increase in effective oxide thickness the oxide capacitance decreases leading to a decrease in lesser electrostatic coupling between the gate and the channel. This results in an effective increase in threshold voltage. In addition to this, the device transconductance is also affected by the increase in effective oxide thickness. The effective increase in threshold voltage due to increase in effective oxide thickness is given as

$$\Delta V_{T_ox_eff} = V_{T_ox_eff} - V_T \qquad \text{-----4.29}$$

4.4 Effect of Insulator nano dimension on ϕ_{eo} :

Use of silicon dioxide as sensing layer in ISFET is rare because of the following problems

i) Low pH sensitivity [11] (25-35 for pH< 7 and 37- 48 pH > 7)
ii) Hysteresis
iii) Sensitivity is pH dependent on pH range. [12]

The reason behind using silicon dioxide as sensing material despite of these drawbacks is its biocompatibility. Pure silicon dioxide is insoluble in vivo. It is indigestible, with zero nutritional value and zero toxicity. When silica is taken orally, it passes unchanged through the gastrointestinal tract, exiting in the feces, leaving no trace behind [13].

The cause of hysteresis and drift is assigned to a charge layer known as buried layer [14] and model for this charge layer effect is already available in [15] using silicon nitride. The same model can be modified for silicon dioxide, by eliminating the term for nitride site as shown below.

$$\frac{\sigma_b}{qN_S} = \left(\frac{[H^+]_{bur}^2 - K_+K_-}{[H^+]_{bur}^2 + K_+[H^+]_{bur} + K_+K} \right) \eta \left(\frac{N_{sil}}{N_S} \right) \quad \text{-----4.30}$$

$$[H^+]_{bur} = [H^+]_s \left[1 + erf\left(\frac{\rho}{2\sqrt{D_{eff}\, t}} \right) \right] \quad \text{-----4.31}$$

Where

$$erf\left(\frac{\rho}{2\sqrt{D_{eff}.t}}\right)=\frac{2}{\sqrt{\pi}}\sum_{n=0}^{\infty}\frac{(-1)^n\left(\frac{\rho}{2\sqrt{D_{eff}.t}}\right)^{2n+1}}{n!(2n+1)} \quad \text{----4.32}$$

$$D_{eff}=\frac{D}{K_{bur}N_{sil}\eta} \quad \text{-----4.33}$$

$$N_S=(1+\eta).N_{sil} \quad \text{-----4.34}$$

η is around 10% of total number of sites [15].

When the cylindrical ISFET is scaled to nano dimension and the factor 'ρ' assumes a very small value leading to ρ <<1. Consequently the error function 'erf' becomes [16]

$$erf\left(\frac{\rho}{2\sqrt{D_{eff}.t}}\right)=\frac{2}{\sqrt{\pi}}\exp\left\{\left(-\frac{\rho}{2\sqrt{D_{eff}.t}}\right)^2\right\}\left[\frac{\rho}{2\sqrt{D_{eff}.t}}+\frac{2\left(\frac{\rho}{2\sqrt{D_{eff}.t}}\right)^3}{1.3}+\frac{4\left(\frac{\rho}{2\sqrt{D_{eff}.t}}\right)^5}{1.3.5}+----\right]$$

-----4.35

It evident from the definition of buried site and form existing literature that buried site lays few nanometer from the insulator surface. Consequently when the thickness of the insulator reduces and should disappear below a particular thickness. If this factor is taken into account, then there will not be any buried site in a nano ISFET and consequently the electrolyte oxide interface

potential will be reduced by η%. The diffusion of hydrogen ions through Silicon Dioxide is still there and will be trapped at the semiconductor insulator interface, but the settling time of the ISFET will be much less, because after diffusion there will not be any buried site for binding.

4.5 Conductance of the nano Cylindrical ISFET:

The channel conductance of a MOSFET is given as [18]

$$g_D = \left.\frac{dI_{DN}}{dV_{DS}}\right|_{V_G = const} = \mu C_{ox}\frac{W}{L}(V_G - V_{th}) \quad \text{for small value of } V_{DS} \qquad \text{----4.36}$$

From this equation the conductance of a cylindrical ISFET at nano size is given as follows

$$g_D = \left.\frac{dI_{DN}}{dV_{DS}}\right|_{V_{reference} = const} = \mu C_{ox_cyl}\left(\frac{\pi\left[t_{Si}^2 - (t_{Si} - t_{inv})\right]^2}{4L.t_{inv}}\right)\left(V_{reference} - V_{th_cyl(isfet)}\right) \qquad \text{--4.37}$$

4.6 Parameter Fluctuation in very small sensor:

In addition to the effects discussed in 4.2, 4.3 and 4.4, some other effects also surfaces in different form leading to parameter fluctuation [19] in a very small sensor.

The variation in number of dopant atom and their position in a decanometer device make each device different [20]. The intrinsic parameter fluctuation associated with discrete random dopant leads to fluctuation in threshold voltage of the device.

Another source of parameter fluctuation in MOS device is trapping of charge near the Si/SiO_2 interface. This may happen in an ISFET during pH measuring process due to diffusion of H^+ ions through the SiO_2 layer [21]. The resulting effect is a local modulation of carrier density and local mobility variation. This will lead to variation of drain current [22].

Atomic scale roughness of the Si/SiO_2 is another source [23] of parameter fluctuation in a nanoscale device. The roughness at the oxide semiconductor interface results in significant oxide thickness variation. This will lead to variation of oxide capacitance and hence the bulk potential and the threshold voltage also vary.

Another leading cause of parameter fluctuation is line edge roughness (LER) [24, 25] caused by

a. Inherent tolerance of the material.
b. Tool used in lithography process.

At nanometer dimension, threshold voltage variation is significant due to line edge roughness [19]. Fortunately cylindrical devices have only two edges as compared to four in a planar device. Hence it can be assumed that parameter fluctuation due to LER effect will be less in a cylindrical ISFET device.

4.7 Simulation results and conclusions

Figure 4.3 shows the threshold voltage shift due to quantum mechanical effects (QME) vs. diameter of the silicon pillar of the cylindrical ISFET. With decrease in diameter of the silicon pillar, the quantum confinement becomes tighter leading to larger shift of threshold voltage at smaller size.

Figure 4.4: shows Δr vs. total carrier concentration. The inversion layer centroid moves away from the oxide semiconductor interface, as the total carrier concentration decreases. In this work, with all the selected parameters, gives a

variation of threshold voltage in the range of 7.7084 (at pH=1) to 8.3994 (at pH=14). When the threshold voltage varies in this range, the total carrier concentration varies from 5.43×10^{17} to 3.83×10^{17}. The corresponding variation in Δr is 0.697nm to 0.784nm. In the following analysis, for the sake of simplicity, the average of these two values has been considered.

Figure 4.5, shows the relationship between the drain current vs. voltage applied to the reference electrode at pH=4 with and without considering QME at t_{si}=10nm. There is considerable reduction in drain current is observed in the curve that includes QME. This is mainly due to two factors. When QME is included, first the conduction band goes up, secondly due to shift of inversion layer centroid, the effective gate capacitance decreases. Both of these causes increase in threshold voltage of the ISFET. The other factor is reduction of device transconductance. This reduction of transconductance occurs due to reduction of gate capacitance.

Figure 4.6 and 4.7 also shows the relationship between the drain current vs. voltage applied to the reference electrode, at pH=7 and pH=10 respectively, with and without considering QME at t_{si}=10nm.

Figure 4.8 shows Drain current vs. voltage applied to the reference electrode at pH=4 and at different diameter of the silicon pillar. As the device dimension decreases, QME becomes more intense and consequently drain current reduces. At t_{si} =20 nm current is highest among the shown curves and as the thickness of the silicon pillar decreases current decreases. At t_{si} =5 nm current is minimum.

Figure 4.9 and 4.10 also shows Drain current vs. voltage applied to the reference electrode, at pH = 7 and pH =10 respectively and at different diameter of the silicon pillar.

Figure 4.11 shows the output characteristics or the relationship between drain current and drain to source voltage of the cylindrical ISFET at t_{si}=10nm.From the figure, it is clearly visible how the current decreases with quantum mechanical effects. At this size of the device, the current reduces up to 16 %.

Figure 4.12 shows the electrolyte oxide interface potential a function of pH at a thickness less than 3nm. At this dimension, the buried sites are not present in the insulator and consequently the total number of binding site decreases. This leads to reduction of electrolyte oxide interface potential. When this effect is included in the cylindrical ISFET equations (including QME) the results given in figure 4.13 is obtained. In this figure it is seen that at pH=4 the current decreases when the effect of nano dimension insulator is considered but at pH=7 and pH=10, the value of drain current increases while considering the same effect. The reason for this opposite nature of the current deviation is pH_{pzc} of the insulator. Here pH_{pzc} =4.2. Consequently at pH=4, the electrolyte oxide interface potential obtained is positive and for the other two value of pH, the electrolyte oxide interface potential is negative. Due to this, the observed trend of variation is obtained.

Fig.4.14 shows relationship between amperometric sensitivity and pH for the cylindrical ISFET with and without considering nano dimension effects (QME and insulator behavior at nano dimension). Reduction of amperometric sensitivity is clear in this figure.

Fig. 4.15 shows the differential conductance of the Cylindrical ISFET at nano dimension vs. pH. The differential conductance decreases wit increase in pH. The threshold voltage of the device increases with increase in pH. This result in decrease in differential conductance as the pH increases. This result is showing a similar trend as demonstrated in [17] and much higher conductance is observed.

Fig.4.16 displays the shift of differential conductance of the Cylindrical ISFET at nano dimension vs. pH, as the voltage applied to the reference electrode is increased.

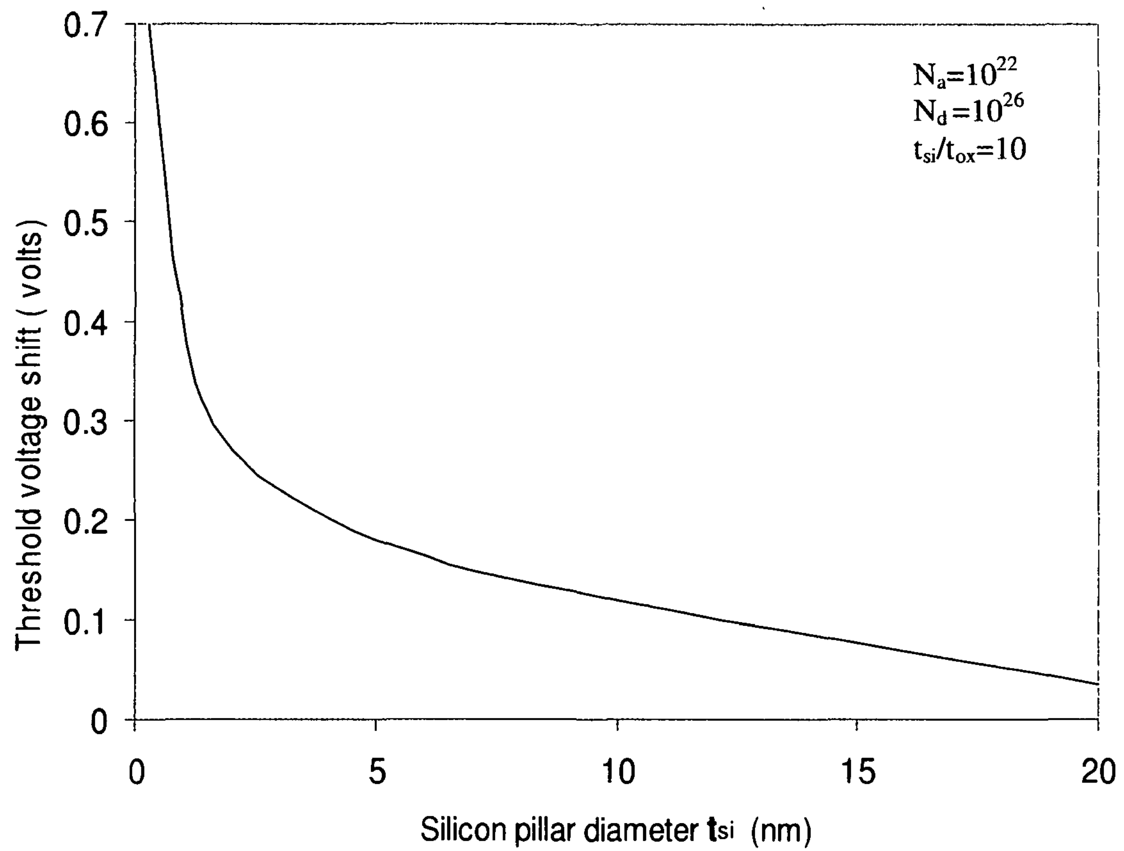

Fig.4.3: Threshold shift vs. silicon pillar diameter

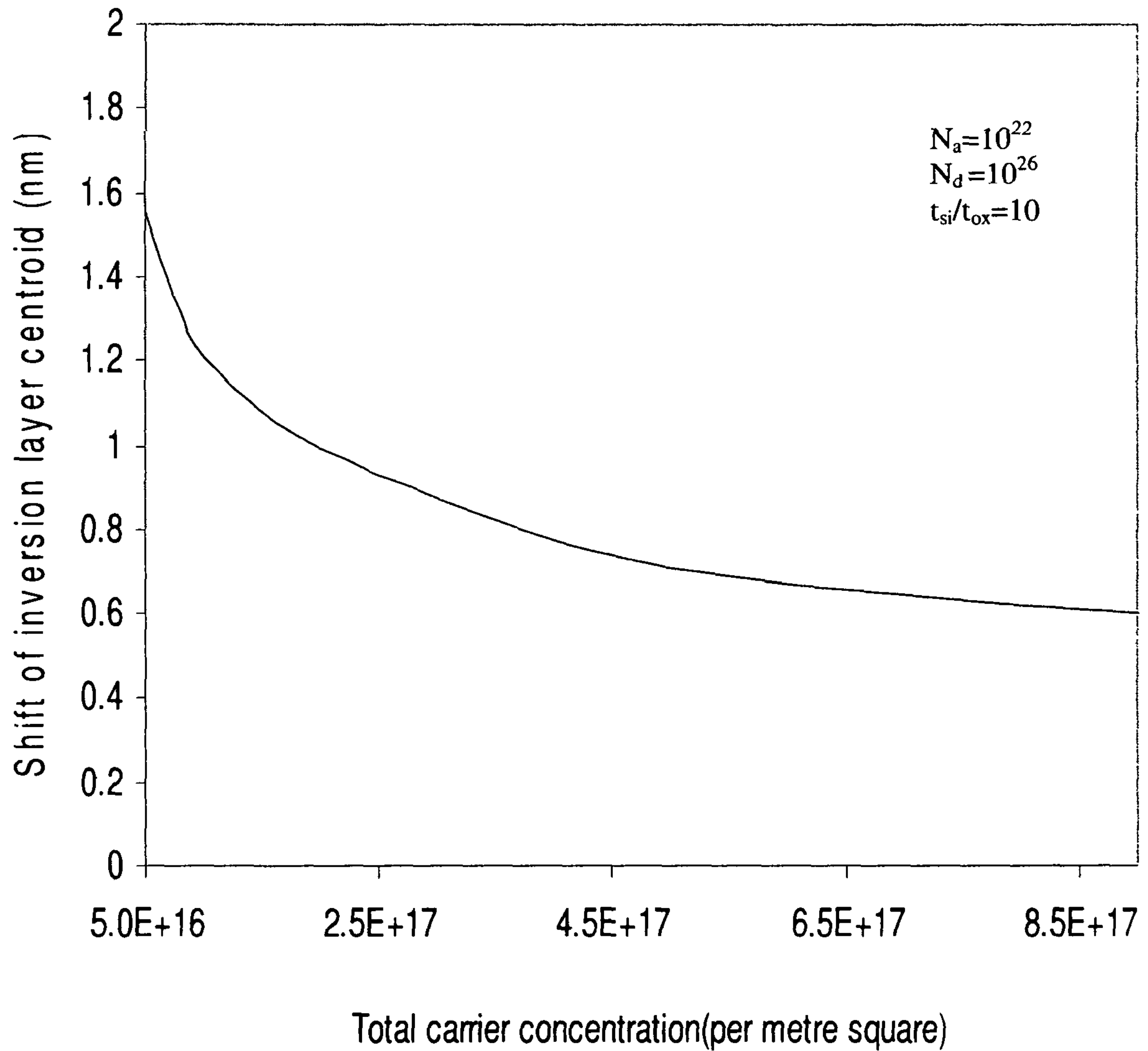

Fig.4.4 shift of inversion layer centroid (Δr) vs. total carrier concentration (Inversion and depletion charges)

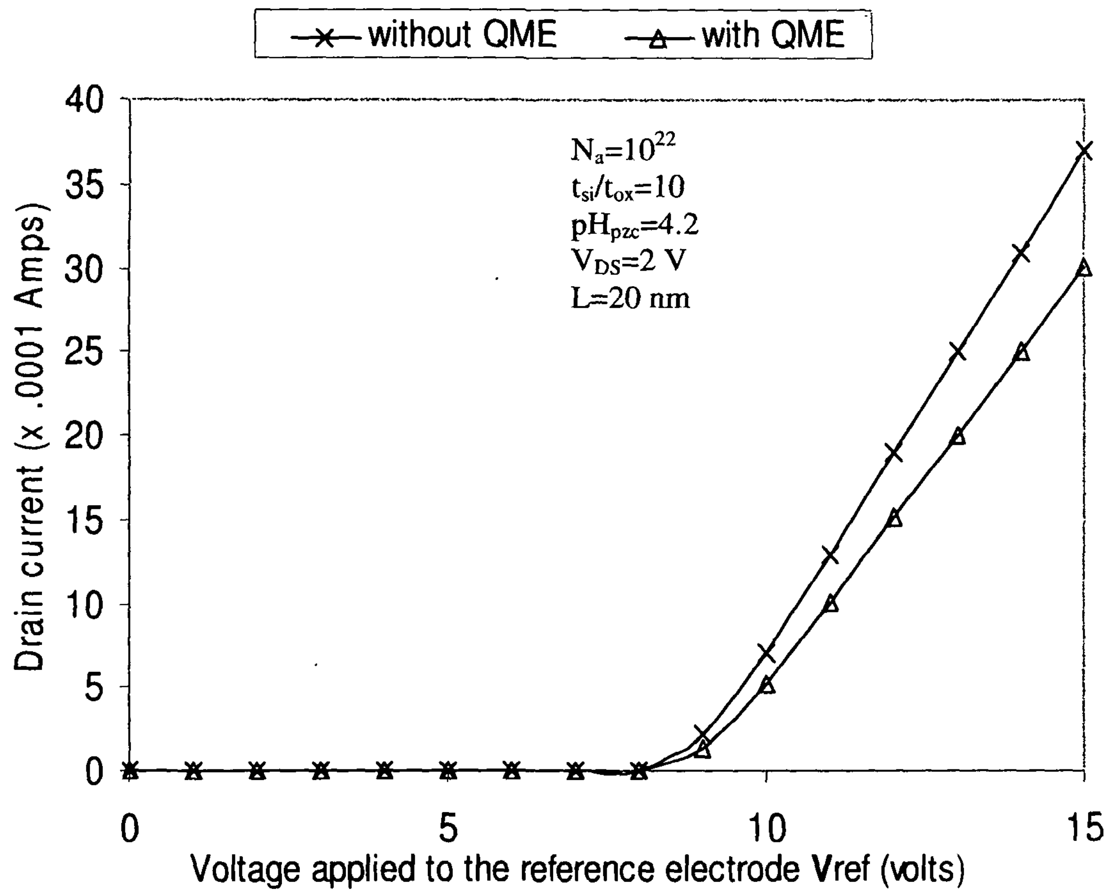

Fig.4.5: Drain current vs. voltage applied to the reference electrode at pH=4, t_{si}=10nm

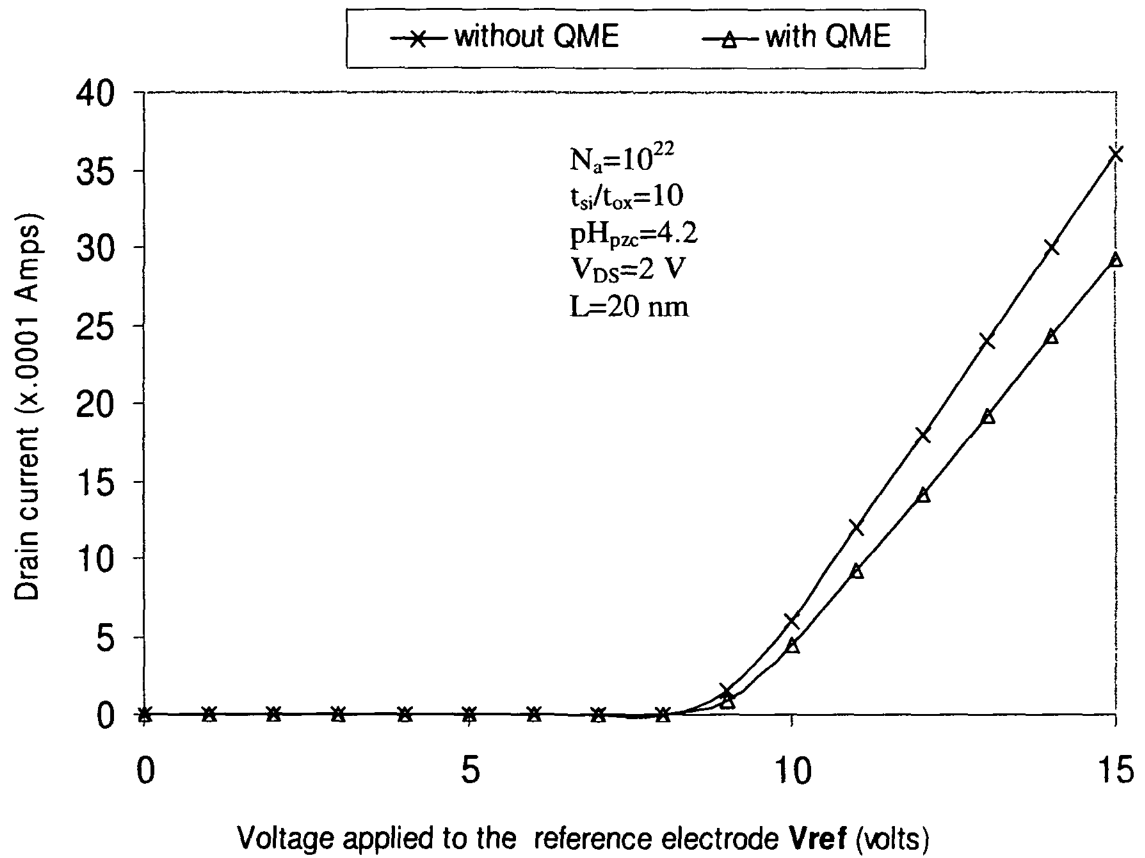

Fig.4.6: Drain current vs. voltage applied to the reference electrode at pH=7, t_{si}=10nm

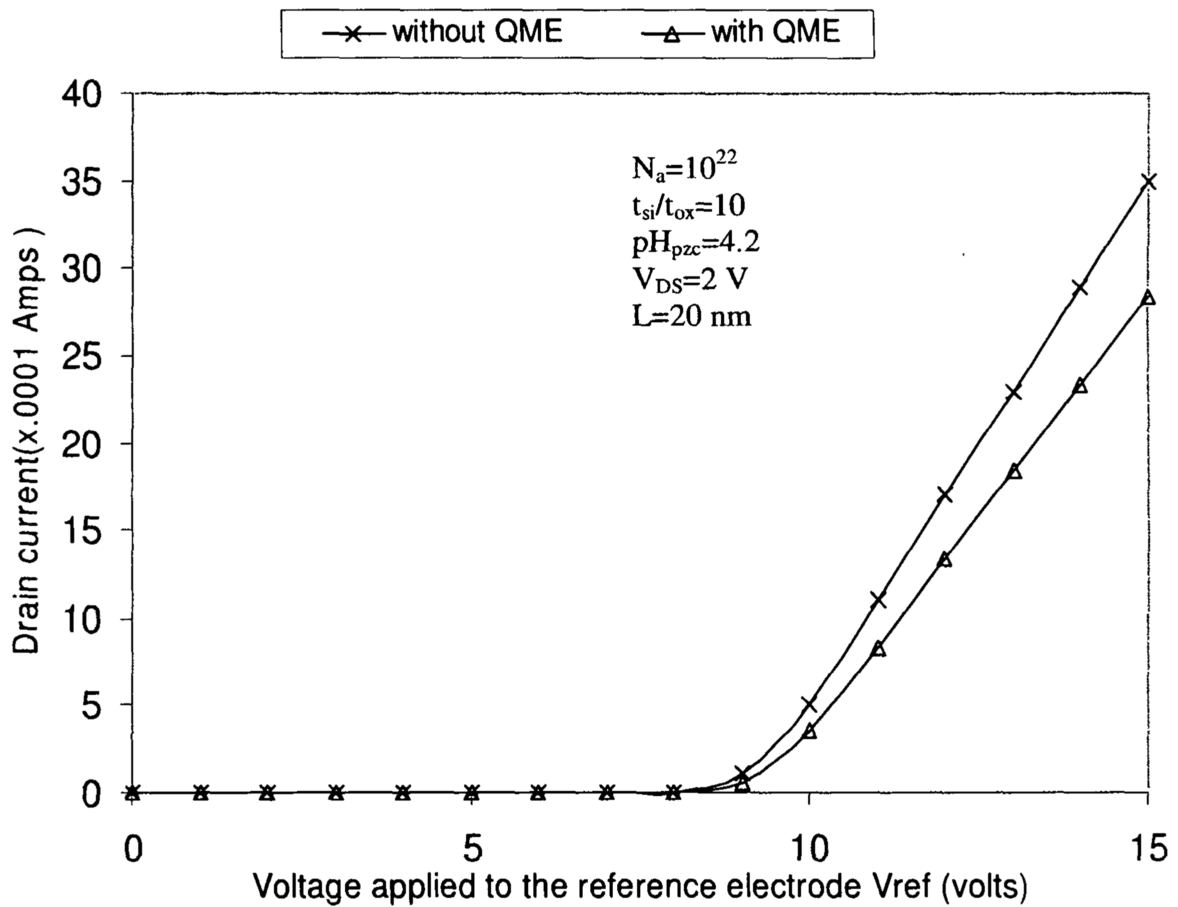

Fig.4.7: Drain current vs. voltage applied to the reference electrode at pH=10 and t_{si}=10nm

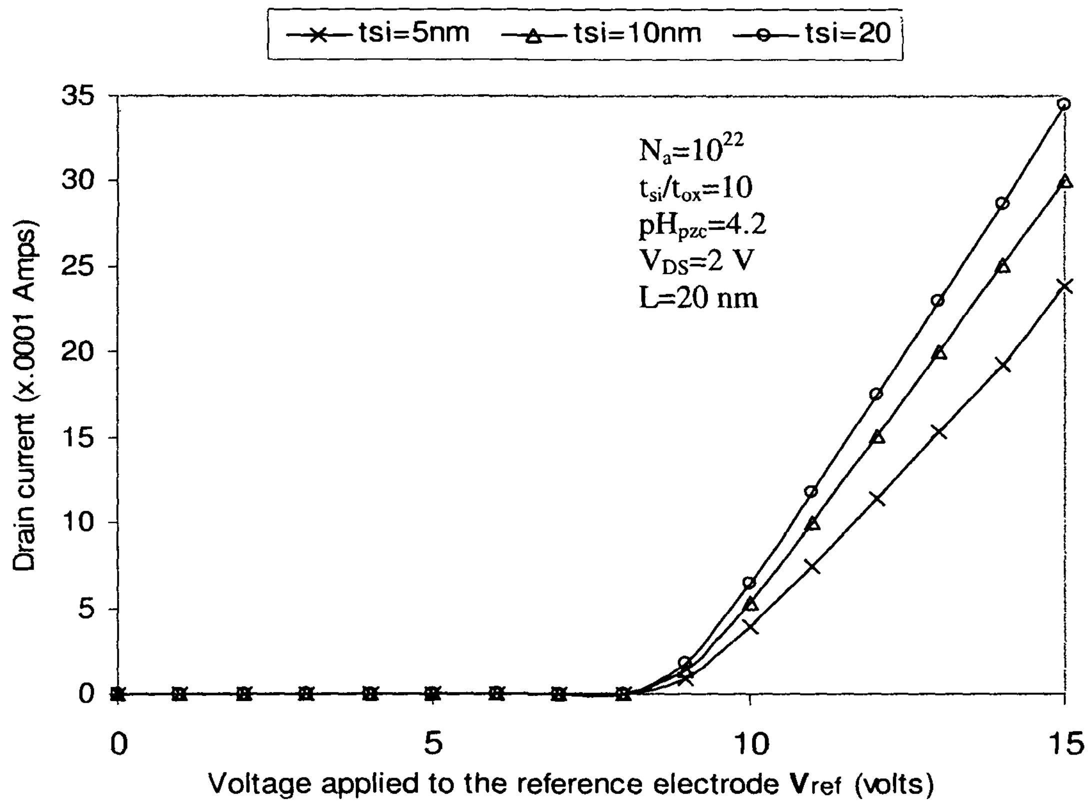

Fig.4.8: Drain current vs. voltage applied to the reference electrode at pH=4, t_{si}=5nm, t_{si}=10nm and t_{si}=20nm

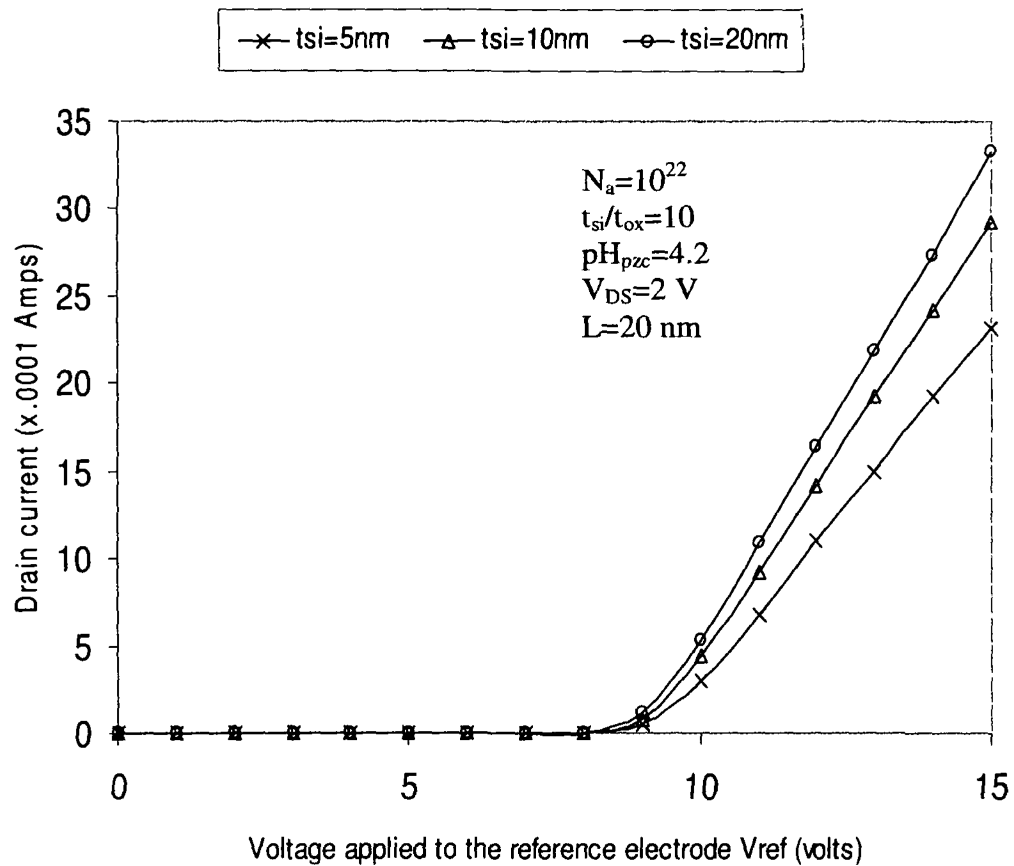

Fig.4.9: Drain current vs. voltage applied to the reference electrode at pH=7, t_{si}=5nm, t_{si}=10nm and t_{si}=20nm

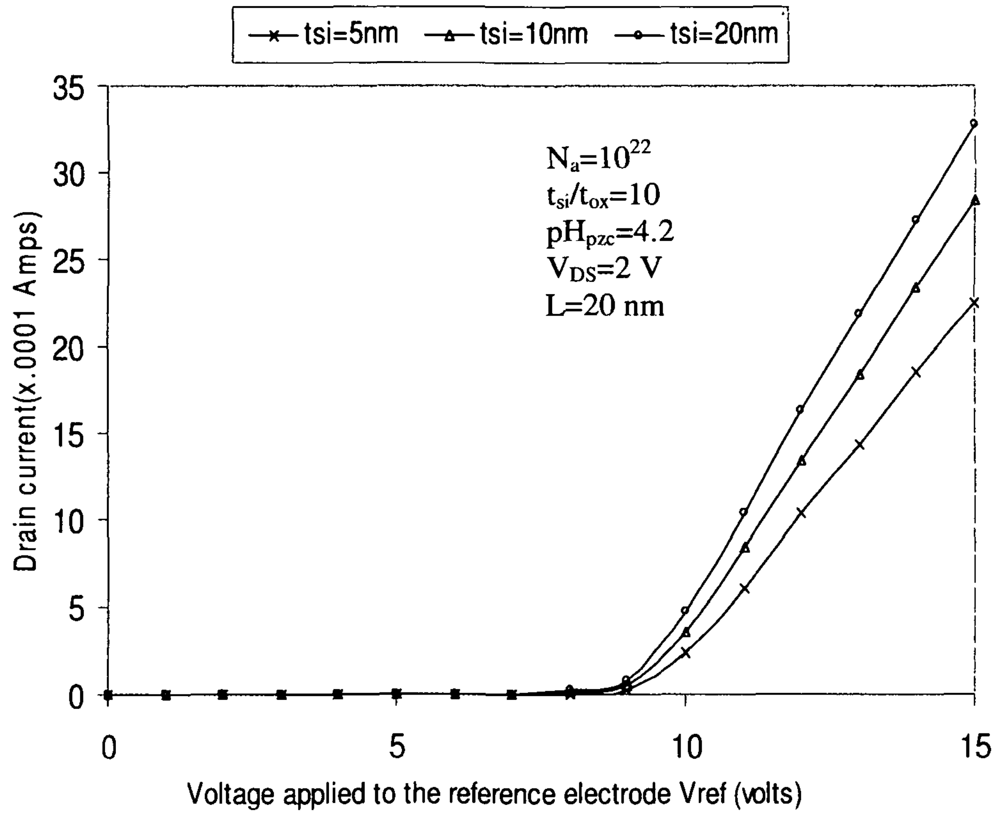

Fig.4.10: Drain current vs. voltage applied to the reference electrode at pH=10, t_{si}=5nm, t_{si}=10nm and t_{si}=20nm

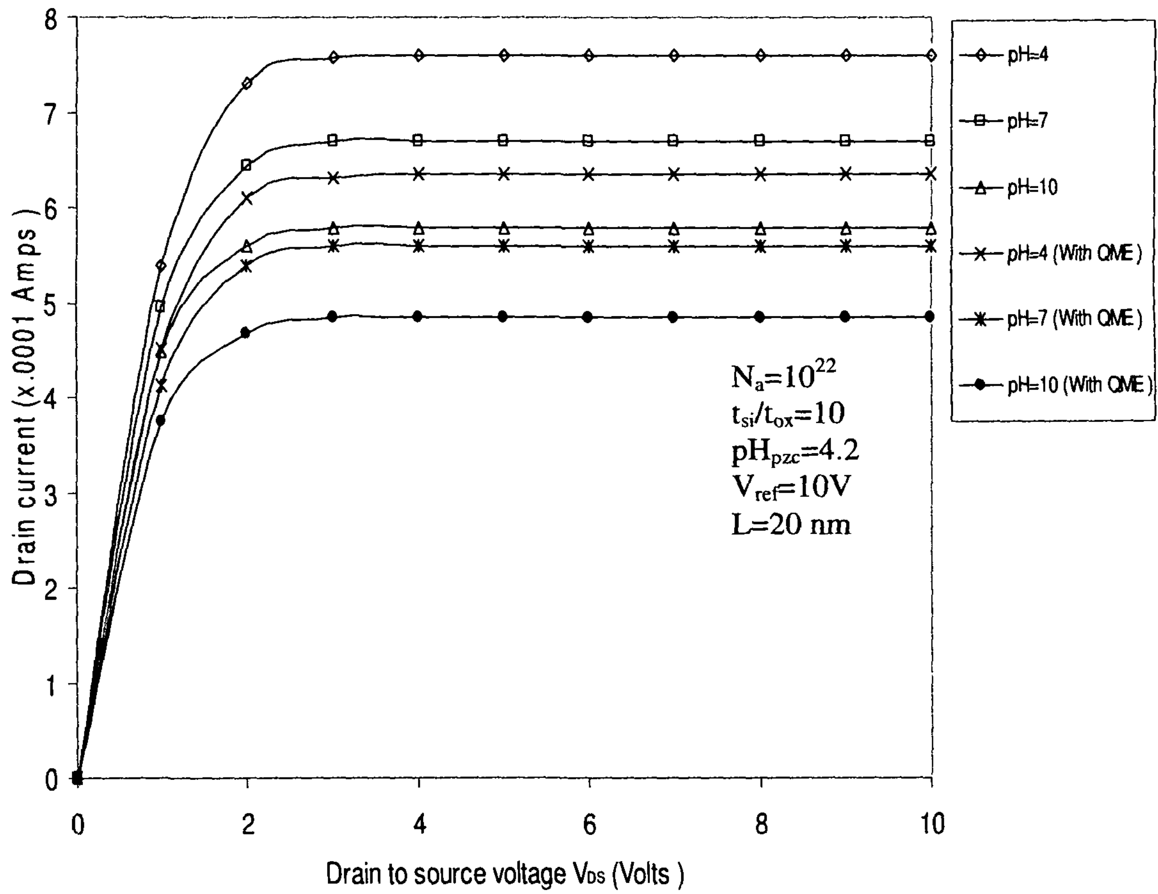

Fig.4.11: Drain current vs. drain to source voltage (t_{si}=10nm)

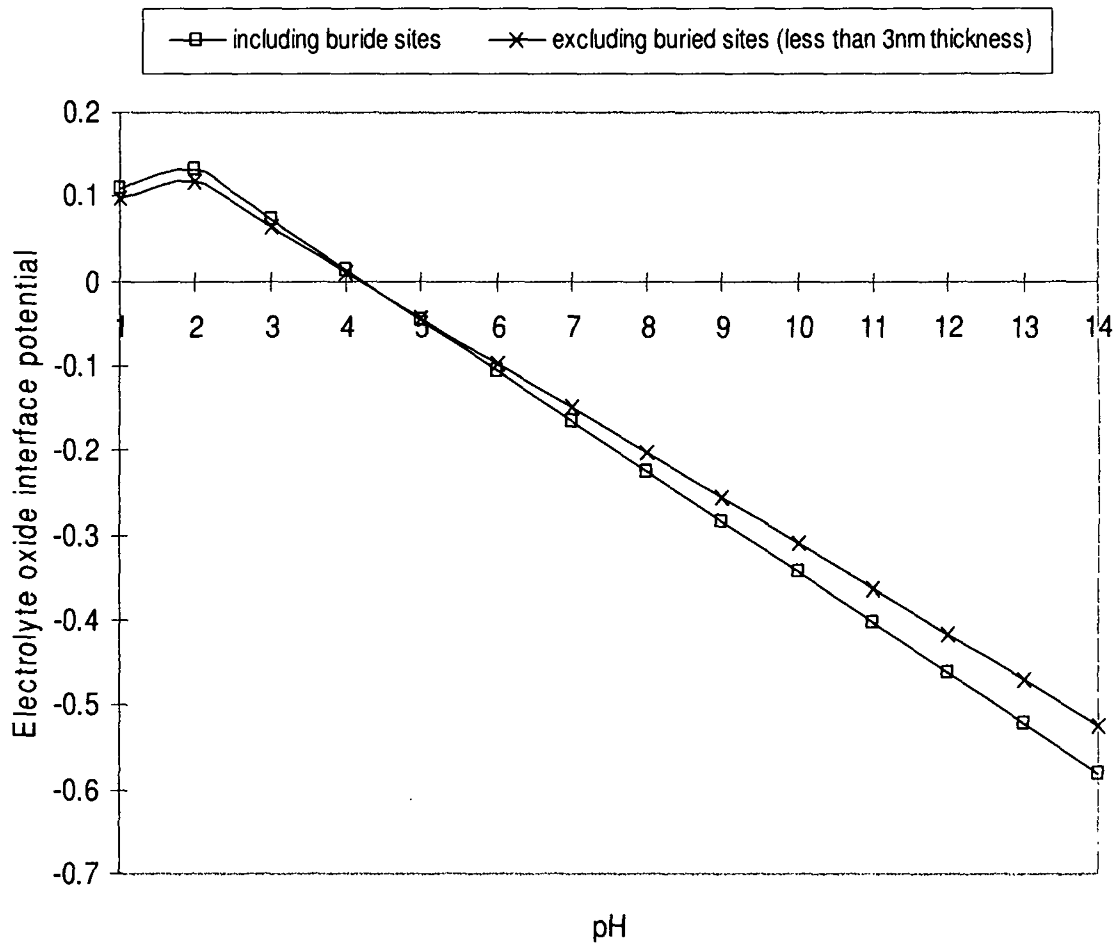

Fig.4.12: Variation of Electrolyte oxide interface potential vs. pH at nano dimension.

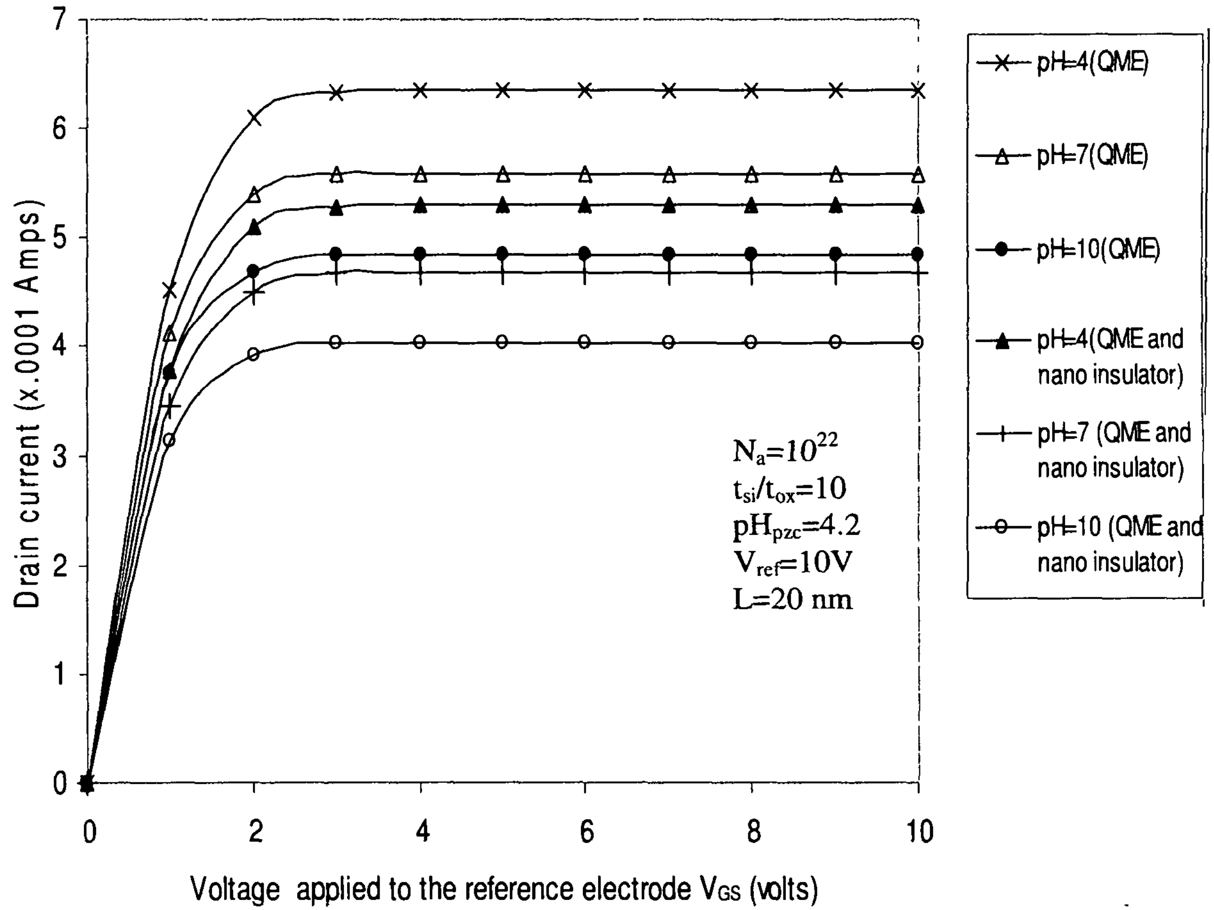

Fig.4.13 Drain current vs. drain to source voltage at t_{si}=10nm (including QME only and QME+ effect of nano dimension insulator)

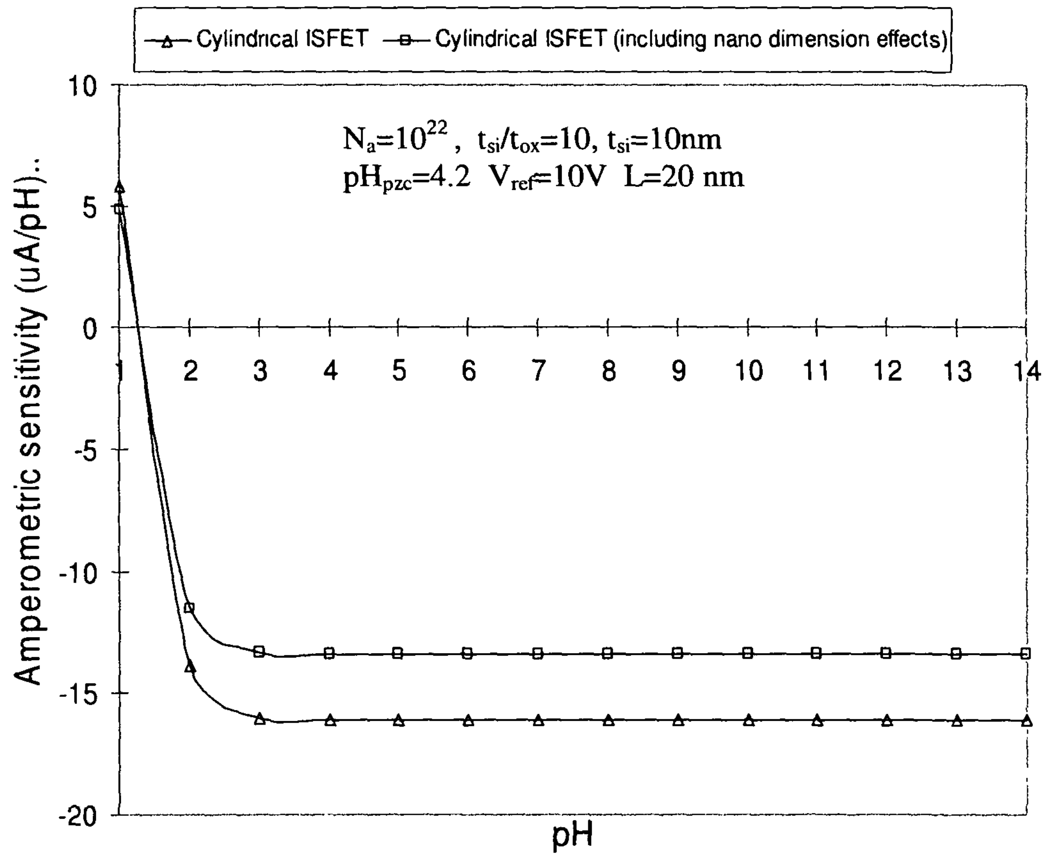

Fig.4.14: Amperometric sensitivity vs. pH

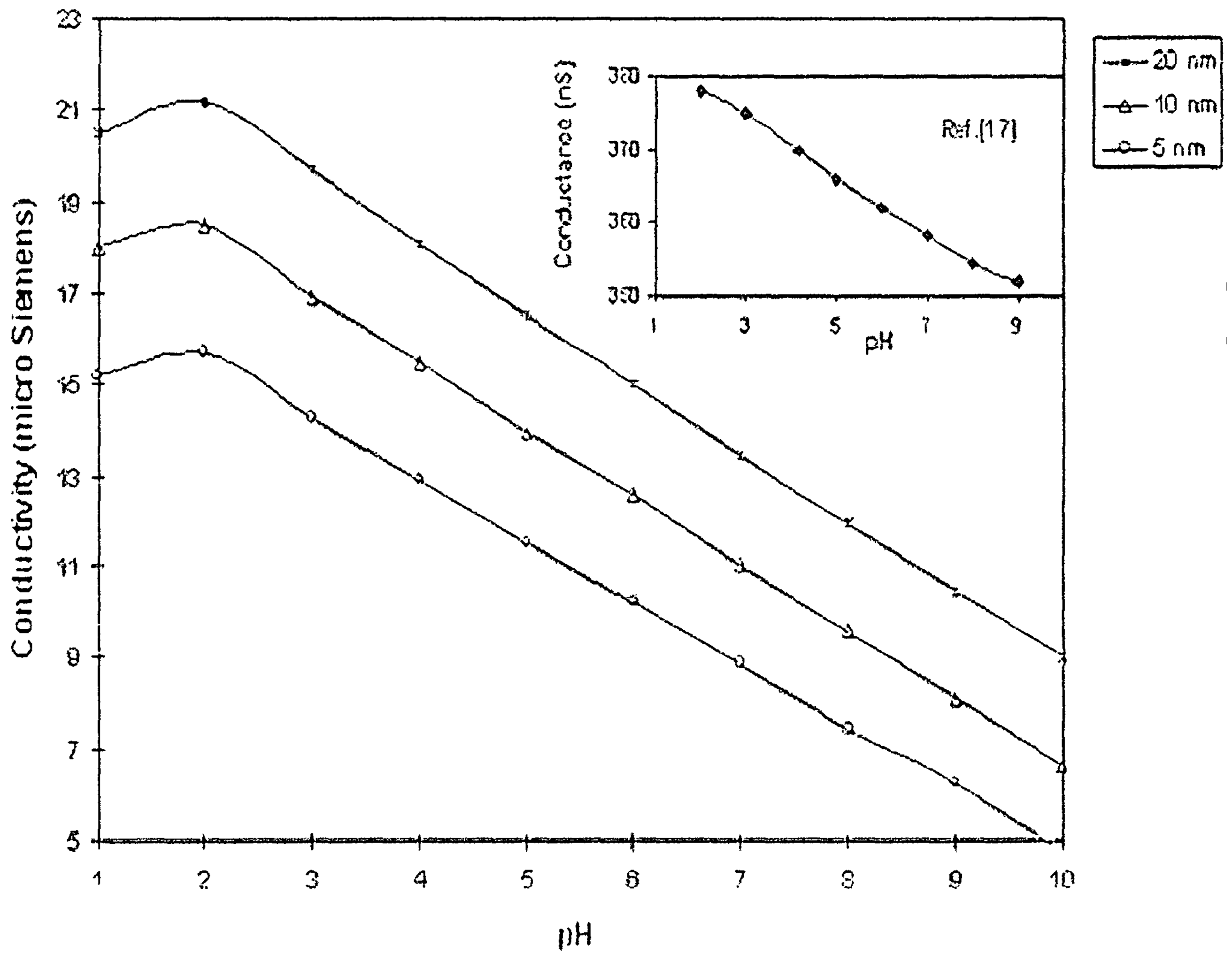

Fig. 4.15: Conductivity of the cylindrical ISFET at nano dimension vs. pH at V_{ref}= 8.5 volts

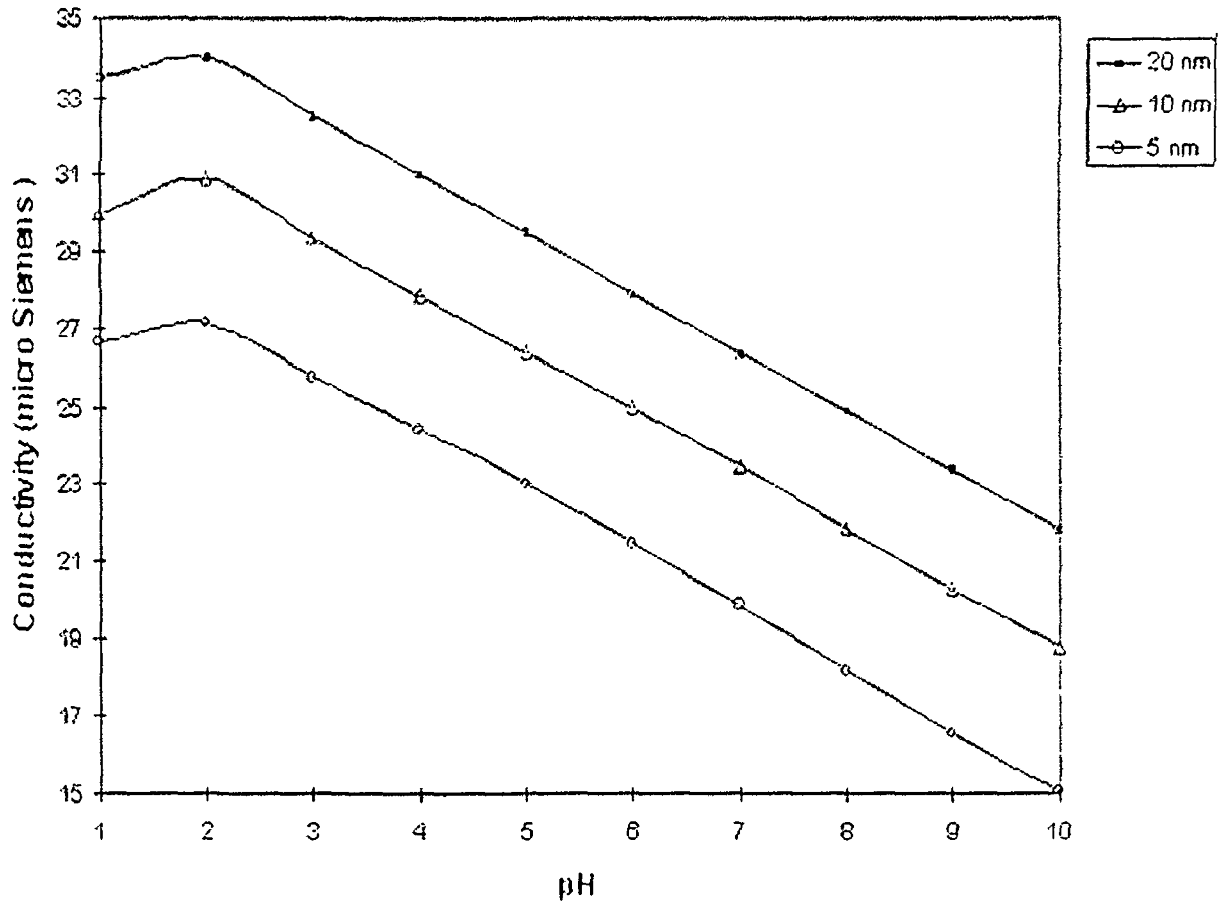

Fig. 4.16: Conductivity of the cylindrical ISFET at nano dimension vs. pH at V_{ref}=9volts

4.8 References

1. Stephen J. Pearton, Tanmay Lele, Yiider Tseng, F Ren "Penetrating living cells using semiconductor nanowires" TRENDS in Biotechnology, Vol. 25, No. 11, pp.481-482, 2007.
2. Tina Mangla, *Modeling, Simulation and Characterization of Nanoscale MOSFETs with quantum mechanical Effects and gate stack engineering for ULSI,* Ph.D Thesis, Delhi University, 2006.
3. D. Vasileska, "SCHRED-2.0 Manual," Arizona State University, Tempe, RZ, Feb. 2000.
4. Jasprit Singh, *Quantum Mechanics Fundamentals and Applications to Technology*, John Wiley and Sons, Inc. 1997
5. Tomasz Janik, Bogdan Majkusiak "Analysis of the MOS Transistor Based on the Self-Consistent Solution to the Schrodinger and Poisson Equations and on the Local Mobility Model" IEEE Transactions on Electron Devices, Vol. 45, No. 6,pp.1263-1271, 1998.
6. S L Jang, S S Liu "An Analytical Surrounding Gate MOSFET Model" Solid State Electronics Vol.42, No.5, pp721-726, 1998.
7. Ben G Streetman, Sanjay Banerjee, *Solid State Electronic Devices,* 5th Ed. Prentice Hall of India Private Limited, 2001.
8. Swagata Bhattacharjee, Abhijit Biswas "Modeling of threshold voltage and subthreshold slope of nanoscale DG MOSFETs" Semiconductor Science and Technology 23(2008) 015010 (8pp), IOP publishing.
9. J P Xu, Y P Li, P T Lai, W B Chen, S G Xu, J G Guan "A 2D threshold voltage model for small MOSFET with quantum –mechanical effects" Microelectronics Reliability Vol. 48, Issue 1, , pp. 23-28, 2008
10. Frank Stern "Self Consistent Results for n-Type Si Inversion Layers" Physical Review B, Vol. 5 No. 12,15 June, pp. 4891-4899,1972

11. T. Matsu, M. Esashi "Methods of ISFET fabrication" Sensors and Actuator, Vol.1, pp.77-96, 1981.
12. Kim R Roger, Ashok Mulchandani, *Affinity Biosensors, Techniques and Protocols,* Humana Press, Totowa, New Jersy , pp77-96,1998.
13. Web source http://en.wikipedia.org/wiki/Silicon_dioxide
14. Massimo Grattarola, Giuseppe Massobrio, *Bioelectronic Handbook: MOSFETs, Biosensors and Neurons,* Mc Graw-HILL, New York. 1998.
15. Sergio Martinoia, Giuseppe Massobrio, Leandro Lorenzelli "Modeling ISFET microsensor and ISFET based Microsystems: a review" Sensor and Actuator, B-105, pp 14-17, 2005.
16. Web source : http://mathworld.wolfram.com/Erf.html
17. Yu Chen, Xihua Wang, Shyamsunder Erramilli and Pritiraj Mohanty "Silicon Based nanoelectronic field effect pH sensor with local gate control" Applied Physics Letter, Vol. 89, Issue 22, 29 November 2006.
18. S.M. Sze, *Semiconductor Devices, Physics and Technology,* 2nd ed, John Wiley and Sons,Inc.
19. Asen Asenov, Andrew R Brown, John H Davies, Savas Kaya and Gabriela Slavcheva " Simulation of Intrinsic parameter Fluctuations in Decananometer and Nanometer Scale MOSFETs", IEEE Transaction on Electron Devices, Vol. 50, No.9, pp.1837-1852,September, 2003.
20. T. Mizuno, J. Okamura, and A. Toriumi, "Experimental study ofthreshold voltage fluctuation due to statistical variation of channel dopant number in MOSFETs," IEEE Trans. Electron Devices, vol. 41,pp. 2216–2221, Nov. 1994.
21. K.K.Hung,P.K.Ko,C.Hu,andY.C.Cheng,"Random telegraph noise of deep-submicrometer MOSFETs," IEEE Electron Device Lett., vol.11, pp. 90–92, Feb. 1990.

22. A. Avellan, W. Krautschneider, and S. Schwantes, "Observation and modeling of random telegraph signals in the gate and drain currents of tunnelling metal-oxide-semiconductor field-effect transistors," Appl. Phys. Lett., vol. 78, pp. 2790–2792, 2001.
23. S. Thompson, M. Alavi, R. Argavani, A. Brand, R. Bigwood, J. Brandenburg, B. Crew, V. Dubin, M. Hussein, P. Jacob, C. Kenyon, E. Lee, M. Mcintyre, Z. Ma, P. Moon, P. Nguyen, M. Prince, R. Schweinfurth, S. Shvakumar, P. Smith, M. Stettler, S. Tyagi, M. Wei, J. Xu, S. Yang, and M. Bohr, "An enhanced 130 nm generation logic technology featuring 60nm transistors optimized for high performance and low power at 0.7–1.4 V," in IEDM Tech. Dig, 2001, pp. 257–260
24. P.Oldiges, Q.Lin,K.Pertillo, M.Sanchez, M.Ieong, and M.Hargrove, "Modeling line edge roughness effects in sub 100 nm gate length devices," in Proc. SISPAD, vol. 31, 2000.
25. S. Kaya, A. R. Brown, A. Asenov, D. Magot, and T. Linton, "Analysis of statistical fluctuations due to line edge roughness in sub 0.1 "m MOSFETs," in Simulation of Semiconductor Processes and Devices, D. Tsoukalas and C. Tsamis, Eds. Vienna, Austria: Springer-Verlag, 2001, pp. 78–81.

Chapter 5

Response of ISFET as a function of Reference electrode position and determination of a rule for reference electrode placement

5.1 Introduction

A Reference electrode is an ideal non polarisable electrode [1]. It has a stable and well-known electrode potential [2]. In a pH measuring system using ISFET, the gate circuit is completed by a reference electrode immersed in the electrolyte [3]. The voltage applied to this reference electrode can suitably change the conductance of the ISFET device. There are debates regarding the need of reference electrode [3]. The gate of a MOSFET or ISFET consists of a capacitance and to turn on the device, it is necessary to charge the capacitance. This means it needs two connections, one is silicon and the other one is the electrolyte [3]. The electrolyte terminal is connected via a reference electrode to the second terminal of the voltage source. The voltage applied to the reference electrode can keep the ISFET in the active/ saturation region so that any change in the electrolyte oxide interface potential (due to change in pH) can directly change the current flowing through the drain. In some cases (Silicon Nanowire) the change in current is obtained only by chemical gating and in the other, the modulation of conductivity of such nanowire is achieved by putting a side gate. A side gate may be very good for modulation of conductivity, but the lateral electric field component will lead to mobility degradation of electrons due to additional scattering from the wire boundary, which is already high in case of a nanowire [4]. A surrounding reference electrode can of course minimize this mobility degradation effect. Introduction of a surrounding electrode with a cylindrical ISFET will increase the size of the pH measuring system. Consequently it is necessary to see how nearer the reference electrode can be placed to the ISFET without compromising the sensor response.

In this chapter a novel attempt is made for modeling ISFET response as a function of position of the reference electrode from the OHP. The potential responsible for the ISFET response is the electrolyte oxide interface potential.

This potential is the potential between the insulator surface and the bulk electrolyte. In this chapter a functional relation has been established between ISFET response (ϕ_{eo}) as a function of the distance of the reference electrode from the OHP. Initially this model is developed for a planar device and then for a cylindrical device and finally a comparison is done between the two. The analysis was done in one dimension.

Potential profile in the Electrolyte Insulator Semiconductor (EIS) structure [5] is shown in fig 5.1.As we proceed from the insulator surface towards the electrolyte bulk through the IHP and OHP, the potential gradually die out. When the reference electrode is placed in bulk electrolyte (at a considerable distance from the OHP), full electrolyte oxide interface potential is available between the insulator surface and reference electrode as shown in fig 5.1. This figure shows the potential profile for $pH>pH_{pzc}$. In the figure 5.2 the reference electrode is placed inside the diffuse layer where the ionic concentration is different from the bulk electrolyte. In this part the potential is also different. From these two figures we can see that when we bring the reference electrode closer from the bulk electrolyte to the diffused layer, the effective electrolyte oxide interface potential available across the reference electrode and insulator surface decreases. Due to this the semiconductor surface potential decreases ($\phi_{s1} < \phi_s$), and leads to lesser charge in the inversion layer. This causes the drain current to decrease.

5.2 Model formulation

As evident from the discussion in the above paragraph and the Fig 5.1 and Fig 5.2 that the variation of potential due to change in the position of reference electrode is dependent on the potential variation inside the diffused layer. This

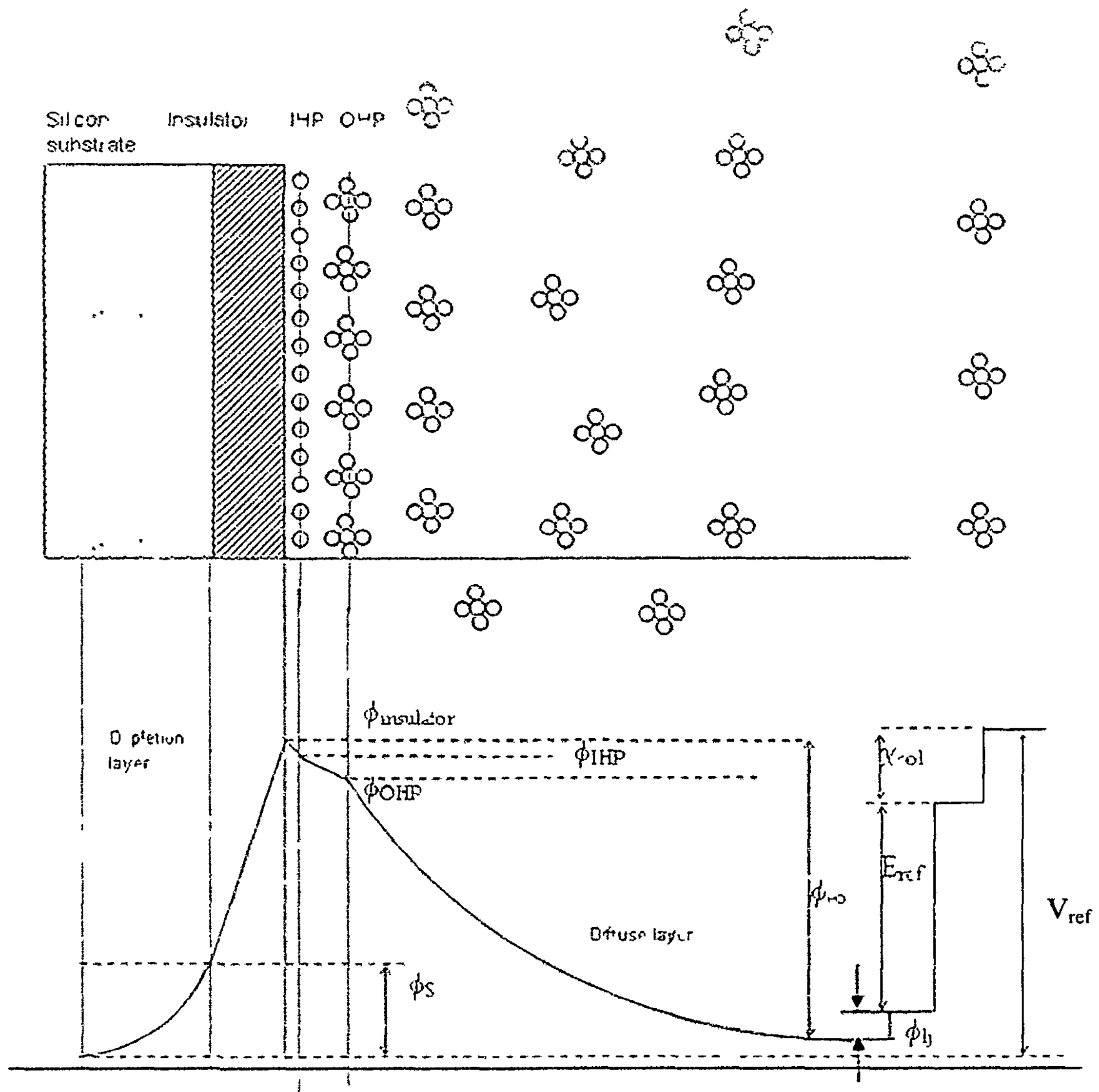

Fig.5 1 Potential profile of the Electrolyte Insulator Semiconductor structure for a planar surface when the reference electrode is placed in the bulk electrolyte i.e. sufficiently away from the OHP

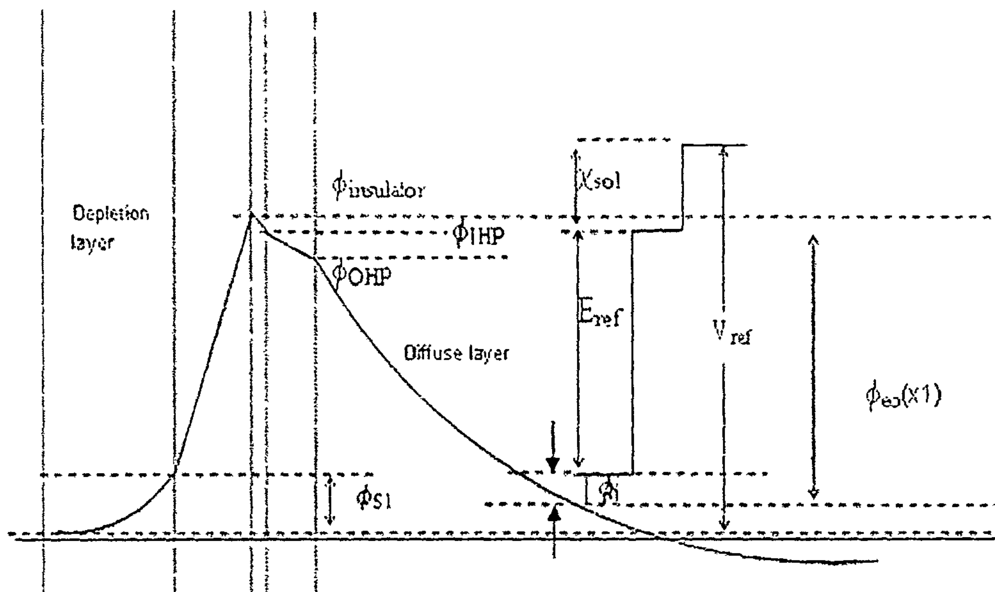

Fig. 5.2: Potential profile of the Electrolyte Insulator Semiconductor structure for a planar surface when the reference electrode is placed inside the diffuse layer.

potential variation can be easily obtained by solving the Poisson Boltzmann Equation (PBE) with the given boundary condition [6]

The PBE for a planer surface

$$\frac{d^2\phi}{dx^2} = -\frac{\sum_{i=1}^{N} c_i^{bulk} z_i q.e^{\frac{-z_i q\phi}{k_B T}}}{\varepsilon_o \varepsilon_r} \qquad \text{---------5.1}$$

With the following simple transformation,

$$\frac{d^2\phi}{dx^2} = \frac{1}{2}\frac{d}{d\phi}\left(\frac{d\phi}{dx}\right)^2 \qquad \text{---------5.2}$$

The above equation can be converted to

$$\frac{1}{2}\frac{d}{d\phi}\left(\frac{d\phi}{dx}\right)^2 = -\frac{\sum_{i=1}^{N} c_i^{bulk} z_i q.e^{\frac{-z_i q\phi}{k_B T}}}{\varepsilon_o \varepsilon_r} \qquad \text{--------5.3}$$

$$\Rightarrow d\left(\frac{d\phi}{dx}\right)^2 = -\frac{2\sum_{i=1}^{N} c_i^{bulk} z_i q.e^{\frac{-z_i q\phi}{k_B T}}}{\varepsilon_o \varepsilon_r} d\phi \qquad \text{---------5.4}$$

$$\Rightarrow \int d\left(\frac{d\phi}{dx}\right)^2 = \int -\frac{2\sum_{i=1}^{N} c_i^{bulk} z_i q.e^{\frac{-z_i q\phi}{k_B T}}}{\varepsilon_o \varepsilon_r} d\phi + C_1 \qquad \text{---------5.5}$$

$$\Rightarrow\left(\frac{d\phi}{dx}\right)^2=\frac{2K_BT}{\varepsilon_o\varepsilon_r}\sum_{i=1}^{N}c_i^{bulk}e^{-z_iq\phi/K_BT}+C_1 \qquad \text{----------5.6}$$

Where C_1 is constant of integration and can be found by using the boundary conditions given below

$$x=0 \qquad \phi=\phi_{co} \qquad \text{----------5.7}$$

$$x=\alpha \qquad \phi=0 \qquad \text{And} \qquad \frac{d\phi}{dx}=0 \qquad \text{----------5.8}$$

Using these conditions, we get

$$C_1=-\frac{2K_BT}{\varepsilon_o\varepsilon_r}\sum_{i}^{N}c_i^{bulk} \qquad \text{---------5.9}$$

Putting this expression of C_1 in the equation 5.6 we get

$$\Rightarrow\left(\frac{d\phi}{dx}\right)^2=\frac{2K_BT}{\varepsilon_o\varepsilon_r}\sum_{i=1}^{N}c_i^{bulk}\left(e^{-z_iq\phi/K_BT}-1\right) \qquad \text{---------5.10}$$

In this analysis a symmetric 1:1 electrolyte is considered i.e.

$$|z_+|=|z_-|=z=1 \qquad \text{--------5.11}$$

$$c_{+}^{bulk} = c_{-}^{bulk} = c^{bulk} \qquad \text{---------5.12}$$

Hence N=2 (one for anionic and one for cationic), z is the valence. Now with this, the equation 5.10 becomes

$$\Rightarrow \left(\frac{d\phi}{dx}\right)^2 = \frac{2K_BT}{\varepsilon_o\varepsilon_r} c^{bulk} \left(e^{z_i q\phi/K_BT} - 1 + e^{-z_i q\phi/K_BT} - 1\right) \qquad \text{---------5.13}$$

$$\Rightarrow \left(\frac{d\phi}{dx}\right)^2 = \frac{2K_BT}{\varepsilon_o\varepsilon_r} c^{bulk} \left(e^{z_i q\phi/2K_BT} - e^{-z_i q\phi/2K_BT}\right)^2$$

$$\Rightarrow \left(\frac{d\phi}{dx}\right)^2 = \frac{2K_BT}{\varepsilon_o\varepsilon_r} c^{bulk} \sinh^2\left(z_i q\phi/2K_BT\right)$$

$$\Rightarrow \frac{d\phi}{dx} = \pm\left(\frac{2K_BT\, c^{bulk}}{\varepsilon_o\varepsilon_r}\right)^{1/2} \sinh\ \left(z_i q\phi/2K_BT\right) \qquad \text{---------5.14}$$

When the electrode is positively charged i.e. pH< pH_{PZC}, $\phi > 0$, sinh (ϕ)>0 and $\frac{d\phi}{dx} < 0$ and hence

$$\frac{d\phi}{dx} = -\left(\frac{2K_BT\, c^{bulk}}{\varepsilon_o\varepsilon_r}\right)^{1/2} \sinh\ \left(z_i q\phi/2K_BT\right) \qquad \text{--------5.15}$$

And when the electrode is negatively charged i.e. pH> pH_{PZC}, ϕ> 0, sinh (ϕ) <0 and $\frac{d\phi}{dx} > 0$ and hence

$$\frac{d\phi}{dx} = \left(\frac{2K_B T\, c^{bulk}}{\varepsilon_o \varepsilon_r} \right)^{1/2} \sinh \left(z_i q\phi / 2K_B T \right) \quad \text{---------5.16}$$

Now for simplicity let us assume that

$$\sinh \left(z_i q\phi / 2K_B T \right) \approx zq\phi / 2K_B T \quad \text{---------5.17}$$

And considering the case when pH< pH_{PZC}

$$\frac{d\phi}{dx} = - \left(\frac{2K_B T\, c^{bulk}}{\varepsilon_o \varepsilon_r} \right)^{1/2} \left(z_i q\phi / 2K_B T \right) \quad \text{---------5.18}$$

$$\Rightarrow \frac{d\phi}{dx} = - \left(\frac{2\, c^{bulk} z^2 q^2}{\varepsilon_o \varepsilon_r K_B T} \right)^{1/2} \phi \quad \text{---------5.19}$$

$$\Rightarrow \frac{d\phi}{dx} = - L_D^{-1}\, \phi \quad \text{--------5.20}$$

Where

$$L_D^{-1} = \left(\frac{2\, c^{bulk} z^2 q^2}{\varepsilon_o \varepsilon_r K_B T} \right)^{1/2} \quad \text{--------5.21}$$

Finally

$$\phi = \phi_{eo} \exp\left(-L_D^{-1}\ x\right)$$ --------5.22

Or

$$\phi(x) = \phi_{eo} \exp\left(-L_D^{-1}\ x\right)$$ --------5.23

$\frac{\phi(x)}{\phi_{eo}} = \exp\left(-L_D^{-1}\ x\right)$ is known as normalized potential

The above expression gives the potential profile at a planer interface. The threshold voltage of ISFET is given by (from equation no. 2.8)

$$V_{th(isfet)} = V_{th(mosfet)} + E_{ref} + \phi_{lj} + \chi_e - \phi_{eo} - \phi_M$$ -------5.24

But from fig 5.1 and 5.2 it is clear that the effective electrolyte oxide interface potential appearing in the above equation should not be ϕ_{eo}, but it should be an effective potential

$$\phi_{eo_eff} = \phi_{eo} - \phi(x)$$ --------5.25

$$\Rightarrow \phi_{eo_eff} = \phi_{eo} - \phi_{eo} \exp\left(-L_D^{-1}\ x\right)$$

$$\Rightarrow \phi_{eo_eff} = \phi_{eo}\left(1 - \exp\left(-L_D^{-1}\ x\right)\right)$$

When the measuring setup is big enough, the reference electrode can be placed at a distance several times the Debye length, under that condition the value of x is large and hence

$$\phi(x) = \phi_{eo} \exp\left(-L_D^{-1}\ x\right) \approx 0 \qquad \text{---------5.26}$$

And consequently

$$\phi_{eo_eff} \approx \phi_{eo} \qquad \text{--------5.27}$$

The PBE for a cylindrical surface is [7]

$$\frac{1}{r}\frac{d}{dr}\left(r\frac{d\phi}{dr}\right) = \frac{2qzc_i}{\varepsilon_{diffuse}}\sinh\left(\frac{zq\phi}{k_B T}\right) \qquad \text{--------5.28}$$

And the approximate solution of this equation is

$$\phi(r) = \phi_0 \frac{K_0(k.r)}{K_0(k.(t_{si} + 2t_{ox}))} \qquad \text{---------5.29}$$

$$\frac{\phi(r)}{\phi_0} = \frac{K_0(k.r)}{K_0(k.(t_{si} + 2t_{ox}))}$$ is normalized potential

Now the effective electrolyte oxide interface potential is given as

$$\phi_{eo_eff} = \phi_{eo} - \phi(r) \qquad \text{---------5.30}$$

$$\Rightarrow \phi_{eo(eff)}(r) = \phi_{eo}\left[1 - \frac{K_0(k.r)}{K_0(k(t_{si} + 2t_{ox}))}\right] \qquad \text{--------5.31}$$

This is the potential that will appear in the ISFET threshold voltage equation, when the reference electrode is placed at a distance 'r' from the OHP.

5.3 Simulation results and conclusions

Figure 5.3: shows the variation of electrolyte oxide interface potential as pH varies from 1 to 14, when the reference electrode is placed at a distance 30.8 nm from the OHP. 30.8nm is the Debye length corresponding to pH=4. From the figure it is clear that up to pH=2 the response of planar as well as cylindrical device is exactly same as that of the ideal case. At pH=3, slight deviation of the curve corresponding to the planar device is observed as compared to the ideal case. Beyond pH=3 both planar as well as cylindrical curve deviates from the ideal curve. Beyond pH=4, the effective electrolyte oxide interface potential becomes almost zero.

In the figure 5.4: the variation of effective electrolyte oxide interface potential vs. pH is shown, when the reference electrode is placed at a distance 3975.15 nm (it is the Debye length corresponding to pH=7) from the OHP. The effective electrolyte oxide interface potential for all the three cases is identical up to pH=6. Beyond this value of pH both the curve becomes non linear and deviates considerably from the ideal case. In this part of curve it can also be noticed that one value of electrolyte oxide interface potential corresponds to two values of pH. For example, ϕ_{eo_eff}= -0.0612 volt corresponds to pH=5.3 and 8 for the planar ISFET and pH=5.3 and 9.1 for the cylindrical ISFET. This is a cause ambiguity. This ambiguity for a planar device starts at lower value of pH then that for a cylindrical device as evident from this figure. For the planar device the ϕ_{eo_eff} becomes zero for pH≥12. But the value of ϕ_{eo_eff} becomes zero at pH_{pzc} also. In between pH_{pzc} and pH=12 each value of ϕ_{eo_eff} corresponds to two values

of pH. Consequently, when the reference electrode is placed at a distance 3975.15 nm from the OHP, the results obtained becomes ambiguous beyond pH=4.2 for a planar ISFET. Similarly for the cylindrical ISFET, for pH $\geq$ 4.7 each value of ϕ_{eo_eff} corresponds to two values of pH.

Figure 5.5: shows the variation of electrolyte oxide interface potential as pH varies from 1 to 14, when the reference electrode is placed at a distance 30837 nm (the Debye length at pH=10)from the OHP. The effective electrolyte oxide interface potential for both planar and cylindrical ISFET is identical to the ideal case up to pH=8.8 and 9 respectively. Beyond this value of pH both the curve becomes non linear and deviates considerably from the ideal case. Deviation in the case of planar ISFET is more than that of the cylindrical ISFET. For the planar device the ϕ_{eo_eff} becomes zero for pH=13.5. But the value of ϕ_{eo_eff} becomes zero at pH_{pzc} also. In between pH_{pzc} and pH=13.5 each value of ϕ_{eo_eff} corresponds to two values of pH. . In case of cylindrical ISFET, for pH$\geq$ 7.5, the ϕ_{eo_eff} corresponds to two value of pH.

From the above discussion it can be concluded that if the reference electrode is placed inside the diffuse layer, then the measurement range of both the ISFETs reduces. In case of planar ISFET this reduction is more than that of a cylindrical ISFET.

For a particular application the pH measurement range may not be 1to 14. If for a particular application the maximum value of pH to be measured is 9, in that case the reference electrode must be placed at a minimum distance of three times the Debye length corresponding to pH=9. Then only for that particular range of measurement, the obtained value of ϕ_{eo_eff} will be close to the ideal case.

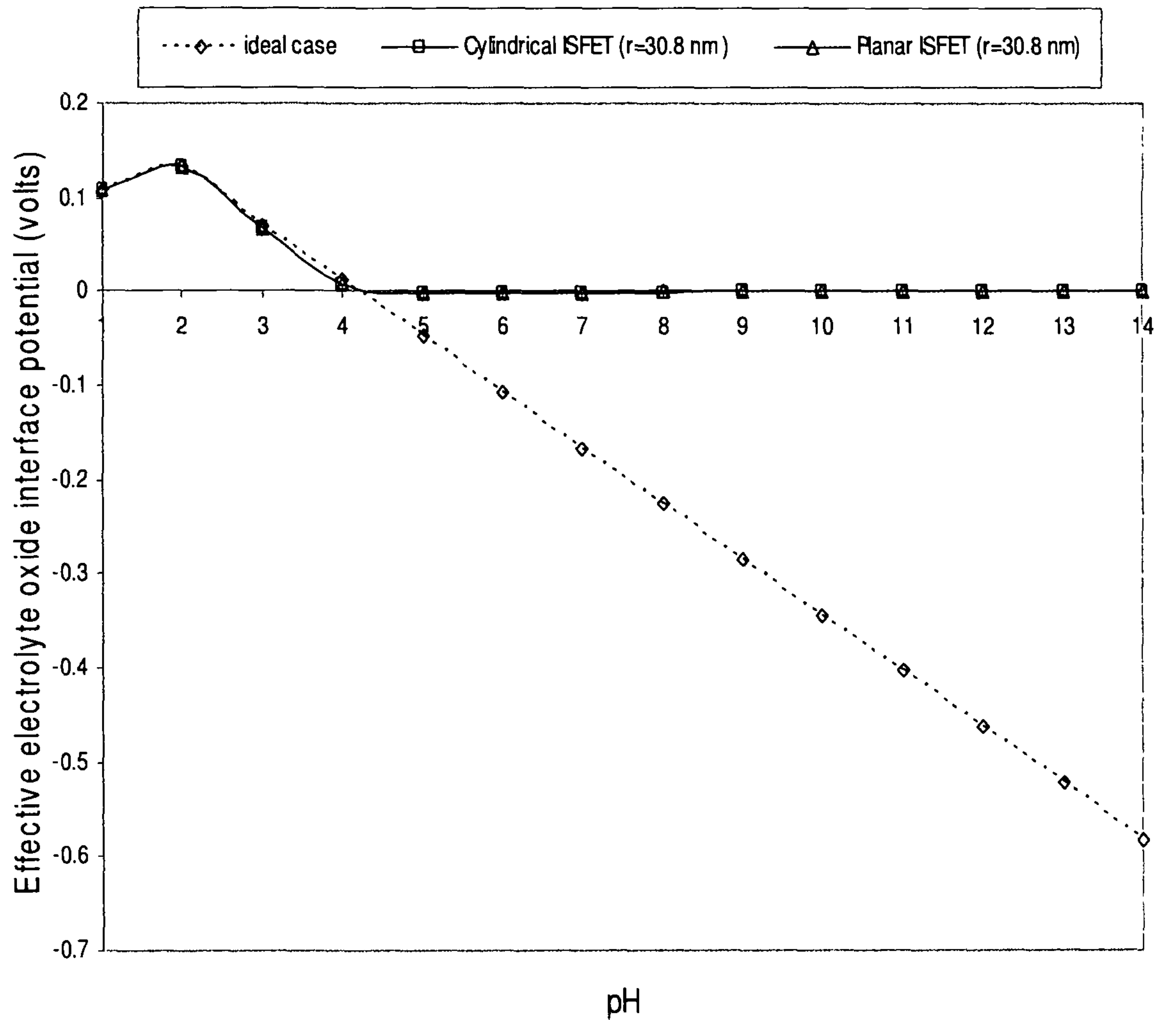

Fig.5.3: Effective electrolyte oxide interface potential (ϕ_{eo_eff}) vs. pH when the reference electrode is placed at a distance of 30.8 nm from the OHP.

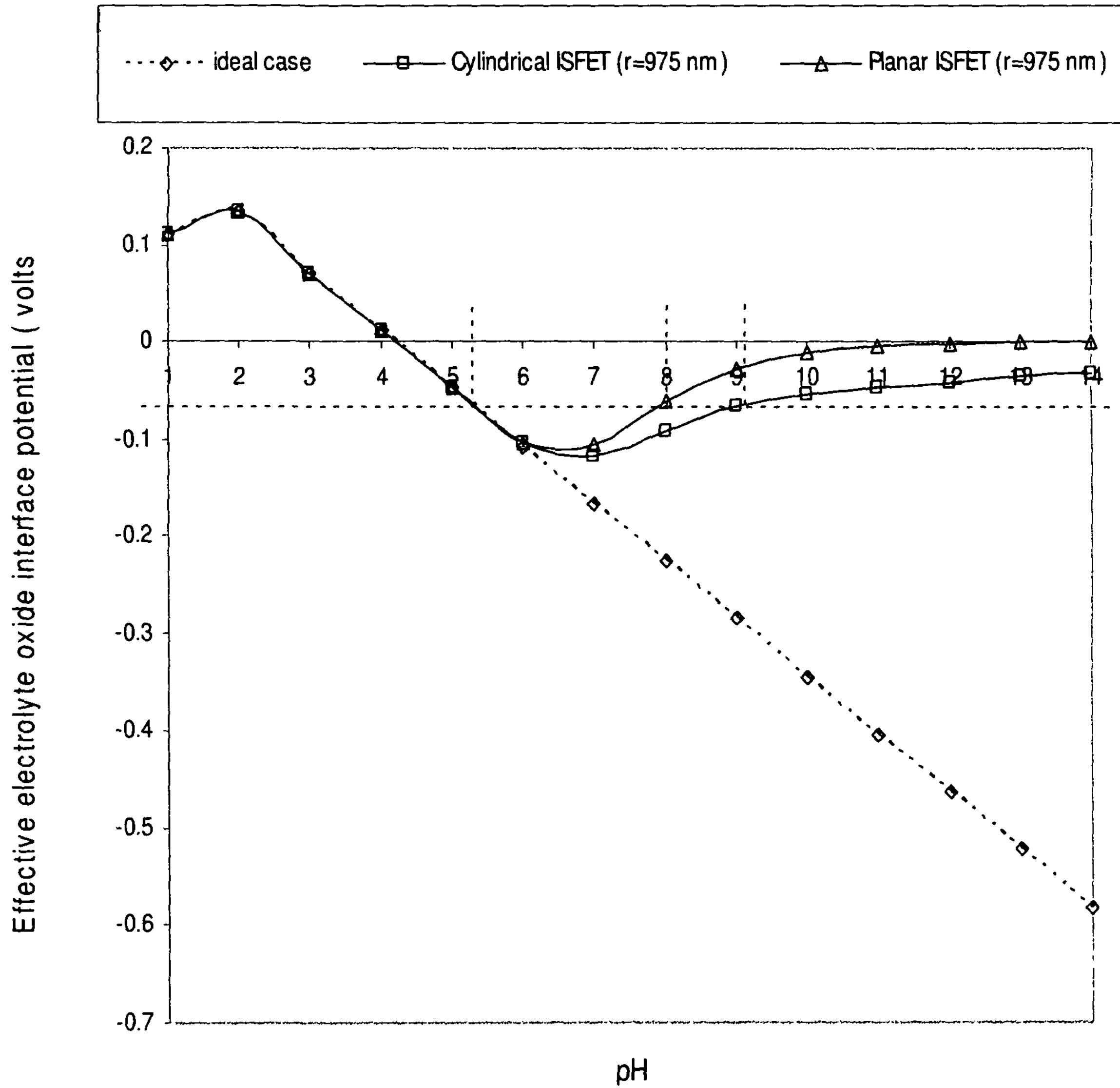

Fig.5.4: Effective electrolyte oxide interface potential (ϕ_{eo_eff}) vs. pH when the reference electrode is placed at a distance of 975 nm from the OHP.

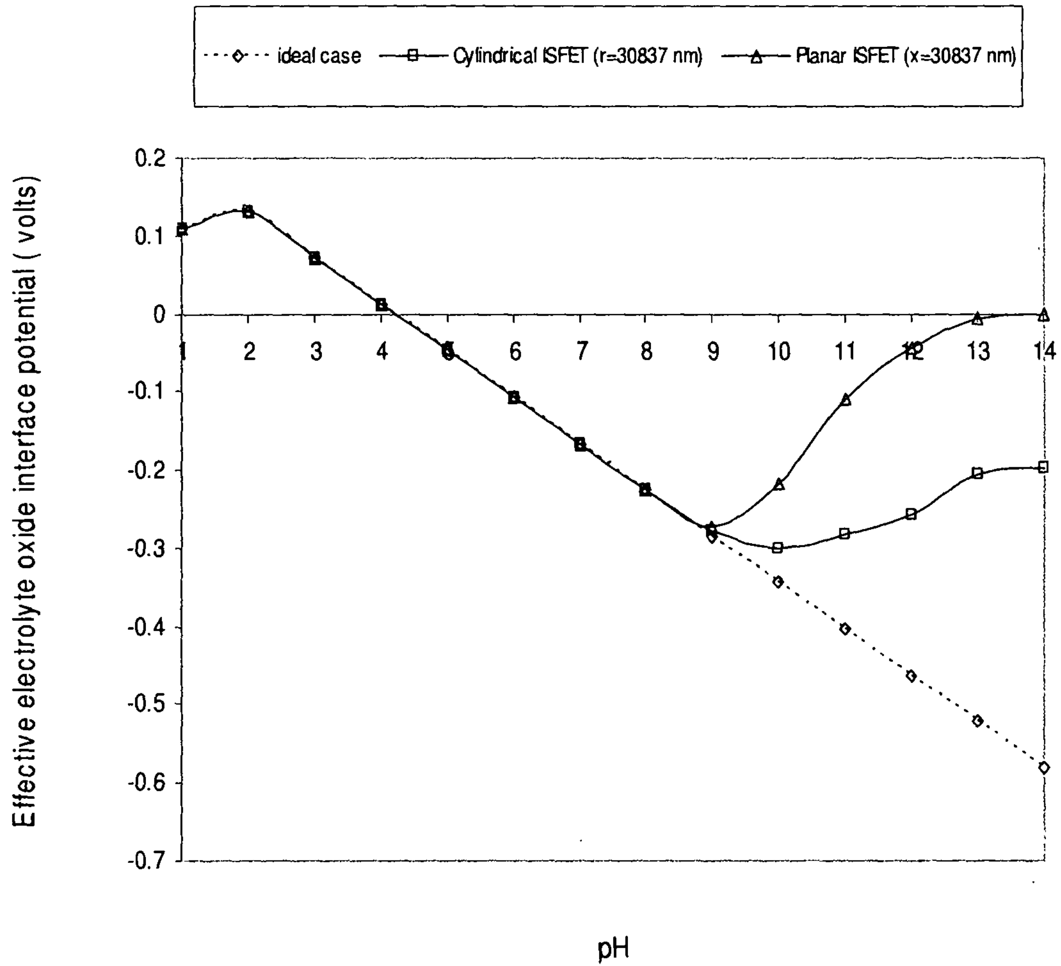

Fig.5.5: Effective electrolyte oxide interface potential (ϕ_{eo_eff}) vs. pH when the reference electrode is placed at a distance of 308375 nm from the OHP.

5.4 References

1. Kasem K Kasem and Stephanie Jones, "Platinum as a Reference Electrode in Electrochemical Measurements", Platinum Metals Review, 2008, 52 (2), pp.100-106.
2. Websource "http://en.wikipedia.org/wiki/Reference_electrode"
3. P.Bergveld, "Thirty years of ISFETOLOGY what happened in the past 30 years and what may happen in the next 30 years", Sensors and Actuators B ,Vol-88, pp. 1-20, 2003.
4. Websource "http://en.wikipedia.org/wiki/Nanowire"
5. G Verzellesi, L Colalongo, D Passeri, B Margesin, M Rudan, G Soneini, P Ciampolini "Numerical analysis of ISFET and LAPS devices" Sensors and Actuators B 44, pp 402-408, 1997.
6. Massimo Grattarola, Giuseppe Massobrio, *Bioelectronic Handbook: MOSFETs, Biosensors and Neurons*, Mc Graw-HILL, New York. 1998
7. Jacob H Masliyah, Subir Bhattacharjee, *Electrokinetic and Colloid Transport Phenomena,* John Wiley & Sons, Inc, 2006

Chapter 6

Conclusions

In this dissertation a new structure for Ion Sensitive Field Effect Transistor has been proposed and the same has been modeled and simulated. This work shows merits and demerits of this new device structure as compared to the conventional planer ISFETs.

In the second chapter a brief review of existing literature is presented. This chapter also discusses the basics of ISFETs and its modeling on the basis of the well known site binding and electrical double layer theory. The pH response of the device is presented using asymptotic solution of the governing equation. Electrolyte oxide interface potential found using this equation shows good agreement with the experimental data available in literature. At the end of this chapter, a term, amperometric sensitivity has been defined to indicate the change in drain current with pH, at a constant drain to source voltage.

In the third chapter, the new, device structure Cylindrical ISFET has been proposed. A one dimensional model for the same has been developed for moderately doped condition. The cylindrical Poisson's equation has been solved using Bessel function for its general solution. The result obtained has been used to find out the threshold voltage of cylindrical MOSFET. This result has been compared with already established model available in literature. The result obtained shows consistency at low to moderate doping concentration. This threshold voltage equation of cylindrical MOSFET has been translated to threshold voltage equation of Cylindrical ISFET after proper modification. In the next part of this chapter the electrolyte potential profile has been modeled by solving the cylindrical Poisson Boltzmann equation for a 1:1 electrolyte. This solution shows that the diffuse layer potential falls more sharply in Cylindrical ISFET as compared to a planar ISFET. As the cylindrical devices have larger aspect ratio as compared to planer device, hence their device transconductance is also more, leading to higher amperometric sensitivity. Here, the potential across

the inversion layer is also presented as a function of pH using depletion approximation.

The fourth chapter analyses the issues when the device is shrunken to nano dimension. Modern sensing applications demand sensors capable of sensing very small volume of measurand efficiently and effectively. For such applications the sensors should also be of small dimension. For example, if we need to extract some information from within a cell, without damaging it, the sensor if penetrates it, must be much smaller than the cell. Available literature shows that a single cell can be penetrated by a nanowire without damaging it. If we need to measure the pH inside a cell, the ISFET used should be of nano dimension. In this chapter ISFET is modeled at nano dimension. The nano dimension effects considered here are quantum mechanical band shift, effective oxide thickness increase and insulator behavior at nano dimension.

1. The first nano dimension effect mentioned here causes an increase in threshold voltage.
2. The second effect also contributes to increase in threshold voltage of the device due to reduction of oxide capacitance. In addition, the effective device transconductance also decreases due to effective oxide thickness increase. This results in reduction of amperometric sensitivity of Cylindrical ISFET, when dimension is reduced to nano level.
3. The third nano dimension effect comes up in an ISFET is reduction of sensitivity of the pH sensing layer. This occurs because of reduction of number of binding sites per unit area at insulator thickness of the order of few nanometers. This reduces the potentiometric sensitivity of the ISFET and consequently the amperometric sensitivity also reduces.

The modeling approach for estimation of quantum mechanical energy band shift uses triangular potential well (TPW) approximation, for decoupling the Schrodinger and Poisson's equation. The Schrodinger equation is formed using the triangular potential well in cylindrical coordinate. This equation is then approximated near the oxide semiconductor interface. The approximated equation finally has been solved asymptotically using Airy functions. The solution has been estimated for n=1, because as per assumption the decoupled Schrodinger and Poisson equation are valid only for low charge density and hence only lowest sub band is considered here.

In the fifth chapter a rule for reference electrode has been framed on the basis of diffuse layer potential profile. This rule says that the reference electrode cannot be placed very close to the sensing area of the ISFET. To get complete effect of electrolyte insulator interface potential, the reference electrode must be placed at a distance much higher than the Debye length. Otherwise a single value of electrolyte oxide interface potential will correspond to two different value of pH. This will lead to ambiguity in the system. So to avoid this ambiguity, the reference electrode must be placed at a minimum distance set by this rule. The compactness of the pH measuring system not only depend on the dimension of the ISFET and reference electrode, but also on the distance allowed between the ISFET and the reference electrode. The simulation result shows electrolyte oxide interface potential as a function of pH. This curve is non liner for small distance between the ISFET and the reference electrode, but approaches linear shape when the distance between the ISFET and the reference electrode is large enough. As far as Debye length is concerned when a Cylindrical ISFET is compared with a planer ISFET, the Debye length for a cylindrical ISFET is smaller than a planer device. Hence , for a cylindrical device, the electrode oxide interface potential becomes linear at a smaller distance between reference

electrode and the sensing surface as compared to a planer device This makes a pH measuring system using Cylindrical ISFET smaller than a system that uses a planer device.

As a future extension of this work, the temperature variation of human body may also be considered in the model because, temperature change in human body under diseased condition may be sufficient to cause drift in the ISFET response in vivo.

APPENDIX

A1 Amperometric sensitivity

$$\frac{dI_{DS}}{dpH}=\frac{d}{dpH}\left[\mu C_{ox}\frac{W}{L}\left\{\left(V_{ref}-V_{th(isfet)}\right)V_{DS}-\frac{V_{DS}^{2}}{2}\right\}\right]$$

$$=\mu C_{ox}\frac{W}{L}\left[-\left(\frac{dV_{th(isfet)}}{dpH}\right).V_{DS}\right]$$

$$=\mu C_{ox}\frac{W}{L}V_{DS}\left(\frac{d\phi_{eo}}{dpH}\right)$$

A2 The cylindrical coaxial capacitance

The cylindrical coaxial capacitance is given as

$$C_{cyl_coax}=\frac{2\pi\varepsilon L}{\left(\ln\left(\frac{b}{a}\right)\right)}$$

Where L = Length of the coaxial cable

b = Outer radius

a = Inner radius

C_{cyl_coax} = coaxial capacitance

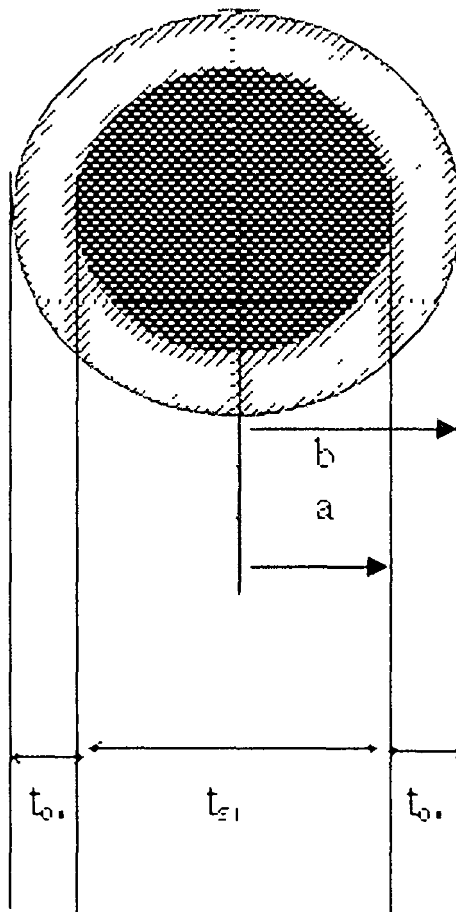

Fig.A1: Cylindrical capacitance cross sectional view

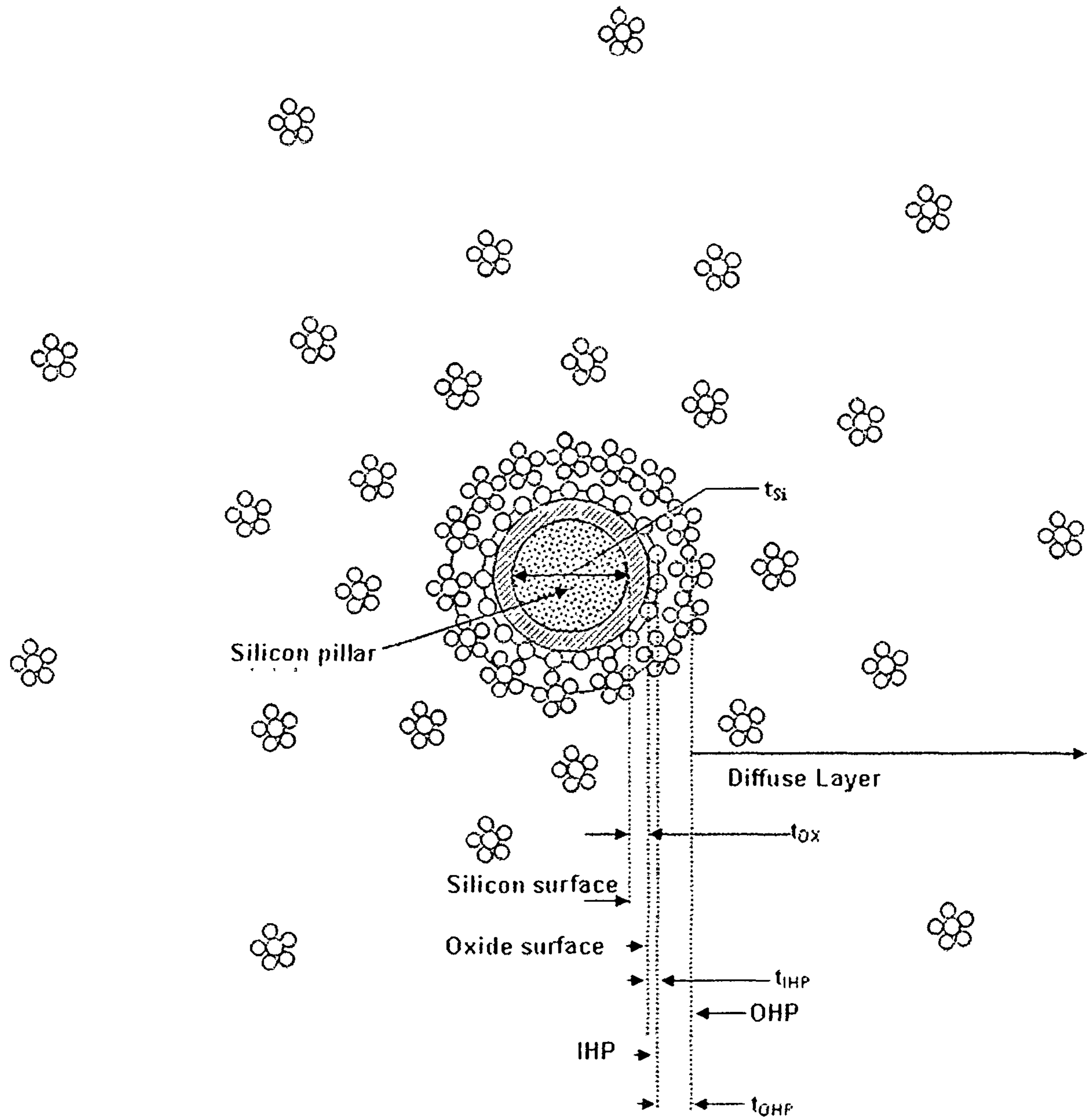

FigA.2: Cross sectional view of a cylindrical ISFET surrounded by electrolyte.

Therefore the coaxial capacitance per unit area is

$$C_{cyl_coax} \Big/ Area = \frac{C_{cyl_coax}}{2\pi a.L}$$

$$= \frac{\varepsilon}{a\left(\ln\left(\frac{b}{a}\right)\right)}$$

If we put $a = \frac{t_{si}}{2}$, $b = \frac{t_{si} + 2.t_{ox}}{2}$

Then cylindrical oxide capacitance per unit area will be

$$C_{OXcyl} = \frac{2\varepsilon_{ox}}{t_{si}\left(\ln(1 + \frac{2t_{ox}}{t_{si}})\right)}$$

From the figure A2 we can see that for IHP capacitance per unit area the inner radius 'a' and outer radius 'b' is given by

$$a = \frac{t_{si} + 2t_{ox}}{2}, \quad b = \frac{t_{si} + 2.t_{ox} + 2t_{IHP}}{2}$$

And the IHP capacitance per unit area becomes

$$C_{IHP_cyl} = \frac{2\varepsilon_{IHP}}{(t_{si} + 2t_{OX})\left(\ln(1 + \frac{2t_{IHP}}{t_{si} + 2t_{OX}})\right)}$$

Similarly for OHP capacitance per unit area the inner radius 'a' and outer radius 'b' is given by

$$a = \frac{t_{si} + 2.t_{ox} + 2t_{IHP}}{2}, \quad b = \frac{t_{si} + 2.t_{ox} + 2t_{IHP} + 2t_{OHP}}{2}$$

And the OHP capacitance per unit area becomes

$$C_{OHP_cyl} = \frac{2\varepsilon_{OHP}}{(t_{si} + 2t_{OX} + 2t_{IHP})\left(\ln\left(1 + \frac{2t_{OHP}}{t_{si} + 2t_{OX} + 2t_{IHP}}\right)\right)}$$

A3 The effective channel width of a cylindrical MOSFET

For a planar device neglecting the effect of drain bias, the shape of the channel can be approximated as shown below.

Here

L = channel length

W = channel width

t_{inv}= thickness of the inversion layer

A = area of the current path

The width 'W' of the channel for a planar can be expressed as

$$W = \frac{A}{t_{inv}}$$

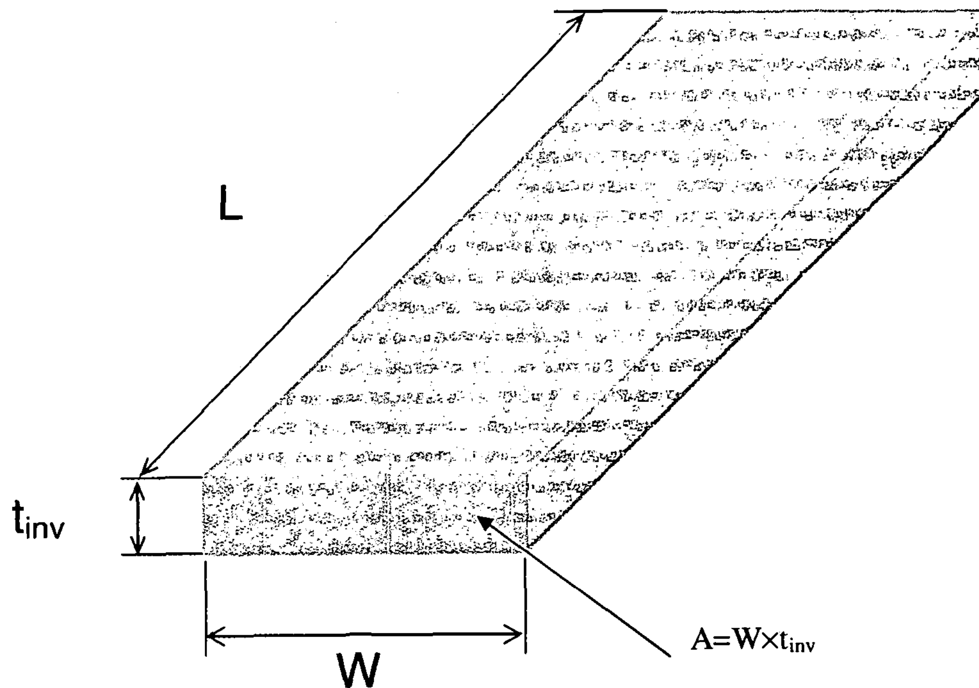

Fig.A3: Channel of a planar MOSFET

For a cylindrical device neglecting the effect of drain bias, the shape of the channel can be approximated as shown in Fig: A4.

The figure A3 shows the body of a cylindrical MOSFET.

L = channel length

W = channel width (not shown in the figure)

t_{inv}= thickness of the inversion layer

The area of the current path 'A' can be expressed as (This is shown in the figure with the dotted texture)

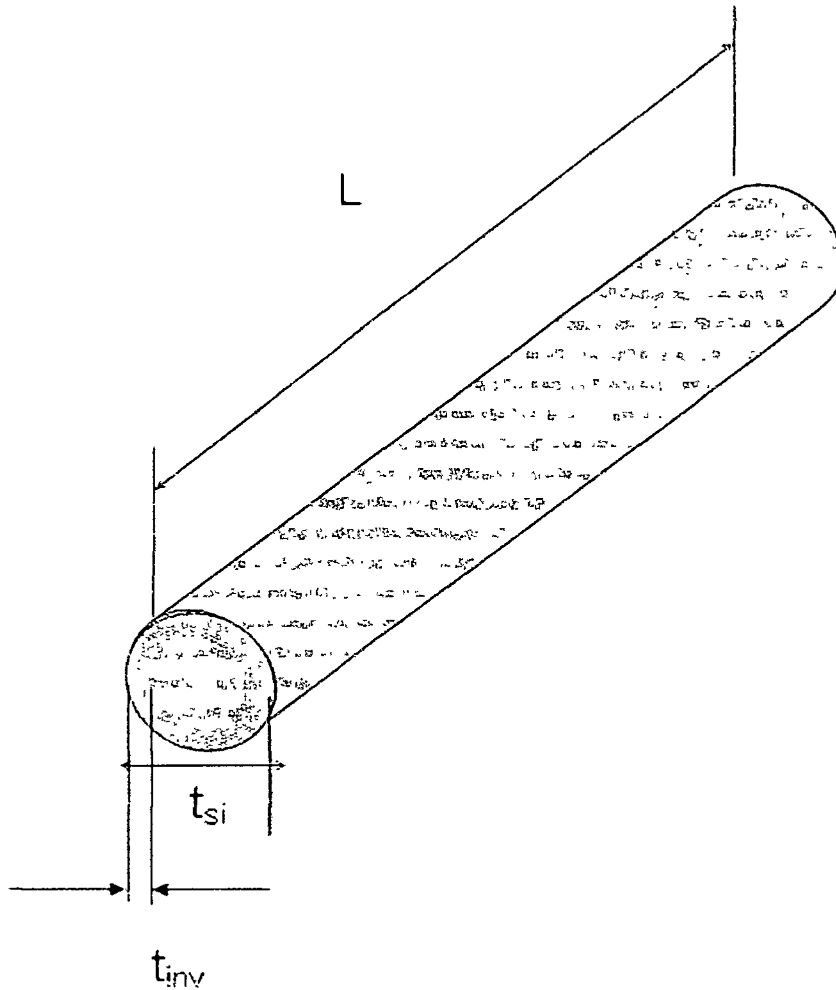

Fig: A4: Cylindrical silicon pillar

A= area of the circle of diameter t_{si} – area of the circle of diameter (t_{si} -2t_{inv})

$$A = \frac{\pi t_{si}^2}{4} - \frac{\pi (t_{si} - 2t_{inv})^2}{4}$$

Now the effective channel width 'W' can be found by dividing the current path area by thickness of the current path (as it was done in the case of a planar device)

$$W = \frac{A}{t_{inv}} = \frac{\pi \left[t_{Si}^2 - (t_{Si} - 2t_{inv})^2 \right]}{4t_{inv}}$$

A4 Calculation of reference electrode potential(E_{ref}) relative to vacuum:

The reference electrode potential is given by the following expression [2],[3]. The filling solution is assumed to be of 3.5M KCl, saturated with AgCl.

$$E_{ref}(T) = E_{abs}(H^+|H_2) + E_{rel}(Ag|AgCl) + \left(\frac{dE_{ref}}{dT} \right)(T - 298.16)$$

$$= 4.7 + .205 + 1.410^{-4}(300 - 298.16)$$

$$= 5.37 volts$$

$E_{abs}(H^+|H_2) =$ Absolute potential of hydrogen electrode

$E_{rel}(Ag|AgCl) =$ Relative potential of Ag/AgCl electrode with reference to hydrogen electrode

$\frac{dE_{ref}}{dT} =$ Temperature coefficient

A5. References

1. S L Jang, S S Liu "An Analytical Surrounding Gate MOSFET model" Solid State Electronics, Vol. 42, No.5, pp721-726, 1998
2. Giuseppe Massobrio, Sergio Martinoia, Massimo Grattarola "Ion Sensitive Field Effect Transistor(ISFET) Model Implemented in SPICE" Simulation of Semiconductor Devices and Processes, Vol.4, Zurich, Switzerland, September 12-14.pp563-570,1991
3. Peter R Barabash, Richard S C Cobbold, Wosciech B. W Lodarski "Analysis of the Threshold Voltage and Its Temperature Dependence in Electrolyte-Insulator-Semiconductor Field-Effect Transistors (EISFET's)" IEEE transaction on Electron Devices, Vol. ED-34,No.6, pp1271-1282, 1987.